Author Response to Interactive Reviews

egusphere-2025-3630 | *The Cryosphere*

Pardo Lara, R., Colliander, A., Tetlock, E., Powers, J., Ambadan, J., and Berg, A.

This document presents our full author response, organized as a thematic letter (Part 1) followed by tables addressing each comment from the editor, RC1, Dr. Jacobs, and Dr. Glaser (Part 2). Revised figures referenced throughout (Figures R1–R5) are included at the end of this document along with Appendix A and B featuring the figures for each pixel-year.

Part 1 Thematic Response

Dear Dr. Hauck, RC1, Dr. Jacobs, and Dr. Glaser,

Thank you for careful and substantive engagement with this manuscript. We address the shared themes below, and respond to individual comments in the tables in Part 2.

A. Threshold Framing and the Extrinsic Hook

RC1 and Dr. Jacobs both found the intrinsic/extrinsic framing imprecise. We appreciate the push to sharpen this, because it is the paper's central scientific argument.

The argument is as follows: freeze/thaw (F/T) transitions are **externally forced** by thermal conditions imposed on the soil. A single microwave observable captures the *consequence* of this transition, a permittivity change that shifts T_{B}^{H}, but not the *cause*. Without anchoring the microwave signal to its thermal driver, a single-variable classifier cannot reliably distinguish phase-change signals from drying, snowpack change, or sub-pixel heterogeneity. This is the reason single-variable classifiers are inherently limited for extrinsically driven phenomena, and why pairing T_{B}^{H} with the thermal coordinate in SurFC–space yields a curve we can interpret physically. The revised manuscript will state this directly in the Abstract and Introduction, replacing the current terminology where it is unclear.

In regard to the 0.15 °C threshold, our results show that the data-driven $T_{\mathrm{B,min}}^{H}$ threshold varies by site, year, and temperature reference. An expanded Table A1 will report these values.

The paper aims to challenge the universal application of the 0.15 °C threshold, not indicate that it is broadly wrong. Assuming it is spatially and temporally invariant is not physically justified, and the SurFC framework provides a way to derive it locally from the system's own response.

B. Revised Figure Set

The editor and both referees found the submitted figures visually busy, we agree. We have reorganized the figure set into four types, each with a single purpose.

1. **Multi-temperature-source SurFC (Figure R1).**

   T_{B}^{H} plotted against all four thermal coordinates (air temperature 2 m, in situ 2.5 cm, in situ 5 cm, and SMAP ancillary T_{eff}/K) for selected pixel-years. This directly addresses the threshold-variability and temperature-source-dependence concerns. Full pixel-year compendium is provided in Appendix A and B.

2. **GEOS-5 T_{eff}/K vs. in situ agreement (Figure R2).**

   Site-level agreement within the −5 to +5 °C transition window (n = 1,942; bias = −0.17 °C; RMSE = 2.0 °C; MAE = 1.4 °C). This replaces the Holmes et al. (2012) citation with a site-specific, winter-valid uncertainty characterization.

3. **SurFC + environmental context (Figures R3–R3b).**

   Three-panel layout per pixel-year: (a) SurFC scatter with freezing and thawing branches as well as the seasonal T_B^H minimum marked ($\star$); (b) rainfall and GlobSnow SWE time series, showing that $\star$ closely coincides with SWE $\to$ 0; (c) T_B^H and soil temperature time series. The 2020–21 drought year (Figure R3b) is shown separately as a confounding case. Full pixel-year compendium is provided in Appendix A and B.

4. **Three-way agreement composition (Figure R4).**

   Replaces the accuracy, F_1, and LR^- bar graphs. Across all 3,000 observations, the three classifiers ($T_{B,min}^H$, NPR, in situ temperature reference) agree in 62.6% of cases; $T_{B,min}^H$ and the temperature reference agree while NPR differs in 29.4%; the remaining $\sim$8% splits between the other two disagreement combinations. We believe this framing removes the circular 'gold standard' logic.

Lastly, an updated study area map (Figure R5) adds SMAP 36 km EASE-Grid pixel boundaries to Figure 1.

C. Temperature Reference Dependence and GEOS-5 Uncertainty

RC1 asked about alternative temperature sources, and Dr. Jacobs identified that GEOS-5 uncertainty had not been characterized for winter conditions at these sites. Figure R1 demonstrates directly that the SurFC trajectory depends on the thermal coordinate: air temperature (2 m) produces the noisiest curve; in situ are the most clear; GEOS-5 T_{eff}/K is in between. Derived thresholds are therefore coordinate-specific, and expanded Table A1 will report them by pixel, year, and temperature source.

We use SMAP ancillary T_{eff}/K because it is the temperature product already packaged in the L3_FT_P pipeline, making the SurFC a coherent extension of the existing SMAP system. Figure R2 establishes a near-zero bias ($-0.17\,^\circ$C) and an RMSE of $2.0\,^\circ$C relative to in situ 5 cm within the transition window ($n = 1{,}942$ overpasses; the larger $n = 3{,}000$ used for the agreement composition in Fig. R4 counts classifier observations, not transition-window overpasses). This RMSE is a point-to-point representativeness statistic; it is larger than in situ sensor uncertainty ($\sim 0.3\,^\circ$C) and characterizes footprint-vs-point mismatch. It is distinct from the precision of a derived threshold (the standard error of the footprint mean) and is different from the $2.0\,^\circ$C scatter (Part 2, G1). Section 2.1.3 will present this explicitly and remove the Holmes et al. (2012) citation for winter conditions.

D. Snow/Soil/Microwave Signal Ambiguity

RC1 and Dr. Jacobs both raised the ambiguity between snowpack and soil contributions to the seasonal T_B^H signal. In the data we analyzed, the seasonal T_B^H minimum was generally tied to snowpack loss as seen in Appendix A and B. It seems, when the snowpack fully melts, the surface temporarily approaches a saturated, high-liquid-water state, producing the lowest observed brightness temperature of the season. The permittivity contrast between liquid water ($\varepsilon_r \approx 80$) and ice ($\varepsilon_r \approx 5$) drives amplitude changes of $\approx$70 K on average; progressive snow grain metamorphism through melt-refreeze cycles contributes secondary T_B^H variations of order 5–15 K (Willmes et al., 2009), and provides useful framing but is not the primary mechanism. As SWE $\to$ 0, the microwave emission transitions from being associated with the snowpack to being associated with exposed-soil. The $\star$ appears to be as tied to soil exposure as much as to snowpack loss. We will quantify this by computing the temporal offset (in days) between the seasonal T_B^H minimum and the nearest date of SWE = 0 across all analyzed pixel-years.

The 2020–21 drought year (Figure R3b) confirms the mechanism. The below-normal snowpack meant the saturated-surface signal was never reached within the $\pm 5\,^\circ$C window, and the minimum

was instead driven by late-season heavy rainfall (42 ± 21 mm over 19–22 May 2021).

We cannot decompose T_B^H into snowpack and soil contributions from passive L-band data alone, this limitation will be stated explicitly throughout the revised manuscript. On Dr. Jacobs's observation that SWE ablation periods do not align with expected air temperature (Fig. 13), this is expected, as ablation is governed by the net surface energy balance—shortwave radiation, rain-on-snow, and ground heat flux—rather than by air temperature alone, so SWE drawdown need not track air temperature. We will note this in the revised text. The SurFC figures along with the SWE time series make the ambiguity visible and show when the method is operating within its physical basis and when it is not.

E. Branch Structure, Hysteresis, and Multiple Thaw Paths

Both referees noted that the branch structure and hysteresis deserve more prominence, and we agree. These distinct T_B^H–T trajectories during cooling/freezing versus warming/thawing are visible across all analyzed pixel-years and are, indeed, among the most physically interesting results of the SurFC representation.

In the revised figures (Figure R1), freezing (blue) and thawing (red) branches are clearly distinguished across all four temperature sources. The branch separation reflects some combination of genuine soil dielectric hysteresis—supported at the laboratory scale by sub-freezing electrical conductivity measurements in Garcia and Glaser (2025) and Liu et al. (2022), raised by Dr. Glaser—and the support mismatch between the SMAP pixel and point-scale temperature measurements (Pardo Lara et al., 2021). We cannot isolate these contributions with the present data, and Section 4.1 will be expanded to discuss both interpretations. A terminology-consistency pass will also ensure SurFC and SurTC are used distinctly throughout Section 3.1, the Results, and all figure captions.

Thank you again for the thorough and constructive reviews.

Sincerely,

Renato Pardo Lara et al.

Part 2 Point-by-Point Tables

Page (p.) and line (L.) references are to the published preprint.

Response to Editor (Dr. Christian Hauck)

#	Comment	Response	Manuscript change	Ref.
E1	Figure and table readability can be improved.	Agreed. Revised figure set (Figs. R1–R5) reduces visual complexity substantially. Each figure has a single purpose; the 9-panel layout is replaced by a 3-panel atlas format; NPR overlays are removed from SurFC figures.	Figs. 3, 5, 7, 9, 14 redesigned.	B, R1–R5, App. A, App. B
E2	Scope of significance; further studies needed.	Agreed. Conclusions scoped explicitly to the two study regions and nine hydrological years across two networks (24 pixel-years analysed).	Conclusions revised with explicit geographic scope.	—

Response to RC1

#	Comment	Response	Manuscript change	Ref.
G1	Active microwave F/T literature missing from Introduction and Discussion.	Accepted fully. We overlooked this literature during drafting and thank RC1 for the direction. Naeimi et al. (2012); Bartsch et al. (2025); Bergstedt et al. (2020), and related papers will be incorporated as established context.	Paragraphs added to Introduction (after L65) and Section 4.	—
G2	p. 1, L7: intrinsic/extrinsic framing confusing.	The argument is: F/T is externally forced, making single-variable classifiers insufficient because they cannot distinguish phase-change signals from drying, metamorphism, or heterogeneity.	L7 and Abstract revised; 'intrinsic/extrinsic threshold' terminology replaced throughout.	A
S1	Sub-grid heterogeneity not discussed.	KSMN/RISMA were selected as SMAP core validation sites (CVS) for footprint-scale homogeneity. A brief land-cover and open-water characterization from SMAP static ancillary data will be added; the CVS designation will be framed as both a study strength and a caveat around generalization.	Section 2.3 expanded with sub-pixel land-cover characterization.	—
S2	Section 2.4.1: active-sensor analogues not mentioned.	We will note precedent multi-variable satellite–thermal state-space studies in the active microwave domain.	Content added to Section 2.4.1.	—
S3	Figs. 3 and 5: visually busy; colour-scale ambiguity; red/blue dual-coding.	Addressed in the revised figure set. Date colour scale replaced by explicit $\star$ annotations; red/blue used only for branch identity; NPR panels removed from SurFC figures; 3-panel atlas layout adopted.	Figs. 3, 5, 7, 9, 14 redesigned.	R1, R3
S4	Table 2: mean (SD) $\rightarrow$ mean $\pm$ SD.	Agreed.	Notation changed.	—

#	Comment	Response	Manuscript change	Ref.
S5	Have you considered ERA5 as a temperature source?	ERA5 is well-motivated; we used GEOS-5 T_{eff}/K for operational consistency with SMAP. ERA5 comparison is future work.	Sentence added to Section 2.1.3 and Discussion.	C
S6	Does the passive approach outperform active methods with a temperature-driven threshold?	No comparison was conducted. Published active backscatter–temperature relationships appear sigmoid-like and monotonic, lacking the hysteretic loop visible in T_{B}^{H}–T space. Whether this reflects a genuine physical difference or unresolved scatter is identified as future work.	Hypothesis added to Section 4.	—
S7	How would the approach perform in Arctic permafrost regions?	Trail Valley Creek (TVC, NWT) data from ECCC provide a permafrost active-layer test case. Identified as planned future work.	Arctic studies added to Conclusions as future work.	—
S8	p. 31, L455–460: points already made in suggested papers.	Citations to Naeimi et al. (2012); Bartsch et al. (2025); Bergstedt et al. (2020).	Citations added.	—

Response to RC2 (Dr. Jennifer Jacobs)

#	Comment	Response	Manuscript change	Ref.
G1	Threshold varies by site and year (add to Table A1); discernible thresholds appear to lie within error (∼2 °C).	Agreed: the threshold is site-, year-, and temperature-source-specific, not universal, and the expanded Table A1 now reports each derived value. On the precision point: the ∼2 °C scatter visible in the figures is single-overpass footprint-vs-point representativeness, not the uncertainty of the derived threshold itself. Because the threshold is a footprint-mean quantity, its uncertainty is the standard error of that mean (≈0.2–0.4 °C), correspondingly smaller than the point-scale spread. Weighting the per-pixel-year thresholds by these uncertainties, a single common threshold is rejected (reduced $\chi^2 \approx 3.6$ on 21 degrees of freedom). The values scatter well beyond measurement error, with clear site/year structure (Kenaston near 0 °C, RISMA near +1.7 °C). Table A1 will list each threshold with its uncertainty.	Table A1 expanded to list the derived threshold and its footprint-mean uncertainty per pixel-year; a brief methods note distinguishes single-overpass representativeness from the precision of the footprint-mean threshold and reports the reduced-χ^2 test of a single common threshold (Vermeesch, 2018).	A

#	Comment	Response	Manuscript change	Ref.
G2	GEOS-5 FP errors not established for study sites; Holmes et al. (2012) valid for non-frozen conditions only.	Accepted. Site-level agreement within the −5 to +5 °C window: bias = −0.17 °C, RMSE = 2.01 °C, MAE = 1.42 °C(n = 1,942 overpasses). This RMSE is a footprint-vs-point *representativeness* statistic, not the precision of a derived threshold: the threshold is a footprint-mean quantity whose uncertainty is the standard error of that mean (≈0.2–0.4 °C) and is smaller than this point-to-point scatter, so the 2.0 °C RMSE should not be compared directly with the across-site threshold spread (see G1). Holmes et al. (2012) citation corrected in scope.	Fig. R2 added and captioned as representativeness; Section 2.1.3 revised with site-specific uncertainty; Holmes et al. (2012) citation corrected in scope.	R2, C
G3	'Gold standard' framing creates a logical inconsistency.	Accepted fully. 'Gold standard' removed. In situ temperature classification described as one imperfect reference among three. Section 3.3 reframed as three-way agreement composition: all three agree 62.6%; $T^{H}_{\mathrm{B,min}}$ and temperature reference agree, NPR differs 29.4%; other combinations ∼8%.	Section 3.3 retitled and reframed; 'gold standard' removed; Table 2 and Figs. 10–12 replaced by agreement composition (Fig. R4).	R4
G4	Could soil moisture sensors provide an alternate comparison?	HydraProbe permittivity and soil temperature data from the study sites were analyzed in Pardo Lara et al. (2020), which introduced the SFCC in permittivity–temperature space for agricultural soils. This framework was subsequently extended to 87 sites across Canadian ecozones, including Kenaston, in Salmabadi et al. (2026). Integration with the present F/T classification is deferred to future work.	Pardo Lara et al. (2020); Salmabadi et al. (2026) cited; direct HydraProbe comparison deferred to future work.	—

#	Comment	Response	Manuscript change	Ref.
G5	Why is single-channel T_{B}^{H} preferable to NPR or DAV? Possible pre-melt DAV phenomenon (cf. Ramage's snow-wetting work).	NPR and DAV-like approaches are complementary rather than superseded. NPR follows the SurFC trajectory closely, but forming the ratio both compresses the dynamic range and propagates larger uncertainty. Emissivity (T_{B}/T) avoids the axis inversion but inherits the representativeness error of the footprint-scale T in its denominator, inflating per-point uncertainty and reordering the trajectory less consistently. We therefore retain single-channel T_{B}^{H} as the lowest-noise coordinate and accept the axis inversion as the cost. DAV Ramage and Isacks (2002) may capture sub-daily melt/ripening near the zero-curtain but requires a separate paired AM/PM analysis, treated as future work.	Discussion paragraph added: NPR ratio-propagated uncertainty and dynamic-range compression; emissivity denominator-inherited error; NPR/DAV framed as complementary.	D, E
S1	Abstract wanders; needs rewriting.	Agreed. Rewritten: problem statement → approach (T_{B}^{H}–T coordinate space, SurFC/SurTC) → key results (hysteresis, $T_{\mathrm{B,min}}^{H}$ threshold, three-way agreement composition) → scope (two mid-latitude sites, nine hydrological years / 24 pixel-years analyzed).	Abstract fully rewritten.	—
S2	p. 2, L52: duplicate text.	Will be removed.	Duplicate at p. 2, L52 deleted.	—
S3	Section 2.1.3: which GEOS-5 FP product was used? What time? Were C and K applied?	NASA SMAP Level-2 ancillary; Choudhury–Schmugge two-layer with $C = 0.246$, $K = 1.007$ O'Neill et al. (2021); co-registered to 6 a.m. descending overpass. We also clarify that the MERRA-Land product underlying Holmes et al. (2012) is not the GEOS-5 FP product used here, so its reported error statistics do not transfer to this study.	Section 2.1.3 revised: product provenance (C, K, overpass time) and site-specific uncertainty added; MERRA-vs-GEOS-5 distinction stated.	R2

#	Comment	Response	Manuscript change	Ref.
S4	Lines 195–199: typos throughout.	Full copyedit pass will be conducted.	Manuscript copyedited.	—
S5	p. 7, L198 needs a reference.	Reference added. L198 introduces the GlobSnow SWE product; we cite Pulliainen et al. (2020) and the GlobSnow v3.0 data record Luojus et al. (2020).	Citation added at L198.	—
S6	Figure 1: add SMAP pixel outlines.	Done. Updated map uses SMAP 36 km EASE-Grid pixel outlines.	Fig. 1 updated (Fig. R5).	R5
S7	p. 11, L250: air or soil temperature?	L250 will list all sources.	p. 11, L250 revised to list all temperature sources.	—
S8	p. 12, LL 259–260: capturing wet snow or soil thaw? Reference needed.	The seasonal $T_{\mathrm{B,min}}^{H}$ corresponds to snowpack disappearance ($\sim$70 K amplitude). Snow grain metamorphism contributes secondary T_{B}^{H} variations (Willmes et al., 2009)<$\sim$5–15 K> but is not the primary mechanism. SWE $\rightarrow$ 0 also marks the transition from snowpack to soil-dominated emission. A day-gap analysis will be added.	p. 12, LL 259–260 revised; snowpack-loss interpretation clarified; day-gap analysis added; Fig. R3b added for drought-year confound.	D, R3b
S9	Figure 2: more examples needed.	Full pixel-year compendium provided Appendix A and B.	Compendium provided on Appendix A and B; representative subset in manuscript.	App. A, App. B
S10	Figure 3: no need to invert y-axis.	Since T_{B}^{H} is inversely correlated with liquid water content, and upon heavy consideration, we chose to keep the y-axis inverted. We believe this preserves visual analogy with the soil freezing characteristic curve. The figure caption will explain this explicitly.	Convention retained; caption revised.	10

#	Comment	Response	Manuscript change	Ref.
S11	Figure 4: show how $T_{\mathrm{B,min}}^{H}$ was obtained.	In revised figures (Fig. R3a and R3b), $\star$ is annotated across all three panels with the associated thermal coordinate readable on the x-axis. The $\pm 5\,^{\circ}\mathrm{C}$ search window is indicated in the time series panel. $T_{\mathrm{B,min}}^{H}$ is defined as the global minimum of T_{B}^{H} observed within this window.	$\star$ annotation added; search window indicated, caption explains selection of global minimum within time and temperature bounds.	R3a, R3b
S12	Figure 5: multiple thaw branches? Label them.	Sub-paths are present but not clearly resolvable using our event-selection method (Pardo Lara et al., 2020): branches merge, split, and restart across transitions, and temporal sampling is insufficient to distinguish them as separate trajectories. Labelling would imply a separability the data do not clearly support within this framework, though finer approaches may yet resolve them. The phenomenon is discussed in Section 4.1 in the context of zero-curtain dynamics.	Added a sentence to Section 4.1 noting that sub-paths are present but not consistently resolvable using our event-selection approach, due to branch merging, false starts, and temporal sampling limits; labelling is therefore omitted to avoid implying separability the data do not clearly support.	R1, E, App. A, App. B
S13	Section 3.3: redefine 'thermodynamic temperature'.	Accepted. Thermodynamic temperature will be defined at first use (Section 2.4.2, ≈L278) as the physical temperature of the soil or atmosphere, as distinct from the radiometric brightness temperature T_{B}^{H} recorded by the satellite.	Definition added at first use in Section 2.4.	—
S14	p. 26, LL 392–393: unclear.	Text rewritten; see manuscript change column. (This is the MB2 HY20-21 series; the within-window minimum described here is distinct from the rainfall-driven seasonal minimum that the $\pm 5\,^{\circ}\mathrm{C}$ window correctly rejects in Fig. R3b.)	"We interpret this period as the zero-curtain, during which soil temperatures fluctuate near 0°C while the snowpack ablates. The $T_{\mathrm{B}}^{H}{}_{min}$ within this window reaches 229.0 K on April 22, 2021, at a thermodynamic temperature of 1.6°C, consistent with the GlobSnow SWE estimate reaching 0 mm on April 26, 2021".	—

#	Comment	Response	Manuscript change	Ref.
C1	Conclusions: Scope too broad; 0.15 °C claim unsupported broadly; p. 33, L515 Point 2 not demonstrated; snowmelt dominance not shown; airborne impractical; Moradi et al. (2023) missing.	*Scope:* narrowed to the two study regions and 24 pixel-years analysed; 0.15 °C claim reframed as a challenge to its universal application, not an assertion that it is broadly wrong; *L515 Point 2:* qualified as a future direction rather than a demonstrated result; the present work supports near-real-time access to the thermal coordinate (GEOS-5 T_{eff}/K, already in the SMAP pipeline); *Snow signal:* the snowpack-loss association ($\star$ coinciding with SWE $\to 0$) is visible across the full pixel-year compendium (Appendix A and B); the 2020–21 drought year (Fig. R3b) is included as the counter-case, where a below-normal snowpack and late rainfall drive the minimum instead. A day-gap analysis quantifying the offset between the seasonal T_{B}^{H} minimum and SWE $= 0$ will be added; *Airborne:* replaced with a SMAP Enhanced product; *Moradi et al. (2023):* added as complementary modeling-side context (Discussion and Conclusions).	Conclusions rewritten: geographic scope made explicit (two regions, nine hydrological years / 24 pixel-years); 0.15 °C claim qualified; L515 Point 2 reframed as future work; airborne removed and SMAP Enhanced noted as the higher-resolution path; day-gap analysis to be added; Moradi et al. (2023) cited in Discussion and Conclusions.	D, R3b, App. A, App. B

Response to Dr. Dan R. Glaser (CRREL)

We thank Dr. Glaser for this substantive connection. Garcia and Glaser (2025); Liu et al. (2022) will be cited in Section 4.1 as laboratory-scale mechanistic support for the T_{B}^{H}–T branch separation, alongside the support-mismatch interpretation described in Section E. Peer-reviewed journal publications are cited; poster presentations are not included as references.

Manuscript change: Garcia and Glaser (2025); Liu et al. (2022) added to Section 4.1 as laboratory-scale supporting evidence for the SurFC/SurTC branch structure.

Response Figures

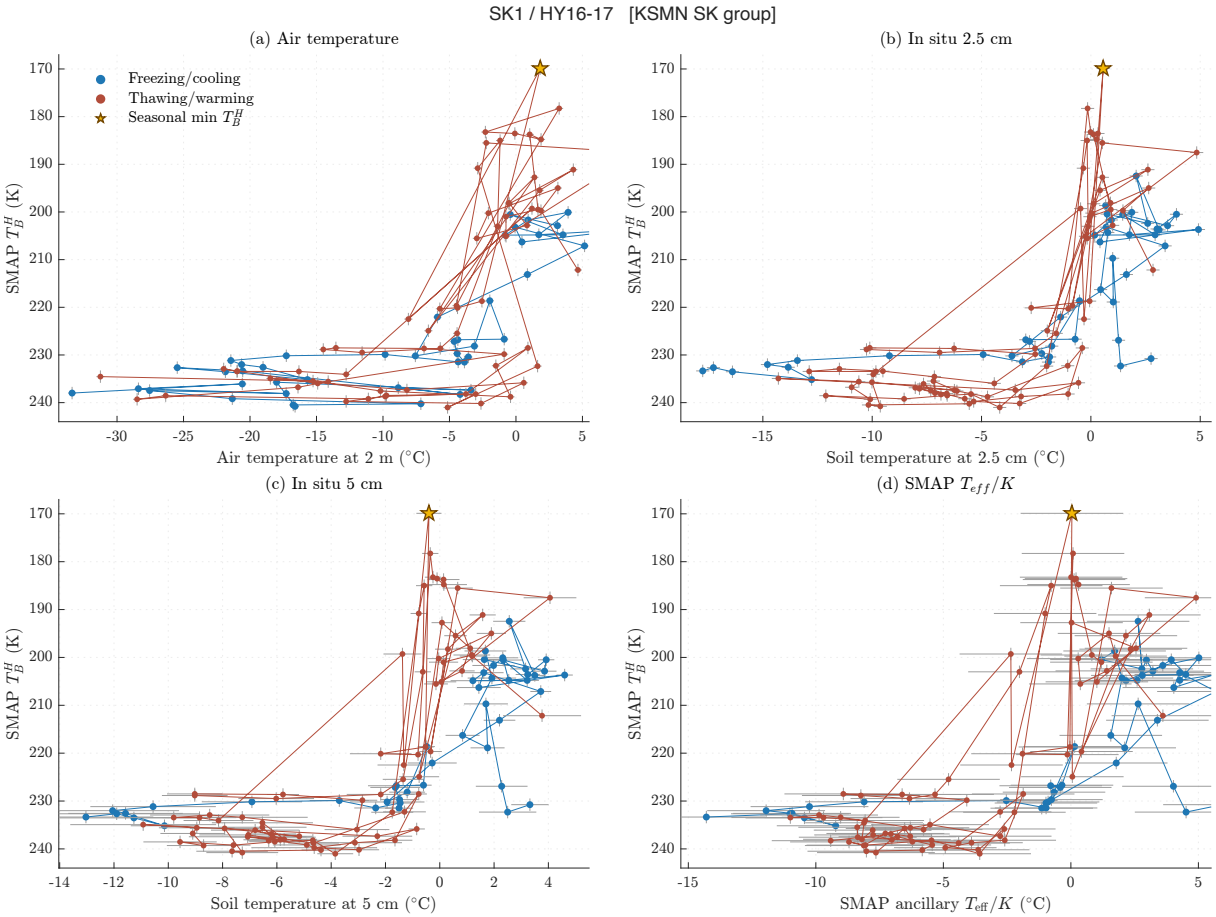

Figure 1: **Figure R1.** Multi-temperature-source SurFC for pixel SK1, hydrological year 2016–17. T_{B}^{H} plotted against: (a) air temperature at 2 m; (b) in situ soil temperature at 2.5 cm; (c) in situ 5 cm; (d) SMAP ancillary T_{eff}/K. Blue = freezing/cooling branch; red = thawing/warming branch; $\star$ = seasonal T_{B}^{H} minimum. Branch structure and hysteresis are visible across all four thermal coordinates; the 5 cm and T_{eff}/K panels (c, d) yield the clearest branch geometry. Horizontal error bars reflect, for each thermal coordinate, the greater of the inter-station spread within the pixel or the instrument uncertainty.

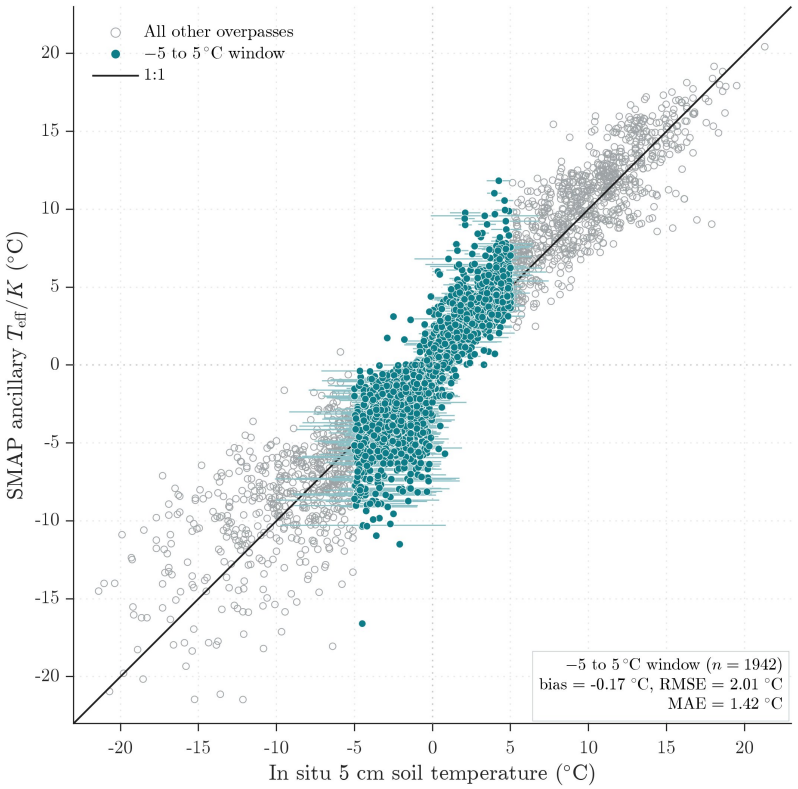

Figure 2: **Figure R2.** SMAP ancillary T_{eff}/K vs. in situ 5 cm soil temperature. Teal points: -5 to $+5\,^{\circ}$C transition window ($n = 1{,}942$; bias $= -0.17\,^{\circ}$C; RMSE $= 2.01\,^{\circ}$C; MAE $= 1.42\,^{\circ}$C). Grey: all other overpasses. Near-zero bias within the transition window is noteworthy given the pixel-to-point support mismatch. The 2.0 °C RMSE is a footprint-vs-point representativeness statistic, it characterizes single-overpass scatter and is not the precision of a derived threshold (the latter is the standard error of the footprint mean, Horizontal error bars reflect, for each thermal coordinate, the greater of the inter-station spread within the pixel or the instrument uncertainty.0.2–0.4 °C; see Part 2, G1).

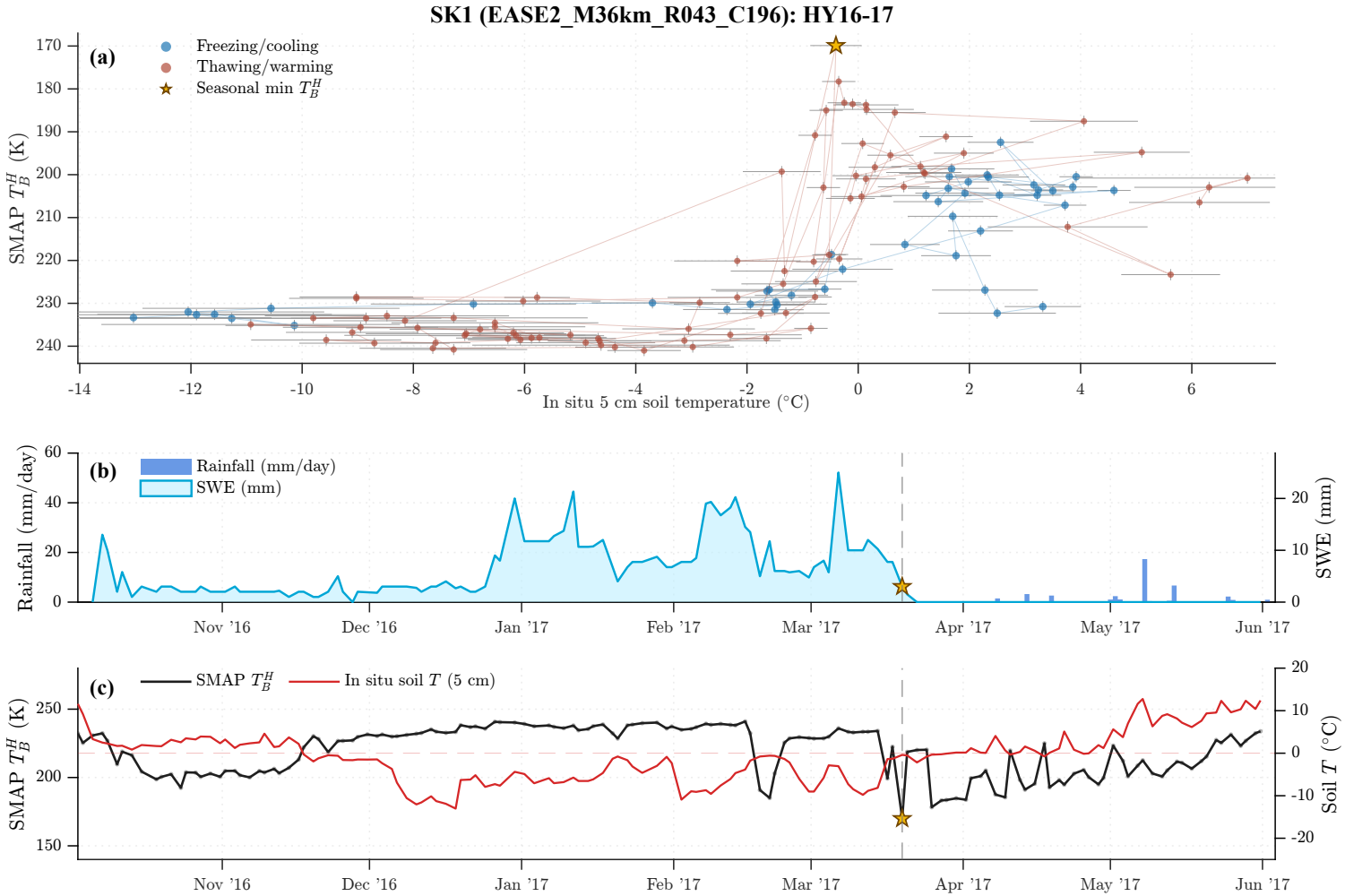

Figure 3: **Figure R3.** Atlas figure: SK1, hydrological year 2016–17 (in situ 5 cm). (a) SurFC scatter; blue = freezing branch, red = thawing branch, ⋆ = seasonal T_{B}^H minimum. (b) Rainfall and GlobSnow SWE time series; ⋆ coincides with SWE → 0 in late March 2017. (c) T_{B}^H and soil temperature time series with ⋆ indicated. This three-panel layout is used throughout the pixel-year compendium.

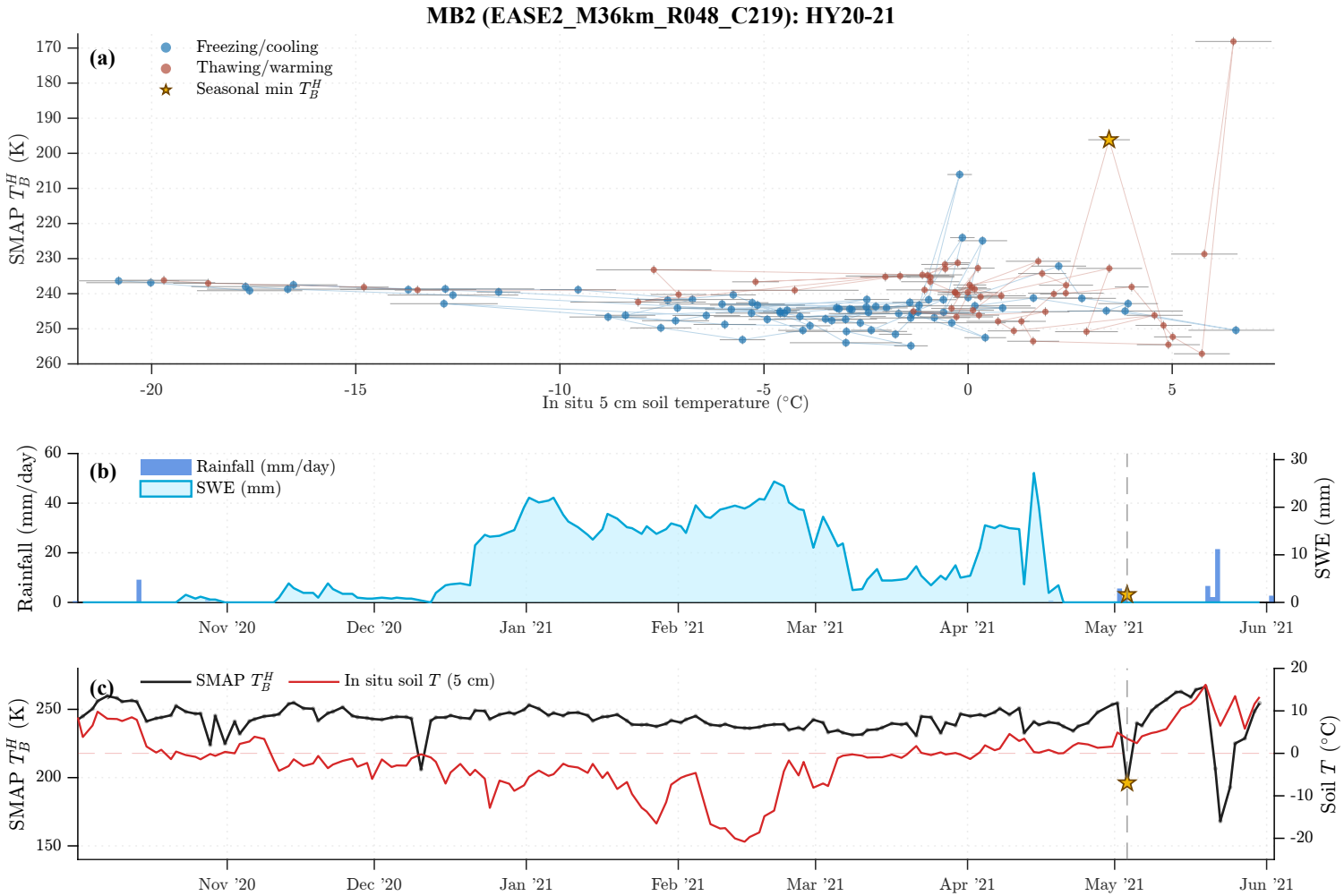

Figure 4: **Figure R3b.** Atlas figure: MB2, hydrological year 2020–21 (in situ 5 cm). The seasonal T_{B}^{H} minimum ($\star$) occurs at soil temperature $\approx$ 5–7 °C in late May 2021, outside the $\pm$5 °C search window. Panel (b) shows a below-normal snowpack (peak SWE $\approx$ 30 mm) and a heavy rainfall event (42 ± 21 mm, 19–22 May 2021) that drove the late T_{B}^{H} depression. In the absence of a substantial snowpack, the method identified a rainfall-driven minimum rather than the snowpack-loss minimum.

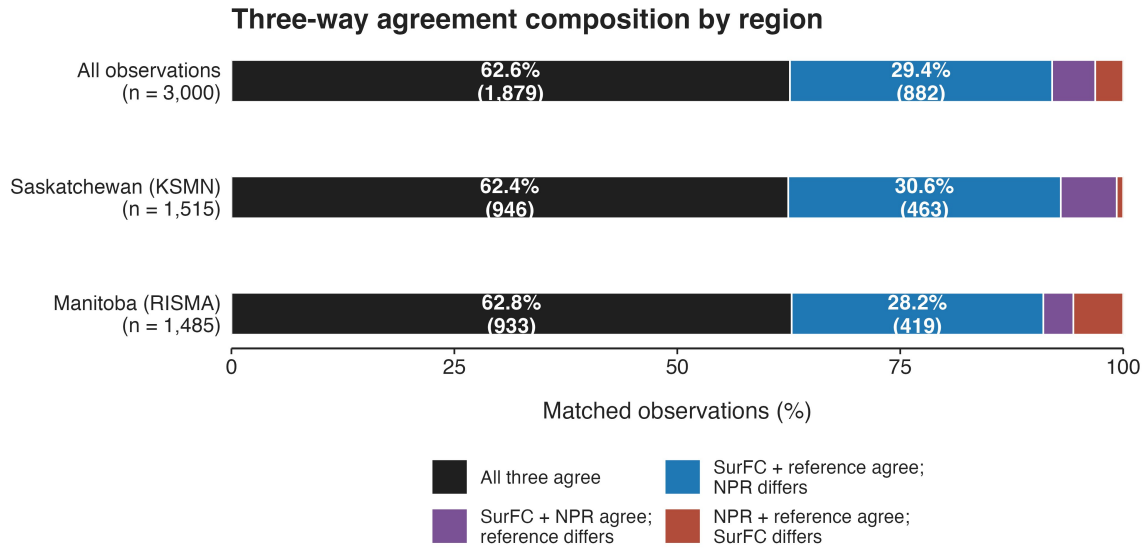

Figure 5: **Figure R4.** Three-way agreement composition by region (n = 3,000 classifier observations; distinct from the n = 1,942 transition-window overpasses in Fig. R2). Black: all three classifiers agree (62.6%). Blue: $T^{H}_{\mathrm{B,min}}$ and in situ temperature reference agree; NPR differs (29.4%). Purple: $T^{H}_{\mathrm{B,min}}$ and NPR agree; temperature reference differs (∼5%). Red: NPR and temperature reference agree; $T^{H}_{\mathrm{B,min}}$ differs (∼3%). This framing replaces the 'gold standard' performance metrics with an honest agreement comparison among three imperfect methods.

Figure 6: **Figure R5.** Study area map showing the Saskatchewan (KSMN) and Manitoba (RISMA) sites. Green rectangles: SMAP 36 km EASE-Grid pixel boundaries for the analysed pixels (SK1–SK4; MB1–MB2). Red dots: in situ soil moisture network stations. Insets show expanded views of each network. Projection: Canada Albers Equal Area Conic (NAD 1983).

References

Bartsch, A., Muri, X., Hetzenecker, M., Rautiainen, K., Bergstedt, H., Wuite, J., Nagler, T., and Nicolsky, D.: Benchmarking passive-microwave-satellite-derived freeze–thaw datasets, The Cryosphere, 19, 459–483, https://doi.org/10.5194/tc-19-459-2025, 2025.

Bergstedt, H., Bartsch, A., Duguay-Tetzlaff, A., Wuite, J., and Nagler, T.: Deriving a frozen area fraction from Metop ASCAT backscatter based on Sentinel-1, IEEE Transactions on Geoscience and Remote Sensing, 58, 6008–6019, https://doi.org/10.1109/TGRS.2020.2967052, 2020.

Garcia, A. and Glaser, D. R.: Sub-freezing complex electrical conductivity hysteresis in frost-susceptible soils, Geophysical Journal International, ggaf335, https://doi.org/10.1093/gji/ggaf335, 2025.

Holmes, T. R., Jackson, T. J., Reichle, R. H., and Basara, J. B.: An assessment of surface soil temperature products from numerical weather prediction models using ground-based measurements, Water Resources Research, 48, https://doi.org/10.1029/2011WR010538, 2012.

Liu, R., Zhu, C., Schmalzel, J., Offenbacker, D., Mehta, Y., Barrowes, B., Glaser, D. R., and Lein, W.: Experimental and numerical analyses of soil electrical resistivity under subfreezing conditions, Journal of Applied Geophysics, 202, 104 671, https://doi.org/10.1016/j.jappgeo.2022.104671, 2022.

Luojus, K., Pulliainen, J., Takala, M., Lemmetyinen, J., and Moisander, M.: GlobSnow v3.0 snow water equivalent (SWE), PANGAEA, https://doi.org/10.1594/PANGAEA.911944, 2020.

Moradi, M., Cho, E., Jacobs, J. M., and Vuyovich, C. M.: Seasonal soil freeze/thaw variability across North America via ensemble land surface modeling, Cold Regions Science and Technology, 209, 103 806, https://doi.org/10.1016/j.coldregions.2023.103806, 2023.

Naeimi, V., Paulik, C., Bartsch, A., Wagner, W., Kidd, R., Park, S.-E., Elger, K., and Boike, J.: ASCAT Surface State Flag (SSF): Extracting Information on Surface Freeze/Thaw Conditions From Backscatter Data Using an Empirical Threshold-Analysis Algorithm, IEEE Transactions on Geoscience and Remote Sensing, 50, 2566–2582, https://doi.org/10.1109/TGRS.2011.2177667, 2012.

O'Neill, P. E., Chan, S., Njoku, E. G., Jackson, T., Bindlish, R., and Chaubell, J.: User Guide: SMAP L3 Radiometer Global Daily 36 km EASE-Grid Soil Moisture, Version 8, Technical report, Jet Propulsion Laboratory, Boulder, CO, 2021.

Pardo Lara, R., Berg, A. A., Warland, J., and Tetlock, E.: In Situ Estimates of Freezing/Melting Point Depression in Agricultural Soils Using Permittivity and Temperature Measurements, Water Resources Research, 56, e2019WR026 020, https://doi.org/10.1029/2019WR026020, 2020.

Pardo Lara, R., Berg, A. A., Warland, J., and Parkin, G. W.: Implications of measurement metrics on soil freezing curves: A simulation of freeze–thaw hysteresis, Hydrological Processes, 35, e14 269, https://doi.org/10.1002/hyp.14269, 2021.

Pulliainen, J., Luojus, K., Derksen, C., Mudryk, L., Lemmetyinen, J., Salminen, M., Ikonen, J., Takala, M., Cohen, J., Smolander, T., and Norberg, J.: Patterns and trends of Northern Hemisphere snow mass from 1980 to 2018, Nature, 581, 294–298, https://doi.org/10.1038/s41586-020-2258-0, 2020.

Ramage, J. M. and Isacks, B. L.: Determination of melt-onset and refreeze timing on southeast Alaskan icefields using SSM/I diurnal amplitude variations, Annals of Glaciology, 34, 391–398, https://doi.org/10.3189/172756402781817761, 2002.

Salmabadi, H., Pardo Lara, R., Berg, A., Mavrovic, A., Hanes, C., Montpetit, B., and Roy, A.: In situ monitoring of seasonally frozen ground using soil freezing characteristic curve in permittivity–temperature space, The Cryosphere, 20, 1635–1654, https://doi.org/10.5194/tc-20-1635-2026, 2026.

Vermeesch, P.: IsoplotR: A free and open toolbox for geochronology, Geoscience Frontiers, 9, 1479–1493, https://doi.org/10.1016/j.gsf.2018.04.001, 2018.

Willmes, S., Haas, C., Nicolaus, M., and Bareiss, J.: Satellite microwave observations of the interannual variability of snowmelt on sea ice in the Southern Ocean, Journal of Geophysical Research: Oceans, 114, C03 006, https://doi.org/10.1029/2008JC004919, 2009.

A Appendix A: Saskatchewan (KSMN) Pixel-Year Compendium

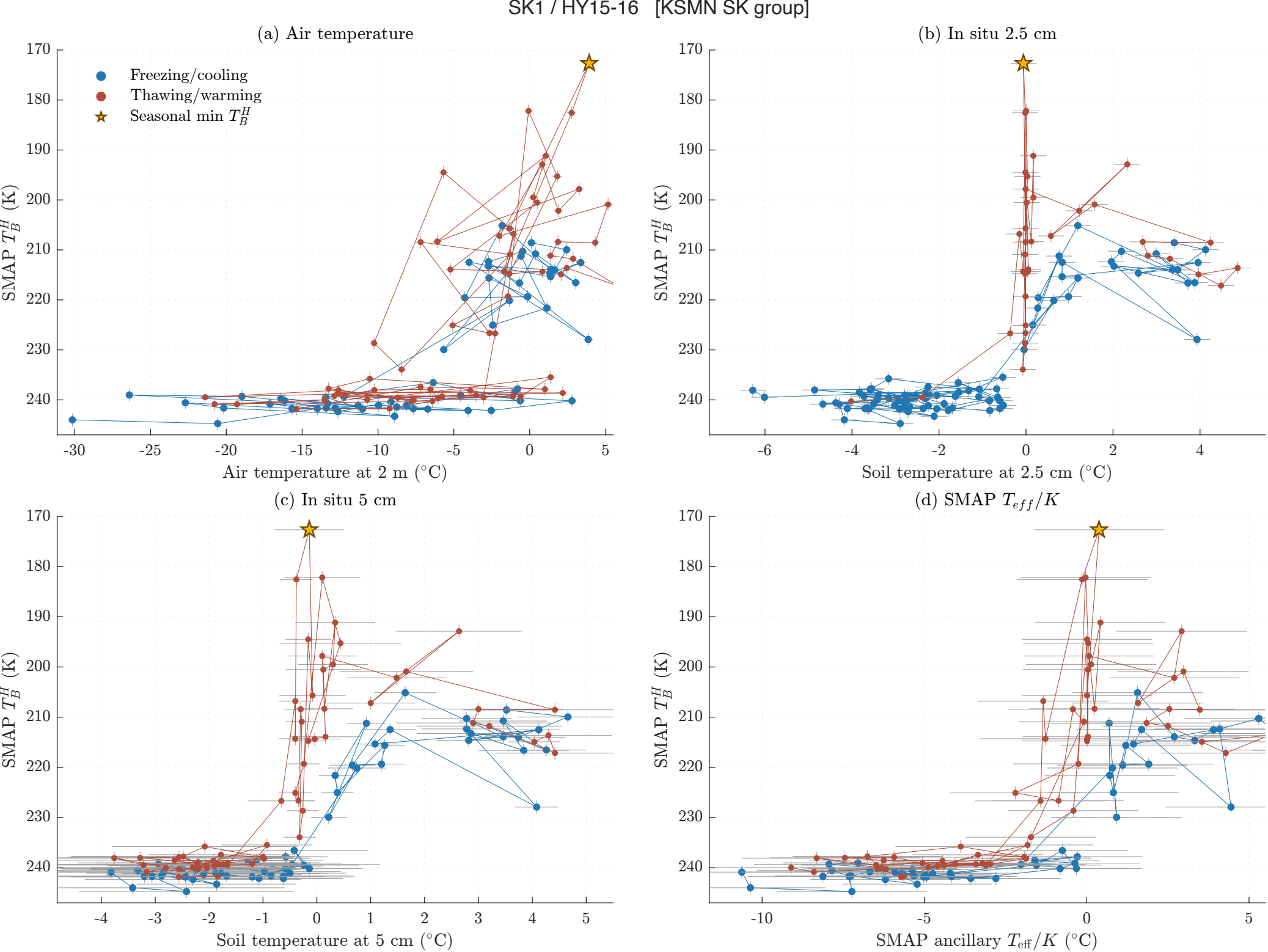
SK1 / HY15-16 [KSMN SK group]
(a) Air temperature
(b) In situ 2.5 cm
(c) In situ 5 cm
(d) SMAP T_{eff}/K
Freezing/cooling
Thawing/warming
Seasonal min T_B^H
SMAP T_B^H (K)
Air temperature at 2 m (°C)
Soil temperature at 2.5 cm (°C)
Soil temperature at 5 cm (°C)
SMAP ancillary T_{eff}/K (°C)

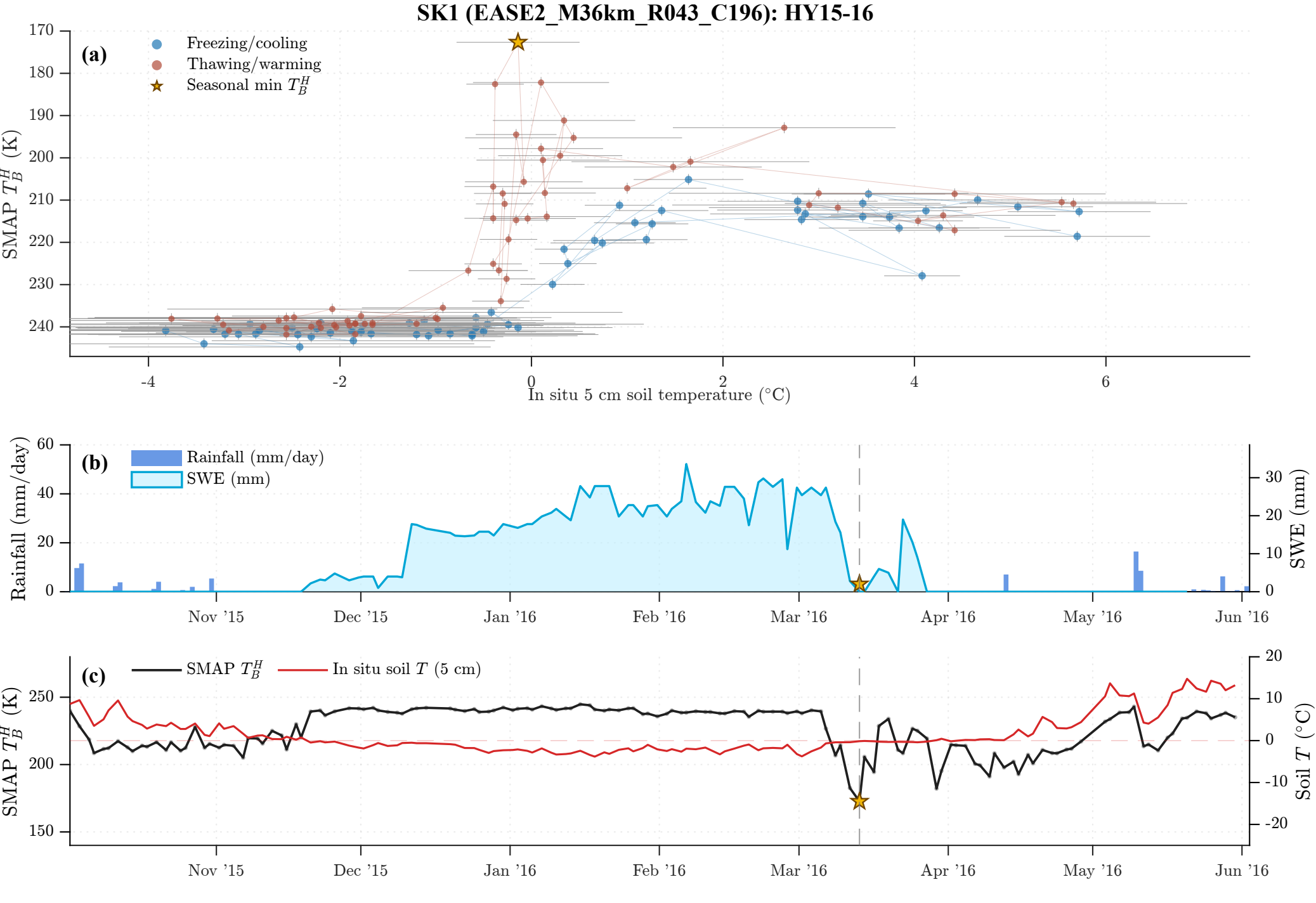
SK1 (EASE2_M36km_R043_C196): HY15-16
(a)
Freezing/cooling
Thawing/warming
Seasonal min T_B^H
SMAP T_B^H (K)
In situ 5 cm soil temperature (°C)
(b)
Rainfall (mm/day)
SWE (mm)
Nov '15
Dec '15
Jan '16
Feb '16
Mar '16
Apr '16
May '16
Jun '16
(c)
SMAP T_B^H
In situ soil T (5 cm)
Soil T (°C)

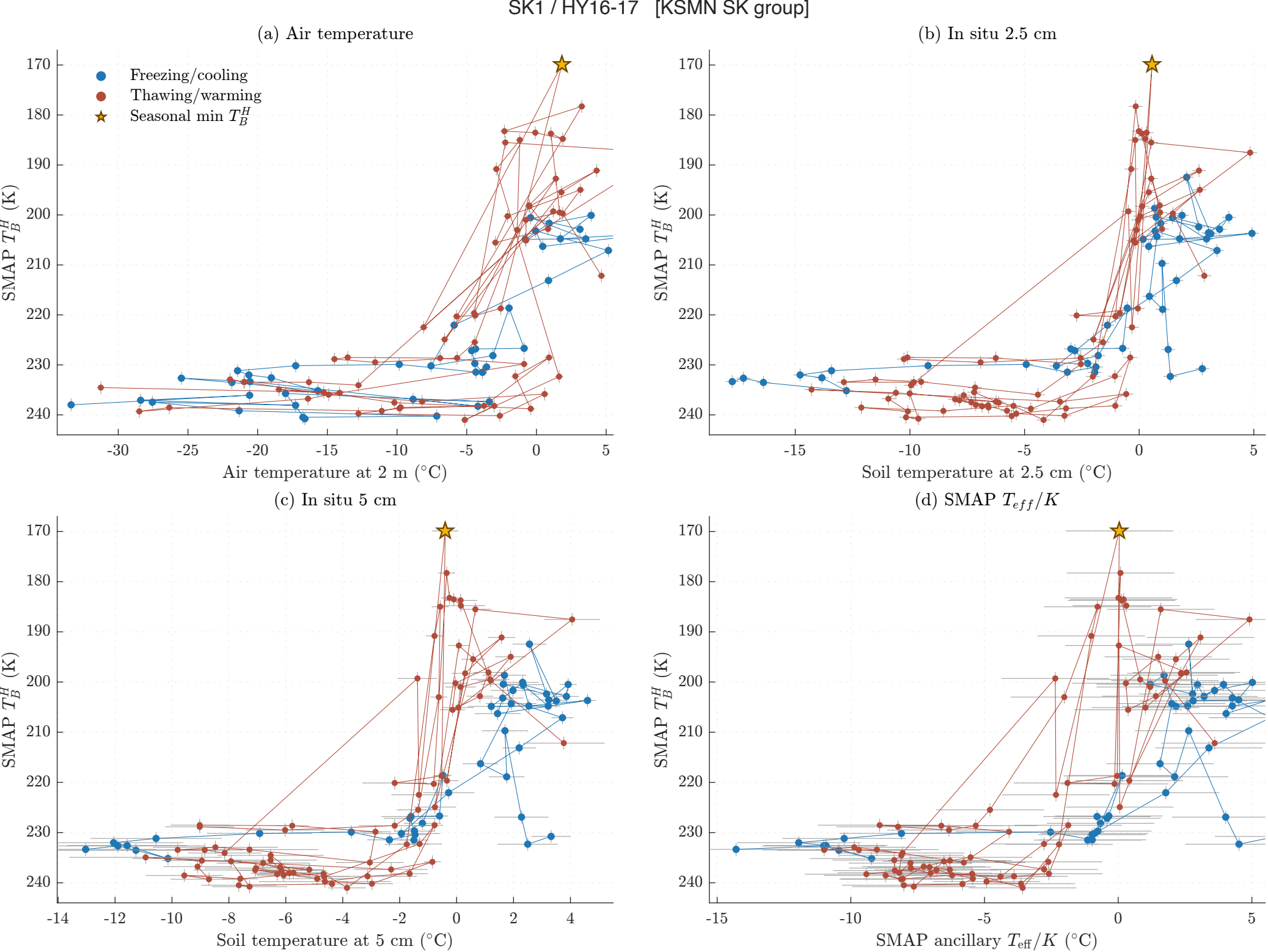
SK1 / HY16-17 [KSMN SK group]
(a) Air temperature
(b) In situ 2.5 cm
(c) In situ 5 cm
(d) SMAP T_{eff}/K
Freezing/cooling
Thawing/warming
Seasonal min T_B^H
SMAP T_B^H (K)
Air temperature at 2 m (°C)
Soil temperature at 2.5 cm (°C)
Soil temperature at 5 cm (°C)
SMAP ancillary T_{eff}/K (°C)

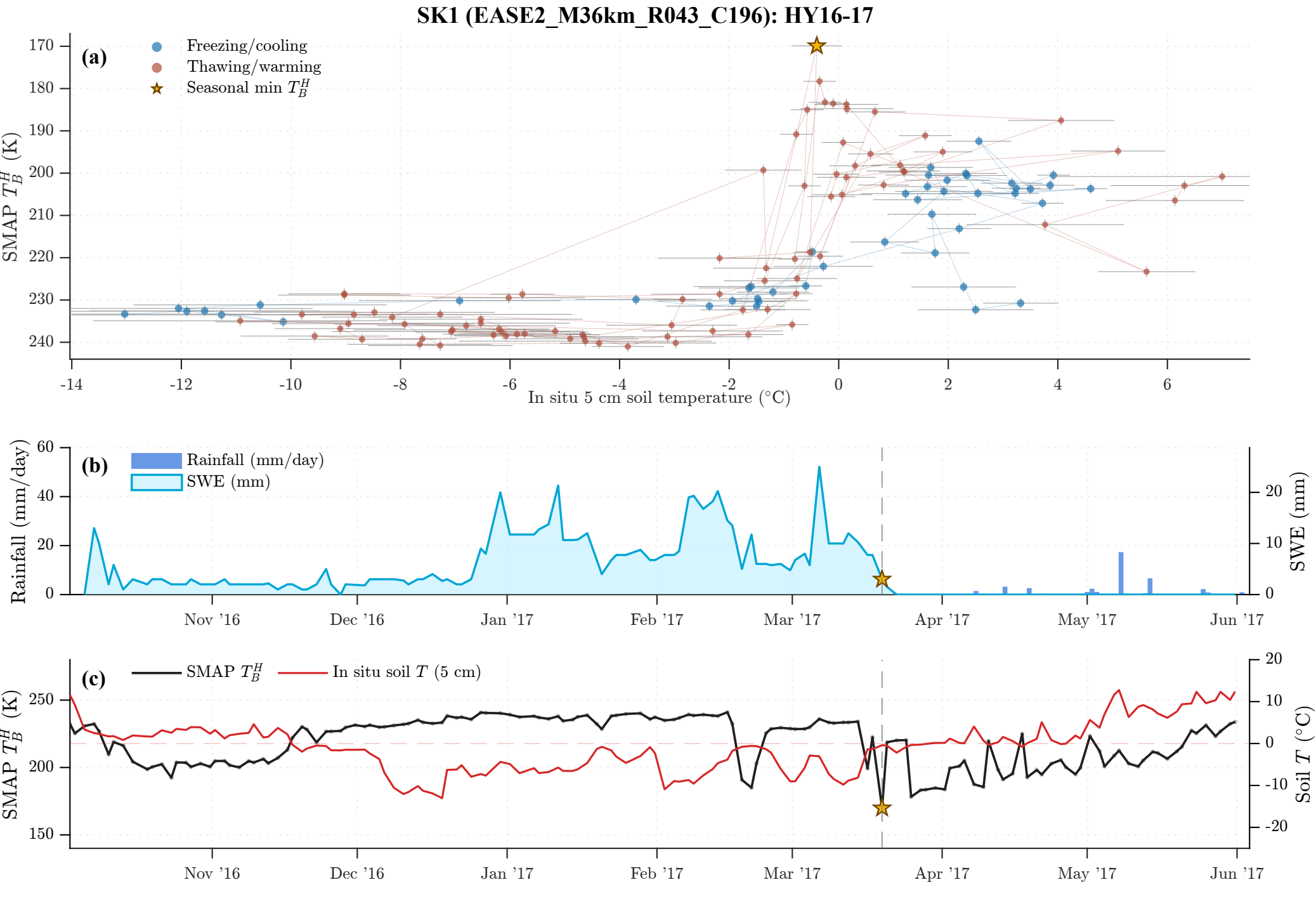
SK1 (EASE2_M36km_R043_C196): HY16-17
(a)
Freezing/cooling
Thawing/warming
Seasonal min T_B^H
SMAP T_B^H (K)
In situ 5 cm soil temperature (°C)
(b)
Rainfall (mm/day)
SWE (mm)
Rainfall (mm/day)
SWE (mm)
Nov '16
Dec '16
Jan '17
Feb '17
Mar '17
Apr '17
May '17
Jun '17
(c)
SMAP T_B^H
In situ soil T (5 cm)
SMAP T_B^H (K)
Soil T (°C)

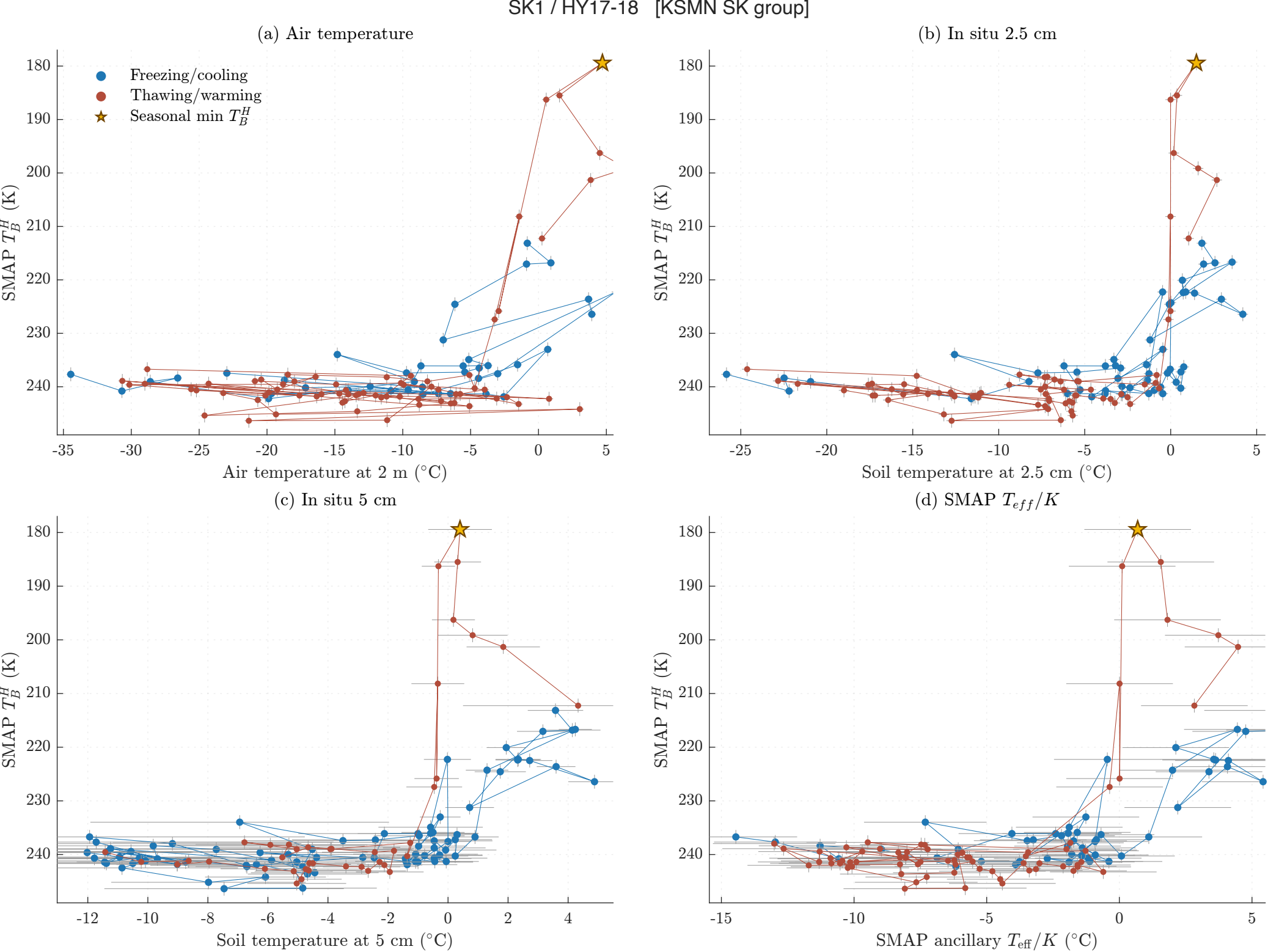
SK1 / HY17-18 [KSMN SK group]
(a) Air temperature
(b) In situ 2.5 cm
(c) In situ 5 cm
(d) SMAP T_{eff}/K
Freezing/cooling
Thawing/warming
Seasonal min T_B^H
SMAP T_B^H (K)
Air temperature at 2 m (°C)
Soil temperature at 2.5 cm (°C)
Soil temperature at 5 cm (°C)
SMAP ancillary T_{eff}/K (°C)

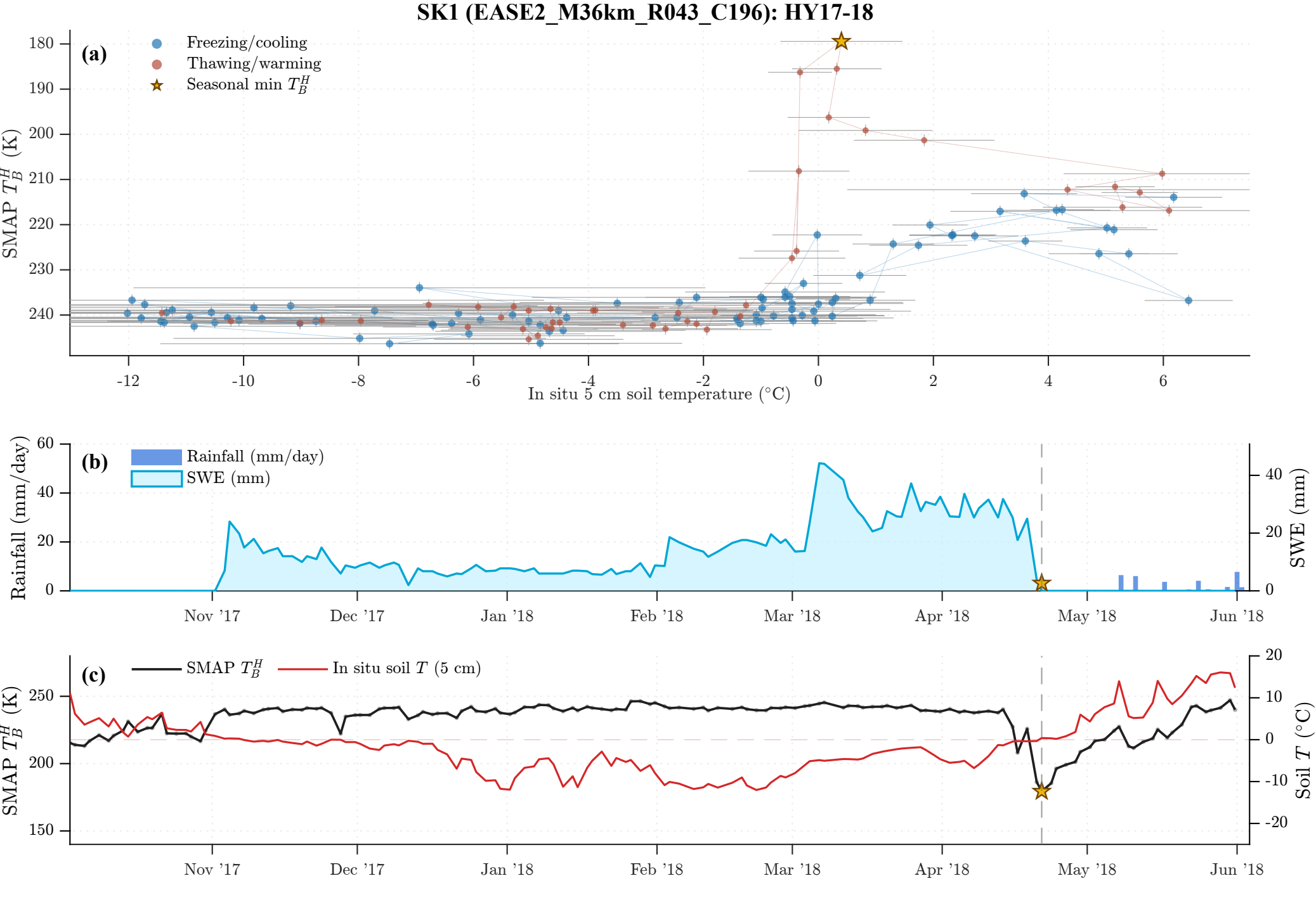
SK1 (EASE2_M36km_R043_C196): HY17-18
(a)
Freezing/cooling
Thawing/warming
Seasonal min T_B^H
SMAP T_B^H (K)
In situ 5 cm soil temperature (°C)
(b)
Rainfall (mm/day)
SWE (mm)
Nov '17
Dec '17
Jan '18
Feb '18
Mar '18
Apr '18
May '18
Jun '18
(c)
SMAP T_B^H
In situ soil T (5 cm)
Soil T (°C)

SK2 / HY15-16 [KSMN SK group]
(a) Air temperature
No data
(b) In situ 2.5 cm
No data
(c) In situ 5 cm
Freezing/cooling
Thawing/warming
Seasonal min T_B^H
SMAP T_B^H (K)
Soil temperature at 5 cm (°C)
(d) SMAP T_{eff}/K
SMAP T_B^H (K)
SMAP ancillary T_{eff}/K (°C)

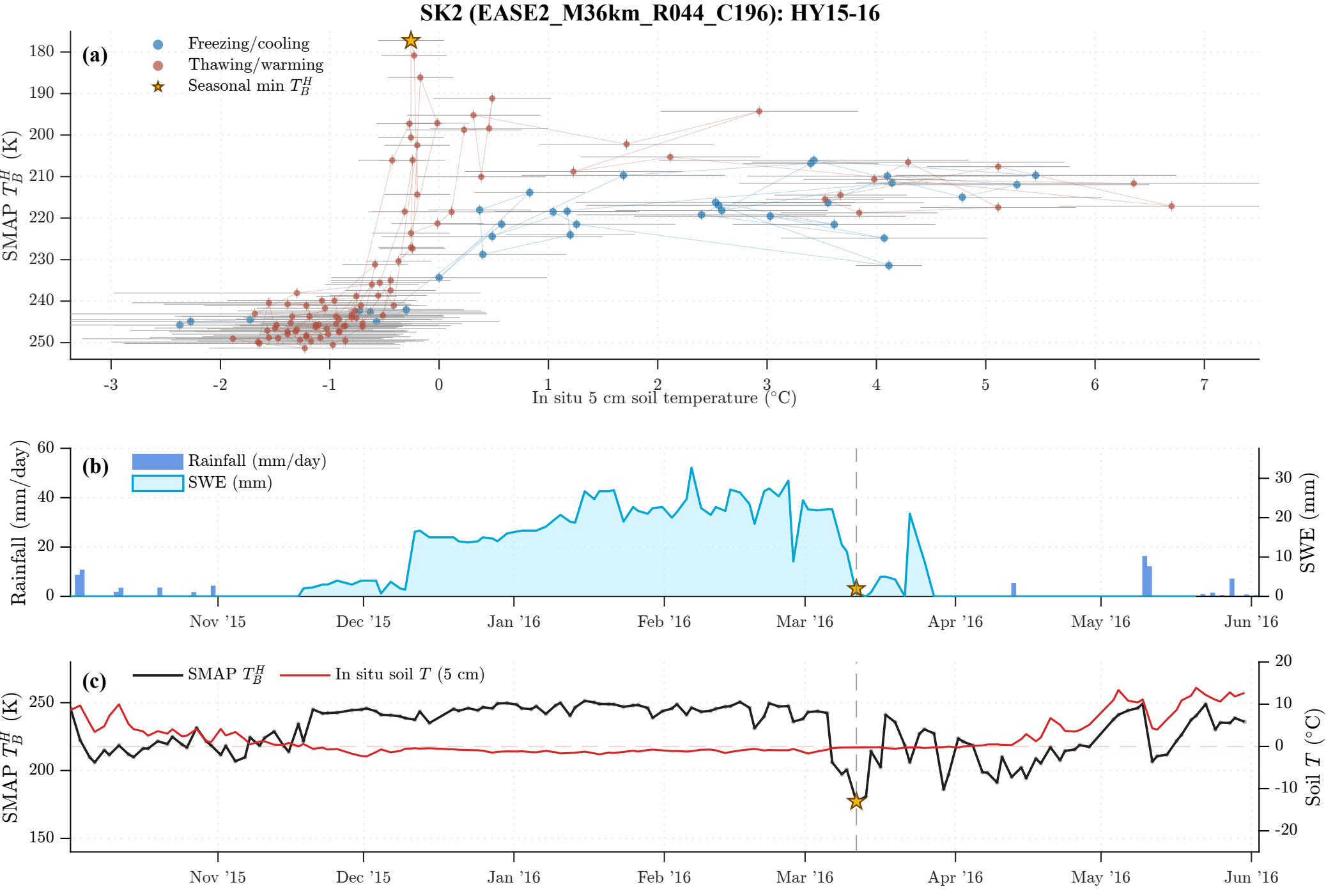
SK2 (EASE2_M36km_R044_C196): HY15-16
(a)
Freezing/cooling
Thawing/warming
Seasonal min T_B^H
SMAP T_B^H (K)
In situ 5 cm soil temperature (°C)
(b)
Rainfall (mm/day)
SWE (mm)
Nov '15
Dec '15
Jan '16
Feb '16
Mar '16
Apr '16
May '16
Jun '16
(c)
SMAP T_B^H
In situ soil T (5 cm)
Soil T (°C)

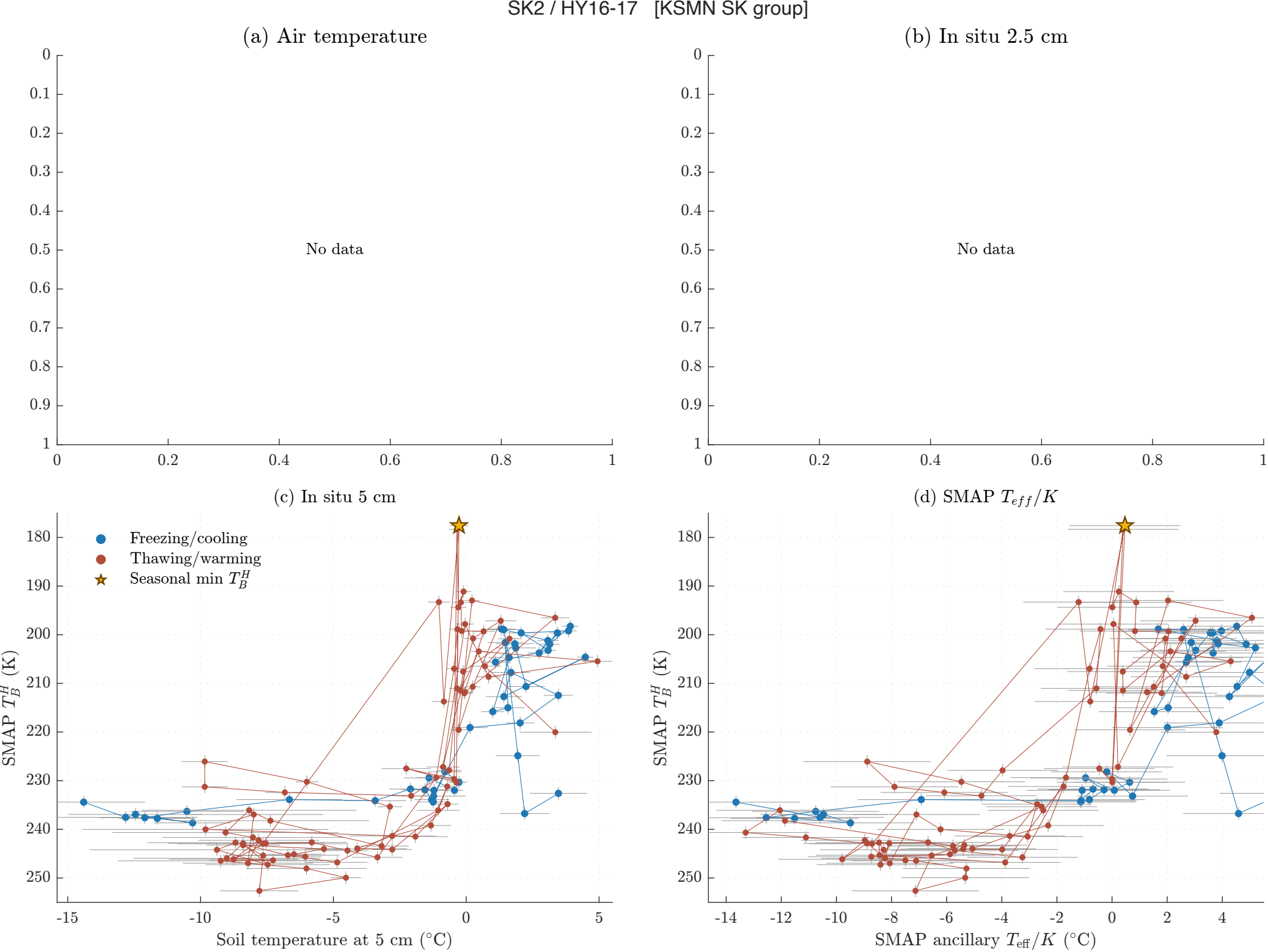
SK2 / HY16-17 [KSMN SK group]
(a) Air temperature
No data
(b) In situ 2.5 cm
No data
(c) In situ 5 cm
Freezing/cooling
Thawing/warming
Seasonal min T_B^H
SMAP T_B^H (K)
Soil temperature at 5 cm (°C)
(d) SMAP T_{eff}/K
SMAP T_B^H (K)
SMAP ancillary T_{eff}/K (°C)

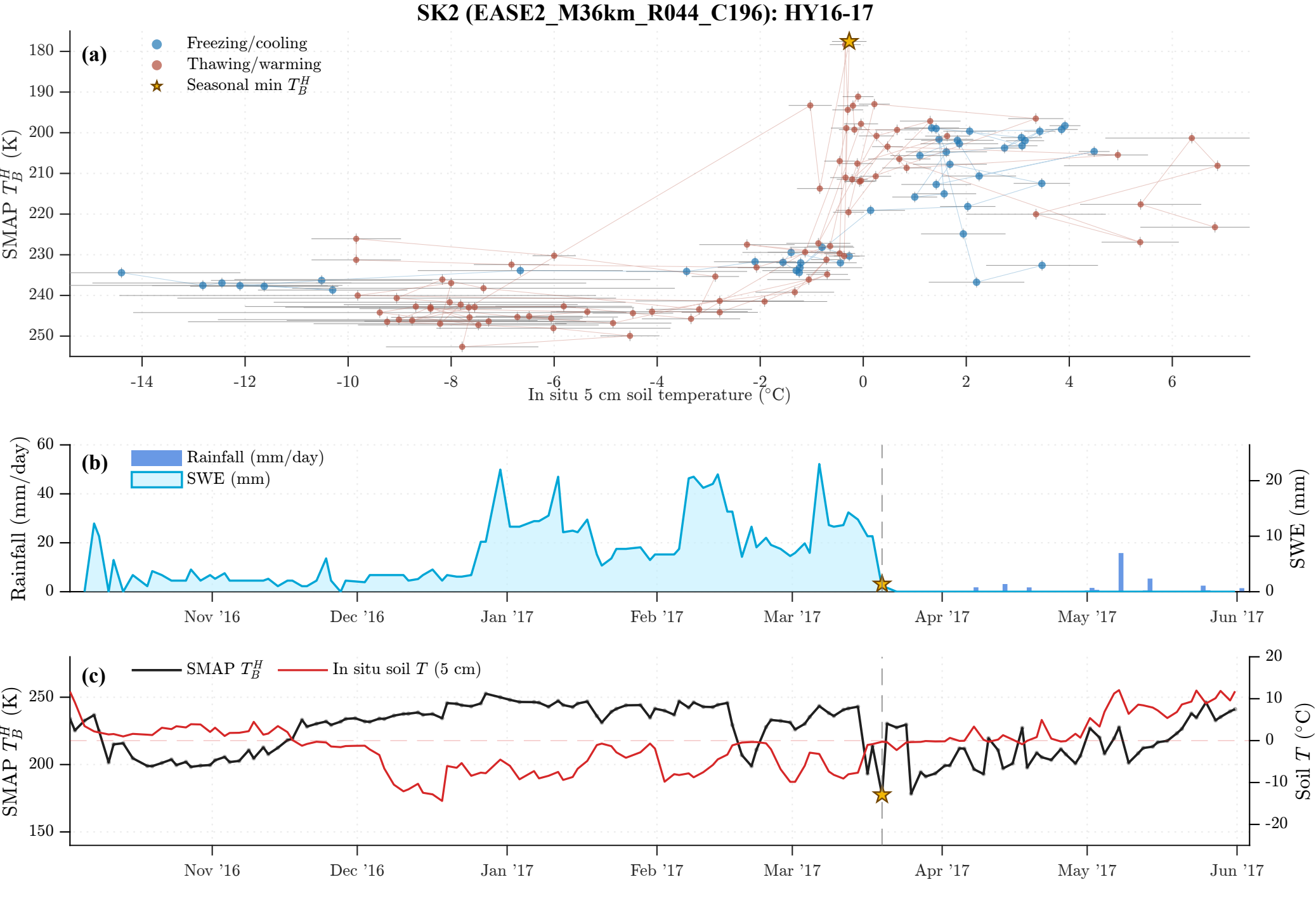
SK2 (EASE2_M36km_R044_C196): HY16-17
(a)
Freezing/cooling
Thawing/warming
Seasonal min T_B^H
SMAP T_B^H (K)
In situ 5 cm soil temperature (°C)
(b)
Rainfall (mm/day)
SWE (mm)
Nov '16
Dec '16
Jan '17
Feb '17
Mar '17
Apr '17
May '17
Jun '17
(c)
SMAP T_B^H
In situ soil T (5 cm)
Soil T (°C)

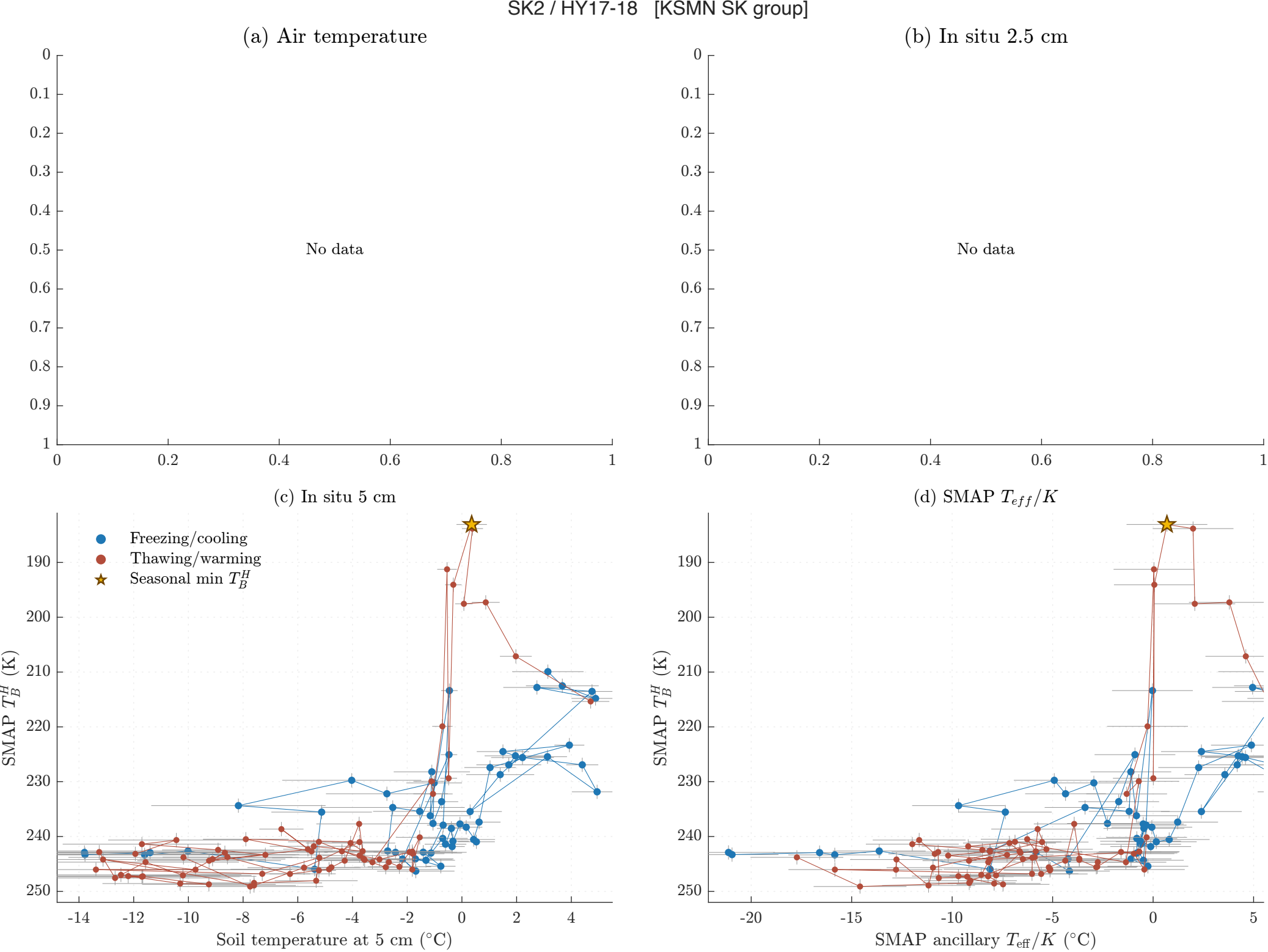
(a) Air temperature
No data
(b) In situ 2.5 cm
No data
(c) In situ 5 cm
Freezing/cooling
Thawing/warming
Seasonal min T_B^H
SMAP T_B^H (K)
Soil temperature at 5 cm (°C)
(d) SMAP T_{eff}/K
SMAP T_B^H (K)
SMAP ancillary T_{eff}/K (°C)

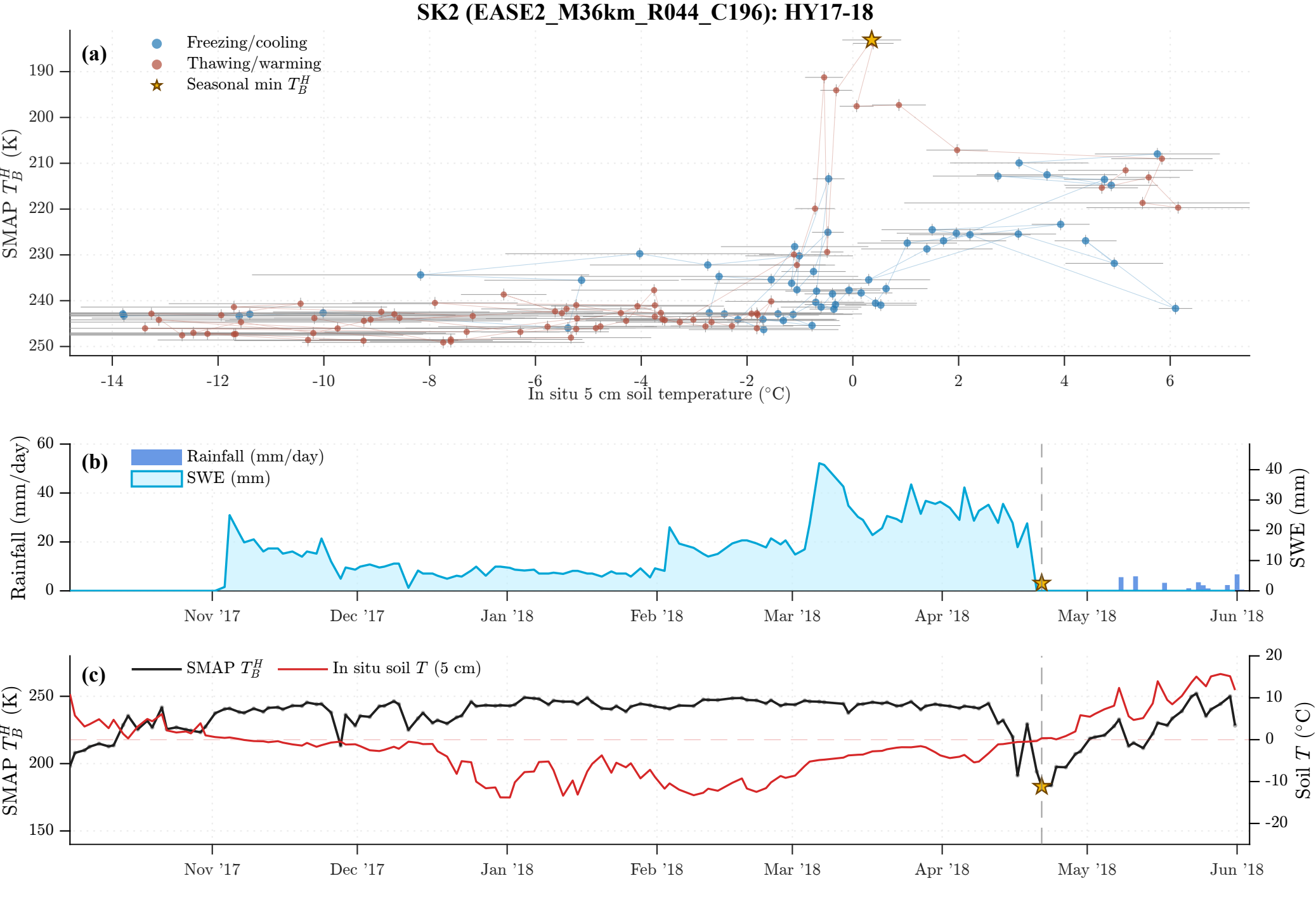
SK2 (EASE2_M36km_R044_C196): HY17-18
(a)
Freezing/cooling
Thawing/warming
Seasonal min T_B^H
SMAP T_B^H (K)
In situ 5 cm soil temperature (°C)
(b)
Rainfall (mm/day)
SWE (mm)
Nov '17
Dec '17
Jan '18
Feb '18
Mar '18
Apr '18
May '18
Jun '18
(c)
SMAP T_B^H
In situ soil T (5 cm)
Soil T (°C)

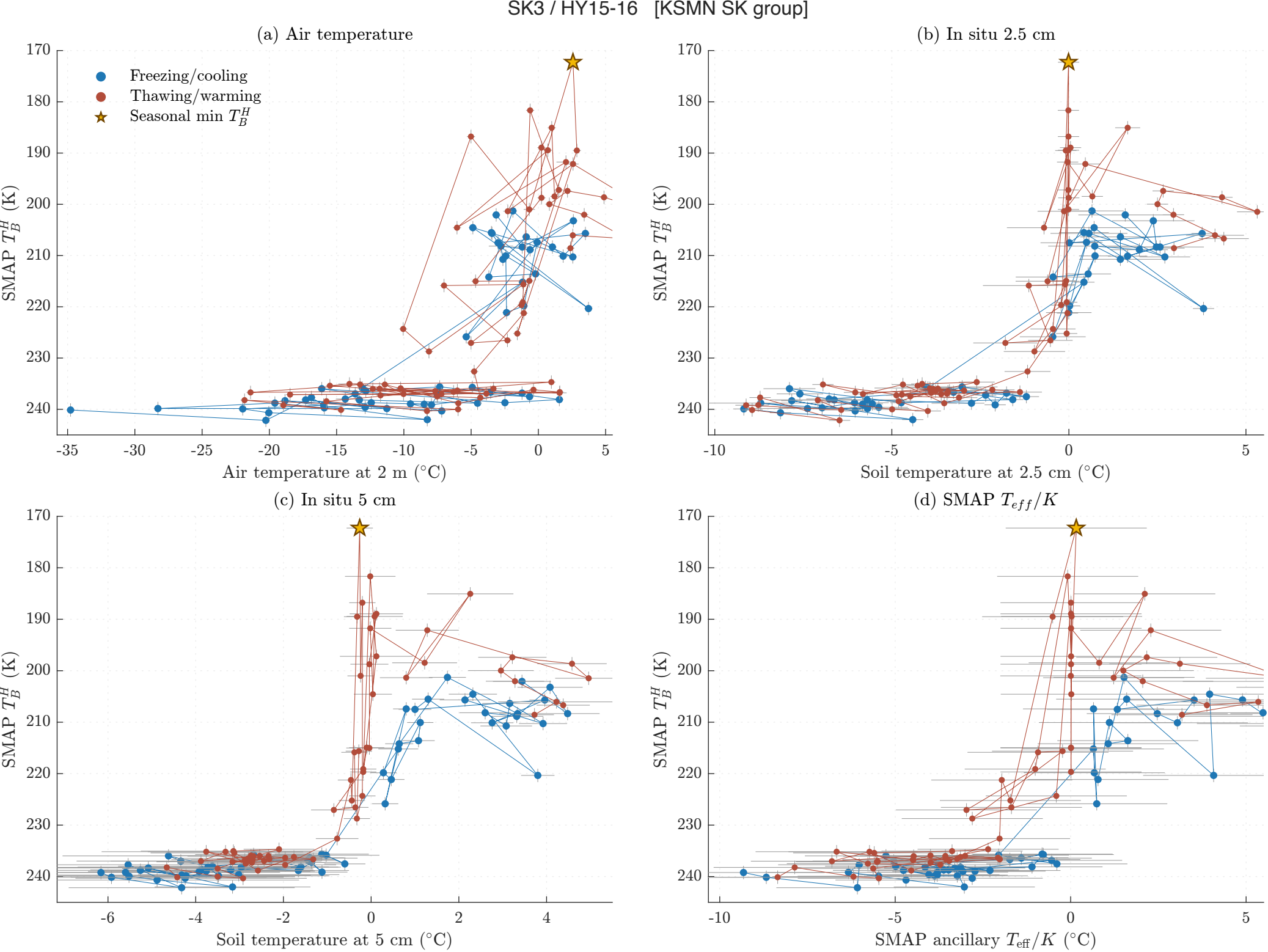
SK3 / HY15-16 [KSMN SK group]
(a) Air temperature
(b) In situ 2.5 cm
(c) In situ 5 cm
(d) SMAP T_{eff}/K
Freezing/cooling
Thawing/warming
Seasonal min T_B^H
SMAP T_B^H (K)
Air temperature at 2 m (°C)
Soil temperature at 2.5 cm (°C)
Soil temperature at 5 cm (°C)
SMAP ancillary T_{eff}/K (°C)

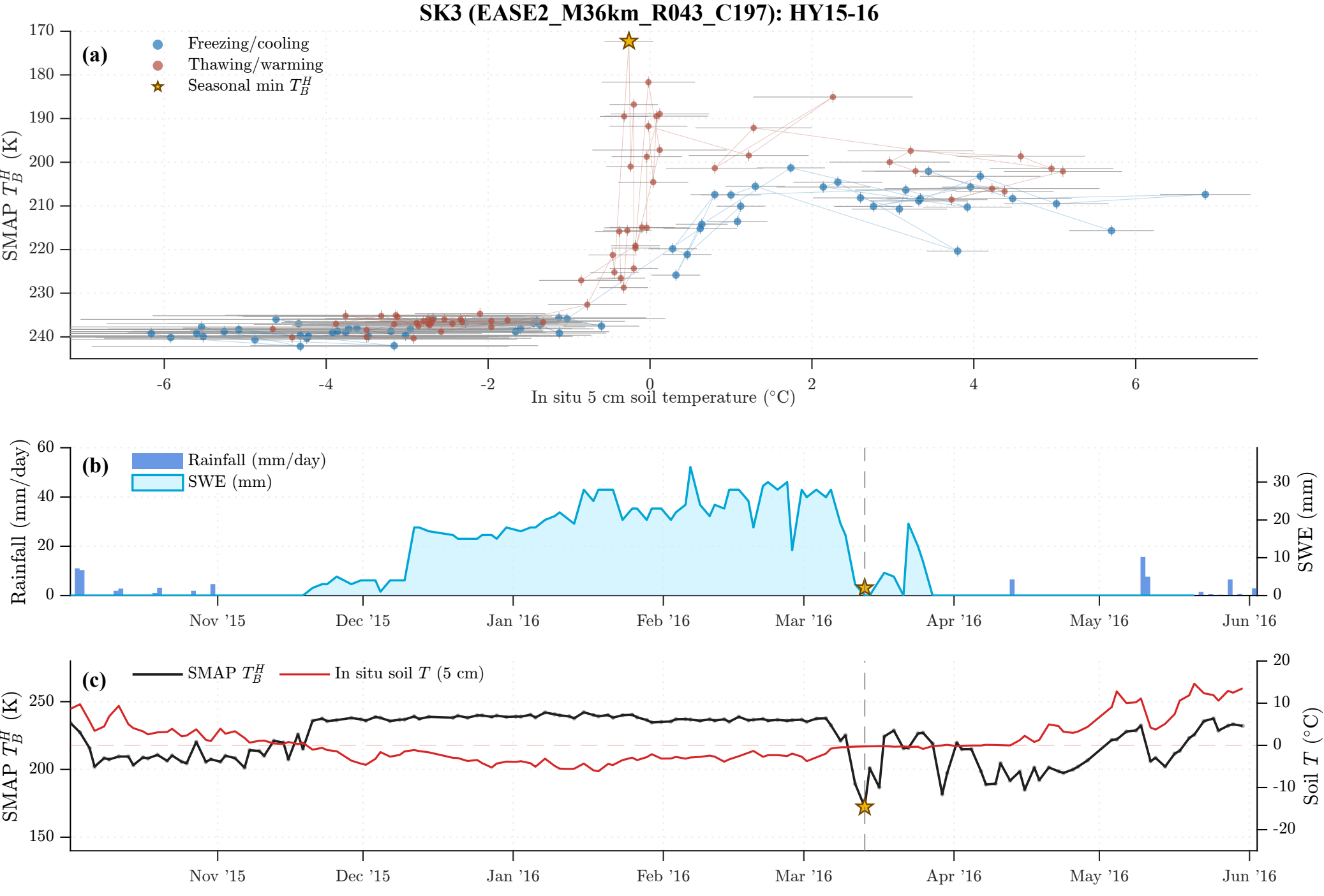
SK3 (EASE2_M36km_R043_C197): HY15-16
(a)
Freezing/cooling
Thawing/warming
Seasonal min T_B^H
SMAP T_B^H (K)
In situ 5 cm soil temperature (°C)
(b)
Rainfall (mm/day)
SWE (mm)
Nov '15
Dec '15
Jan '16
Feb '16
Mar '16
Apr '16
May '16
Jun '16
(c)
SMAP T_B^H
In situ soil T (5 cm)
Soil T (°C)

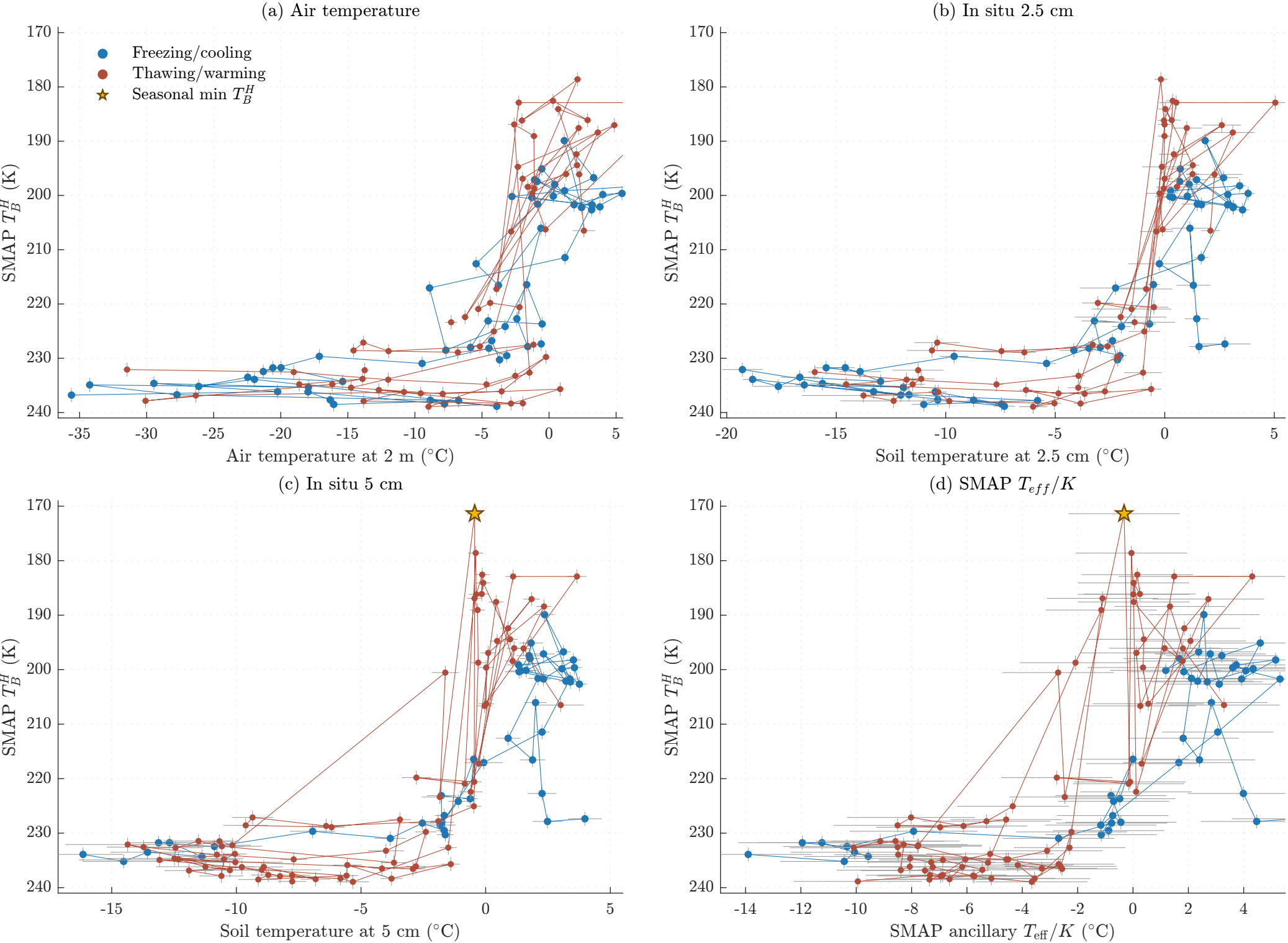
(a) Air temperature
(b) In situ 2.5 cm
(c) In situ 5 cm
(d) SMAP T_{eff}/K
Freezing/cooling
Thawing/warming
Seasonal min T_B^H
SMAP T_B^H (K)
Air temperature at 2 m (°C)
Soil temperature at 2.5 cm (°C)
Soil temperature at 5 cm (°C)
SMAP ancillary T_{eff}/K (°C)

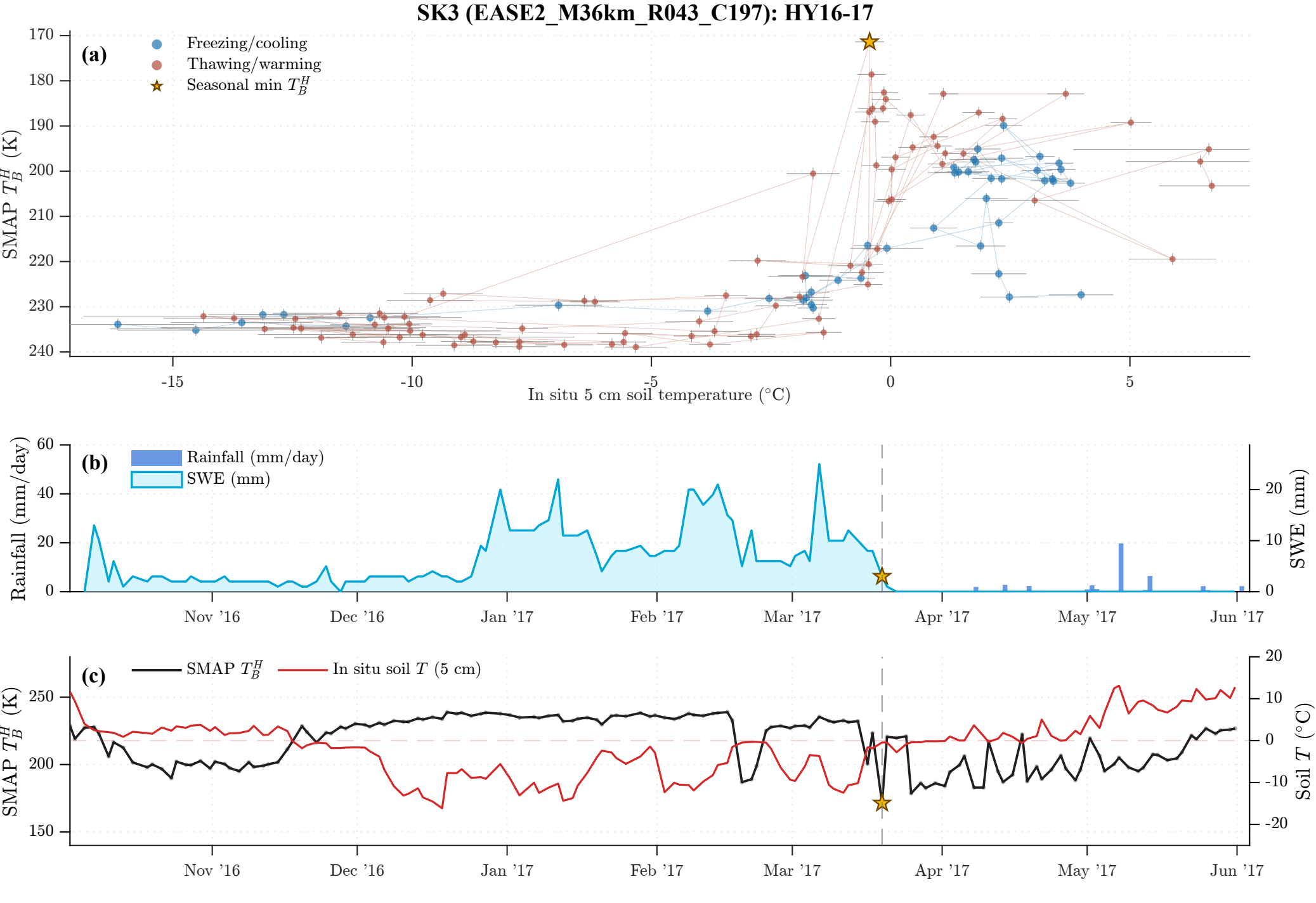
SK3 (EASE2_M36km_R043_C197): HY16-17
(a)
Freezing/cooling
Thawing/warming
Seasonal min T_B^H
SMAP T_B^H (K)
In situ 5 cm soil temperature (°C)
(b)
Rainfall (mm/day)
SWE (mm)
Nov '16
Dec '16
Jan '17
Feb '17
Mar '17
Apr '17
May '17
Jun '17
(c)
SMAP T_B^H
In situ soil T (5 cm)
Soil T (°C)

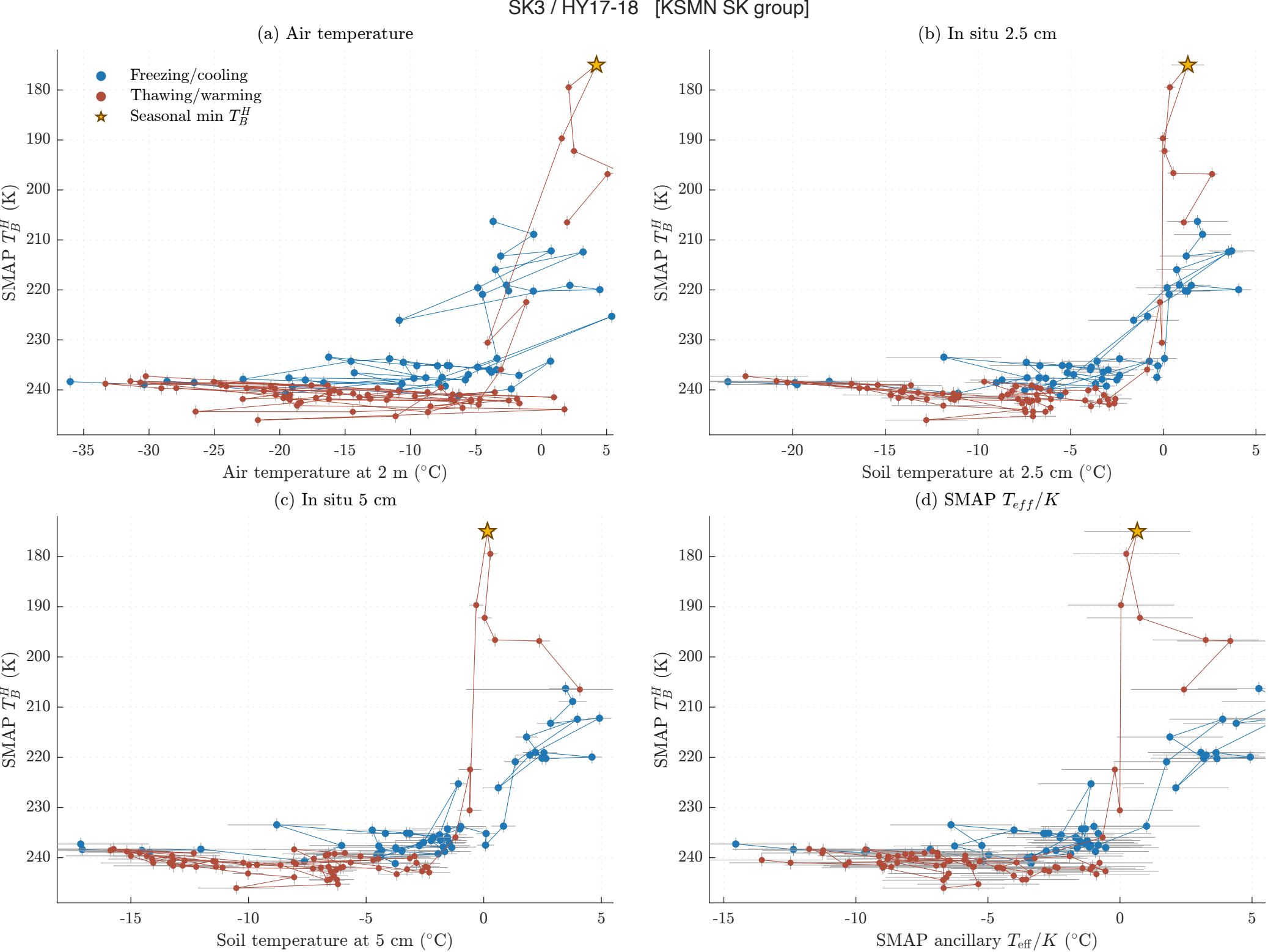
SK3 / HY17-18 [KSMN SK group]
(a) Air temperature
(b) In situ 2.5 cm
(c) In situ 5 cm
(d) SMAP T_{eff}/K
Freezing/cooling
Thawing/warming
Seasonal min T_B^H
SMAP T_B^H (K)
Air temperature at 2 m (°C)
Soil temperature at 2.5 cm (°C)
Soil temperature at 5 cm (°C)
SMAP ancillary T_{eff}/K (°C)

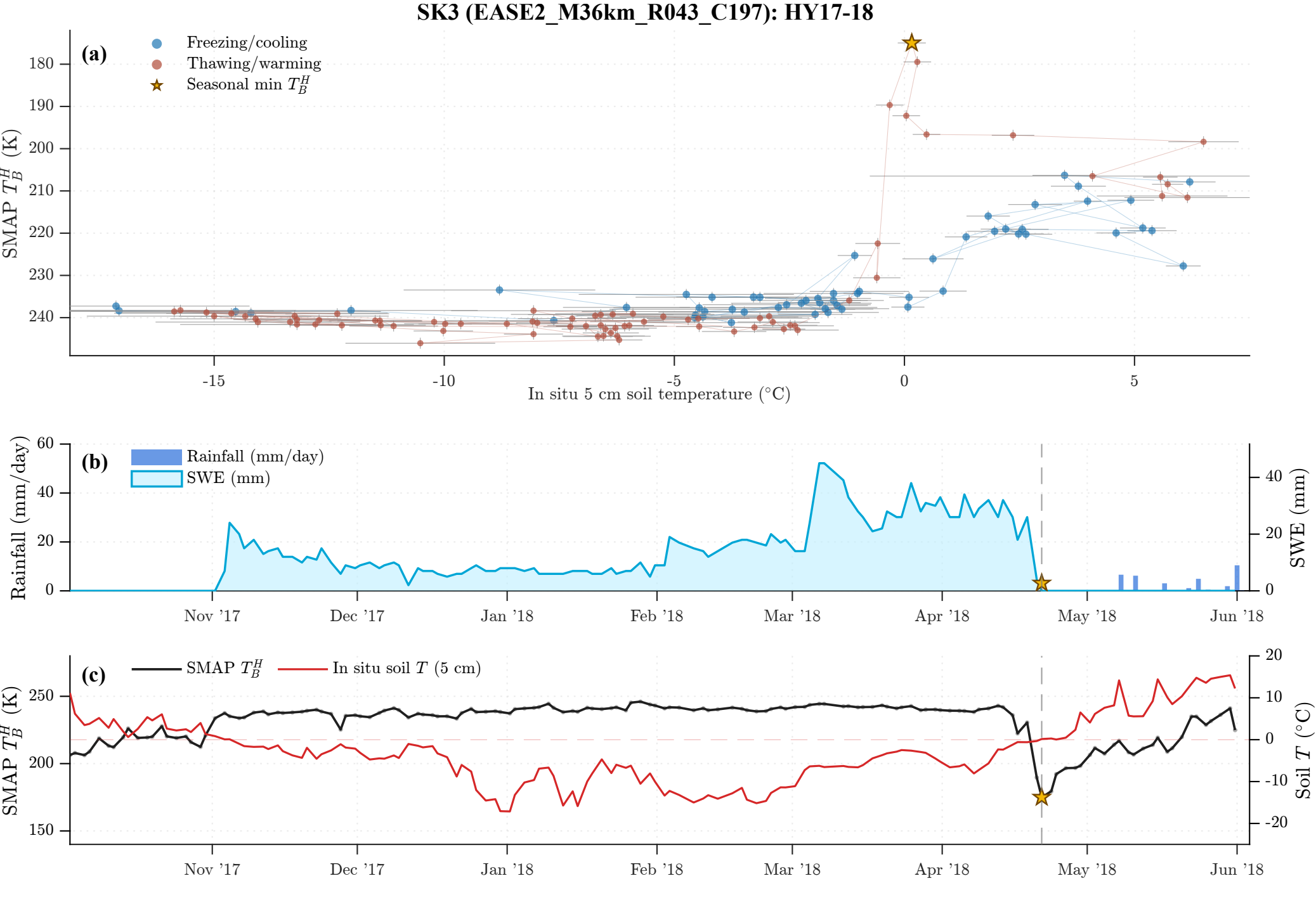
SK3 (EASE2_M36km_R043_C197): HY17-18
(a)
Freezing/cooling
Thawing/warming
Seasonal min T_B^H
SMAP T_B^H (K)
In situ 5 cm soil temperature (°C)
(b)
Rainfall (mm/day)
SWE (mm)
Nov '17
Dec '17
Jan '18
Feb '18
Mar '18
Apr '18
May '18
Jun '18
(c)
SMAP T_B^H
In situ soil T (5 cm)
Soil T (°C)

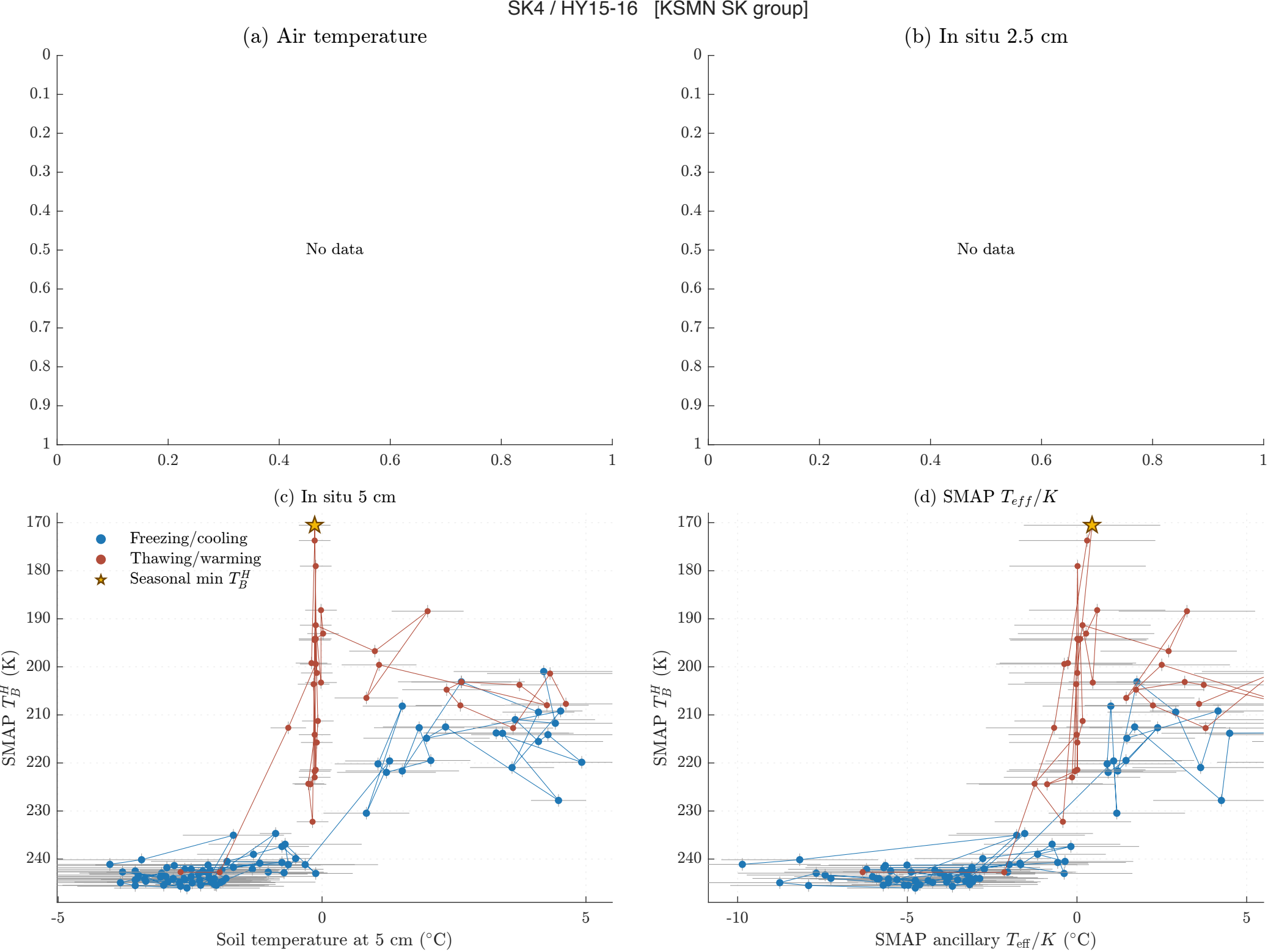
(a) Air temperature
No data
(b) In situ 2.5 cm
No data
(c) In situ 5 cm
Freezing/cooling
Thawing/warming
Seasonal min T_B^H
SMAP T_B^H (K)
Soil temperature at 5 cm (°C)
(d) SMAP T_{eff}/K
SMAP T_B^H (K)
SMAP ancillary T_{eff}/K (°C)

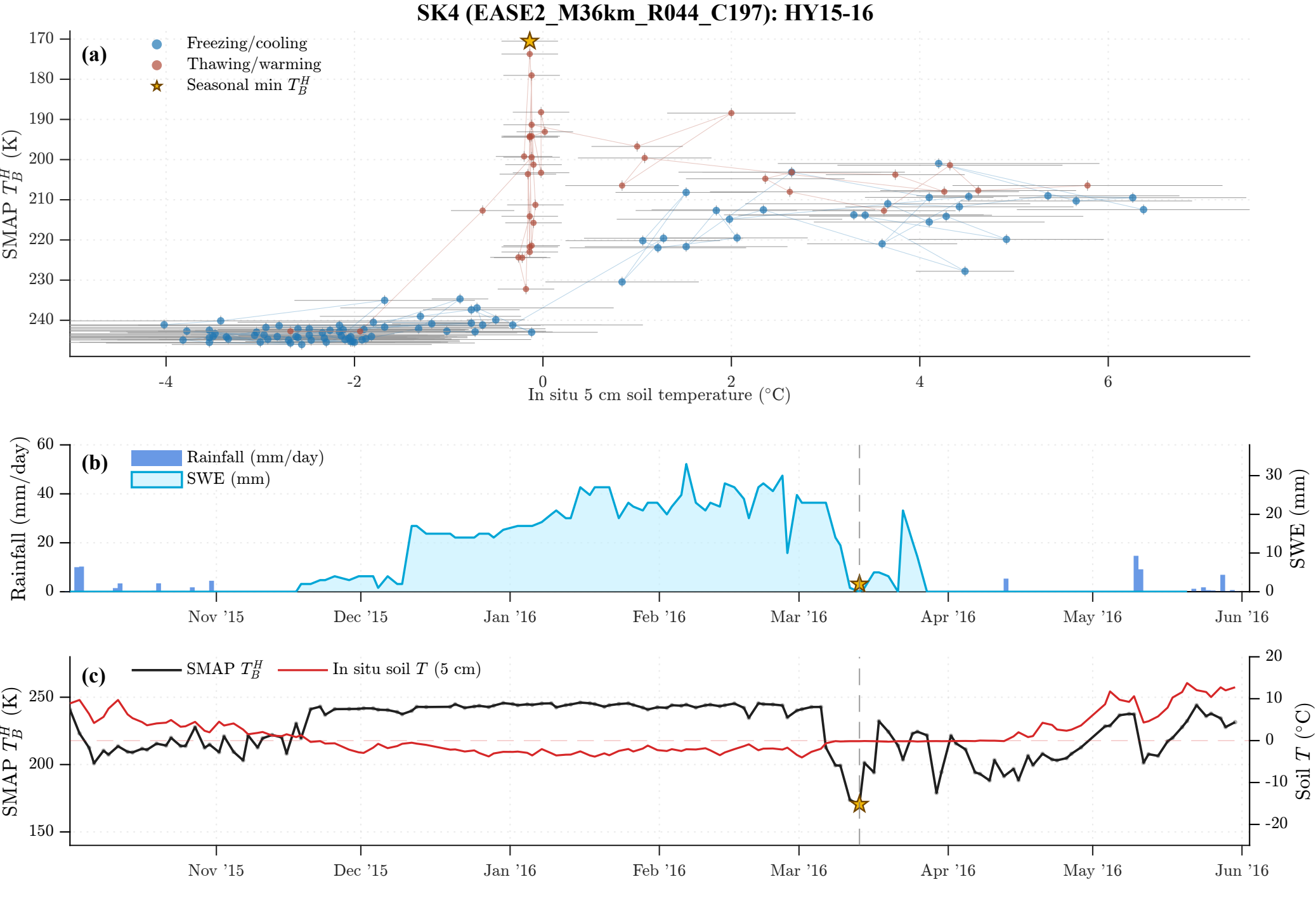
SK4 (EASE2_M36km_R044_C197): HY15-16
(a)
Freezing/cooling
Thawing/warming
Seasonal min T_B^H
SMAP T_B^H (K)
In situ 5 cm soil temperature (°C)
(b)
Rainfall (mm/day)
SWE (mm)
Nov '15
Dec '15
Jan '16
Feb '16
Mar '16
Apr '16
May '16
Jun '16
(c)
SMAP T_B^H
In situ soil T (5 cm)
Soil T (°C)

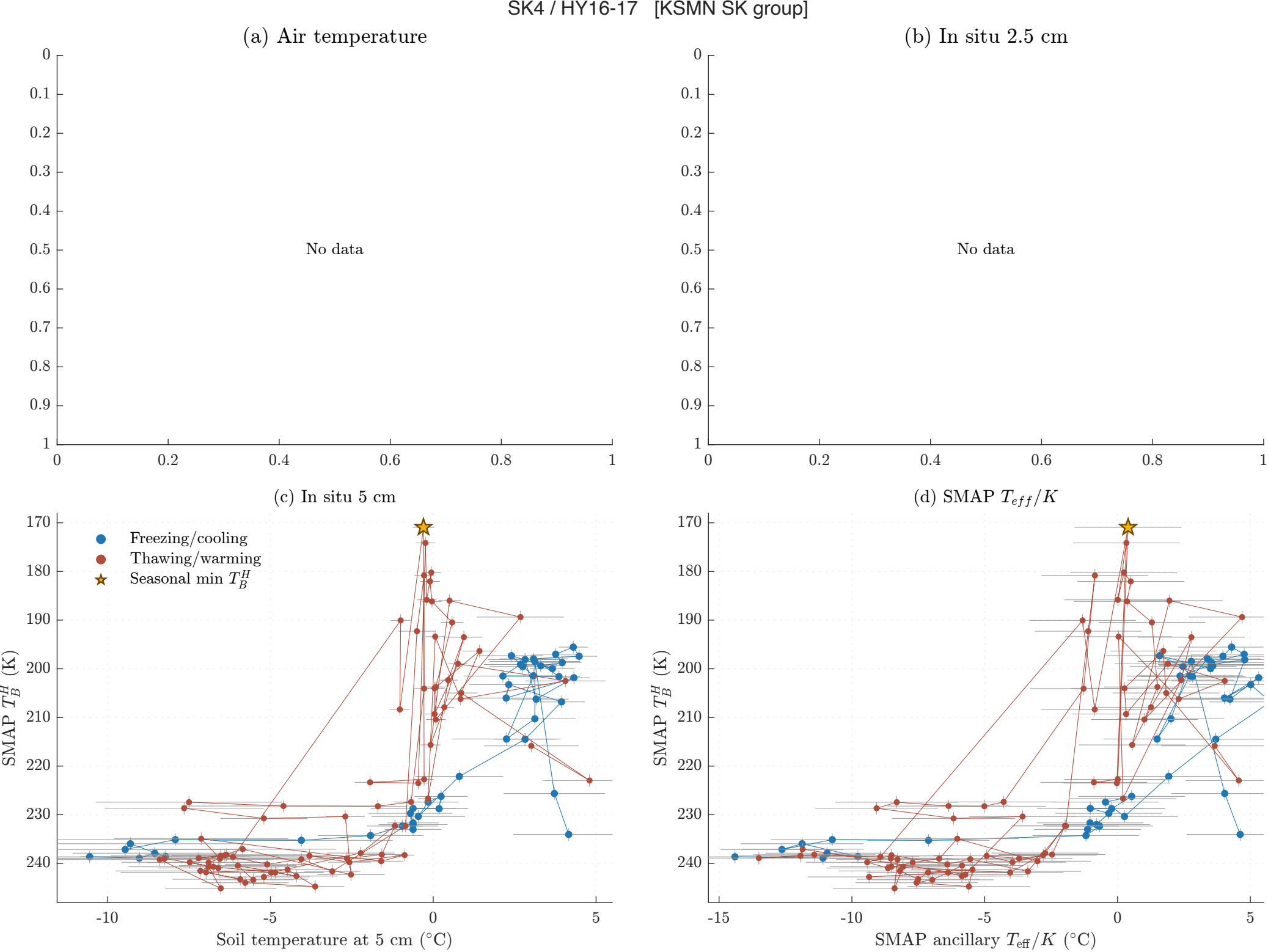
(a) Air temperature
No data
(b) In situ 2.5 cm
No data
(c) In situ 5 cm
Freezing/cooling
Thawing/warming
Seasonal min T_B^H
SMAP T_B^H (K)
Soil temperature at 5 cm (°C)
(d) SMAP T_{eff}/K
SMAP T_B^H (K)
SMAP ancillary T_{eff}/K (°C)

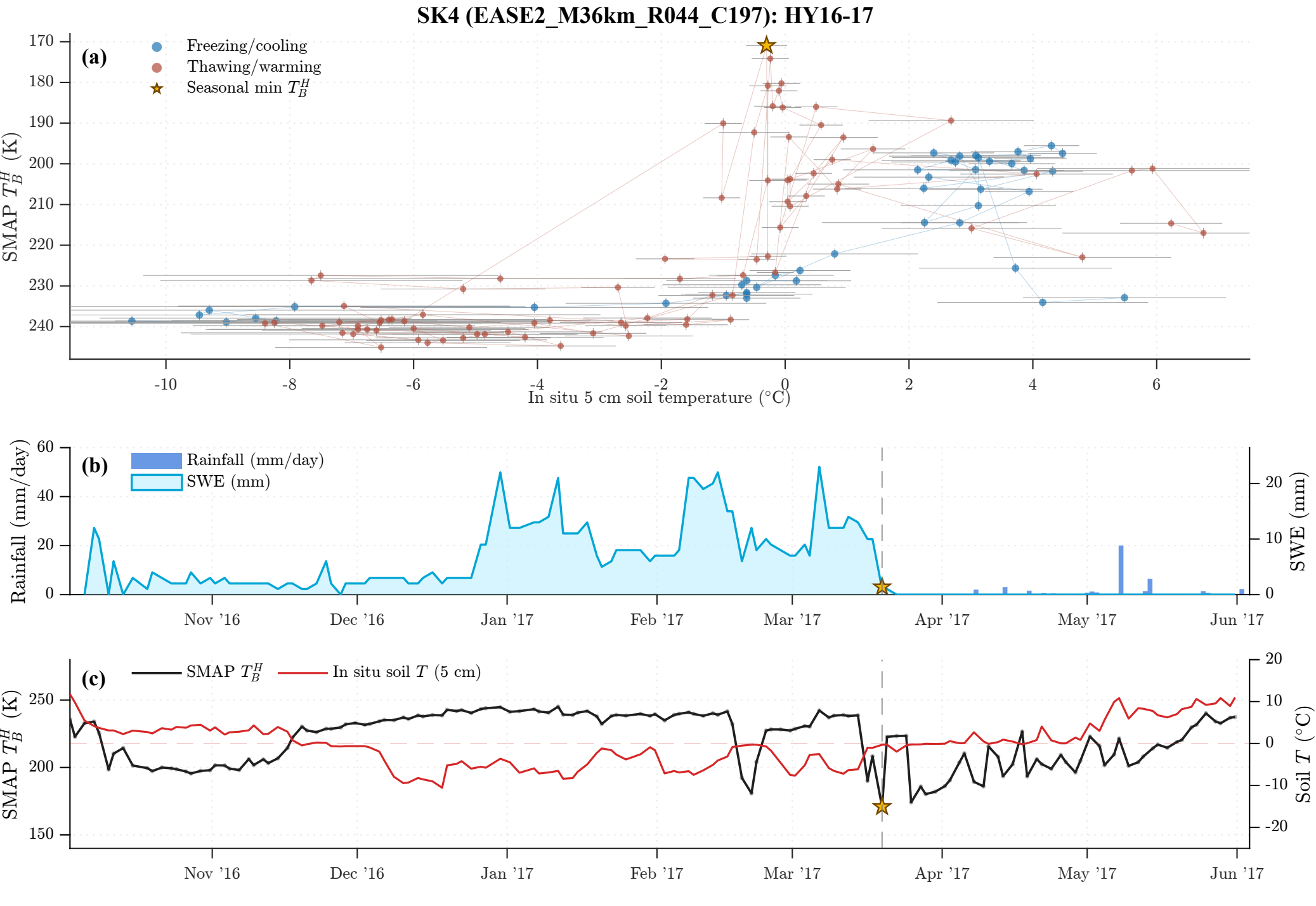
SK4 (EASE2_M36km_R044_C197): HY16-17
(a)
Freezing/cooling
Thawing/warming
Seasonal min T_B^H
SMAP T_B^H (K)
In situ 5 cm soil temperature (°C)
(b)
Rainfall (mm/day)
SWE (mm)
Rainfall (mm/day)
SWE (mm)
Nov '16
Dec '16
Jan '17
Feb '17
Mar '17
Apr '17
May '17
Jun '17
(c)
SMAP T_B^H
In situ soil T (5 cm)
SMAP T_B^H (K)
Soil T (°C)

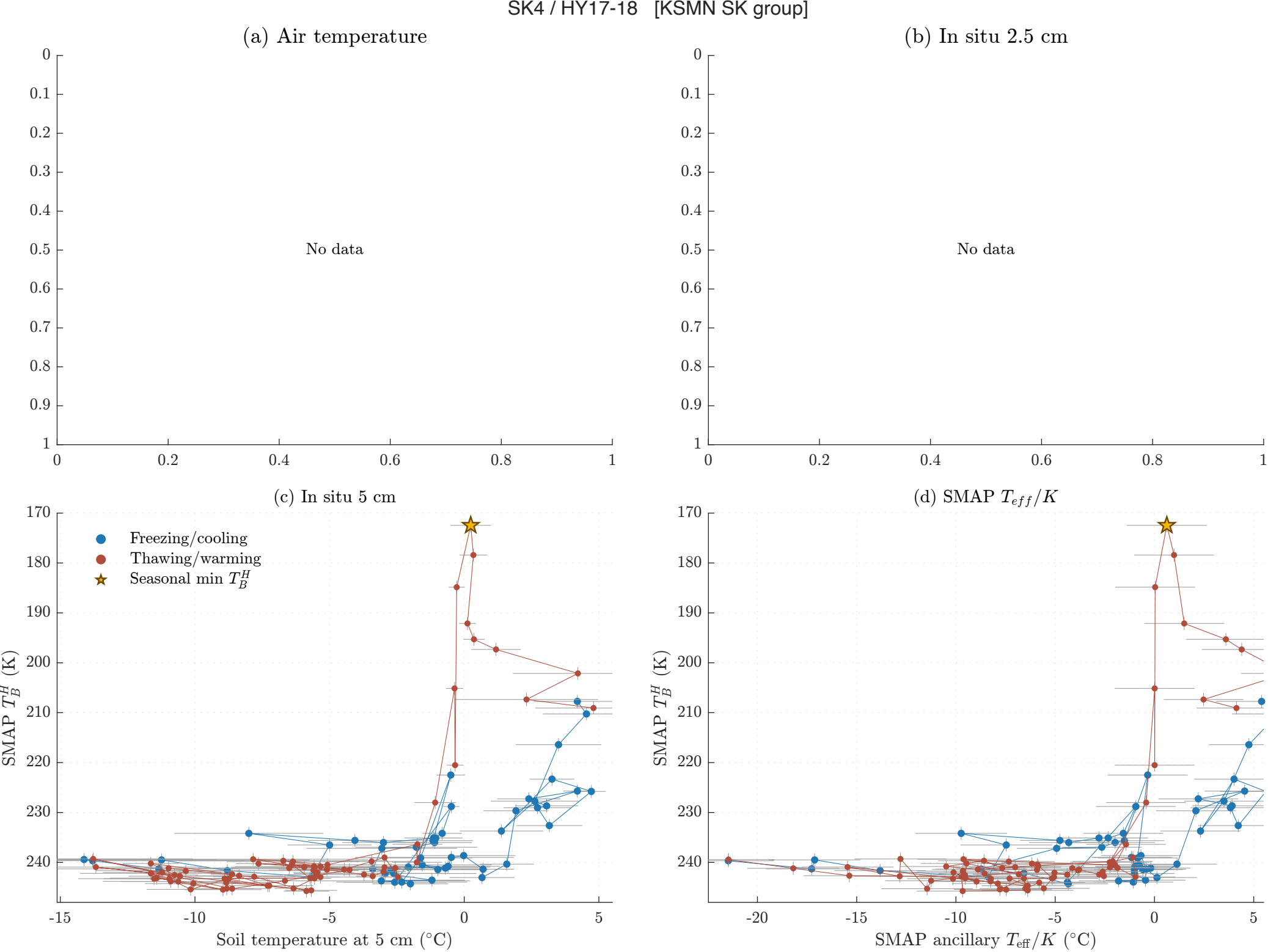
SK4 / HY17-18 [KSMN SK group]
(a) Air temperature
No data
(b) In situ 2.5 cm
No data
(c) In situ 5 cm
Freezing/cooling
Thawing/warming
Seasonal min T_B^H
SMAP T_B^H (K)
Soil temperature at 5 cm (°C)
(d) SMAP T_{eff}/K
SMAP T_B^H (K)
SMAP ancillary T_{eff}/K (°C)

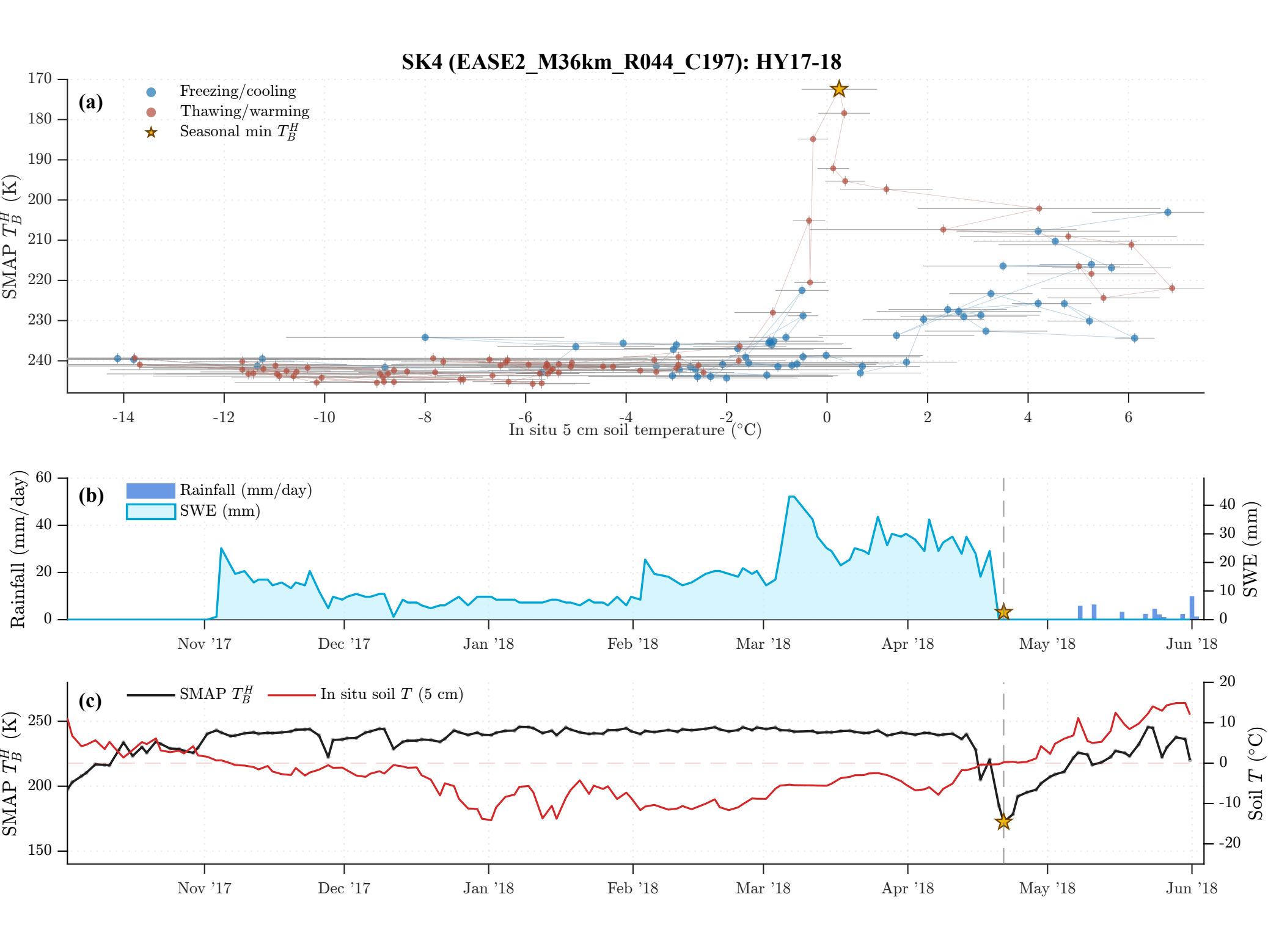
SK4 (EASE2_M36km_R044_C197): HY17-18
(a)
Freezing/cooling
Thawing/warming
Seasonal min T_B^H
SMAP T_B^H (K)
In situ 5 cm soil temperature (°C)
(b)
Rainfall (mm/day)
SWE (mm)
Nov '17
Dec '17
Jan '18
Feb '18
Mar '18
Apr '18
May '18
Jun '18
(c)
SMAP T_B^H
In situ soil T (5 cm)
Soil T (°C)

B Appendix B: Manitoba (RISMA) Pixel-Year Compendium

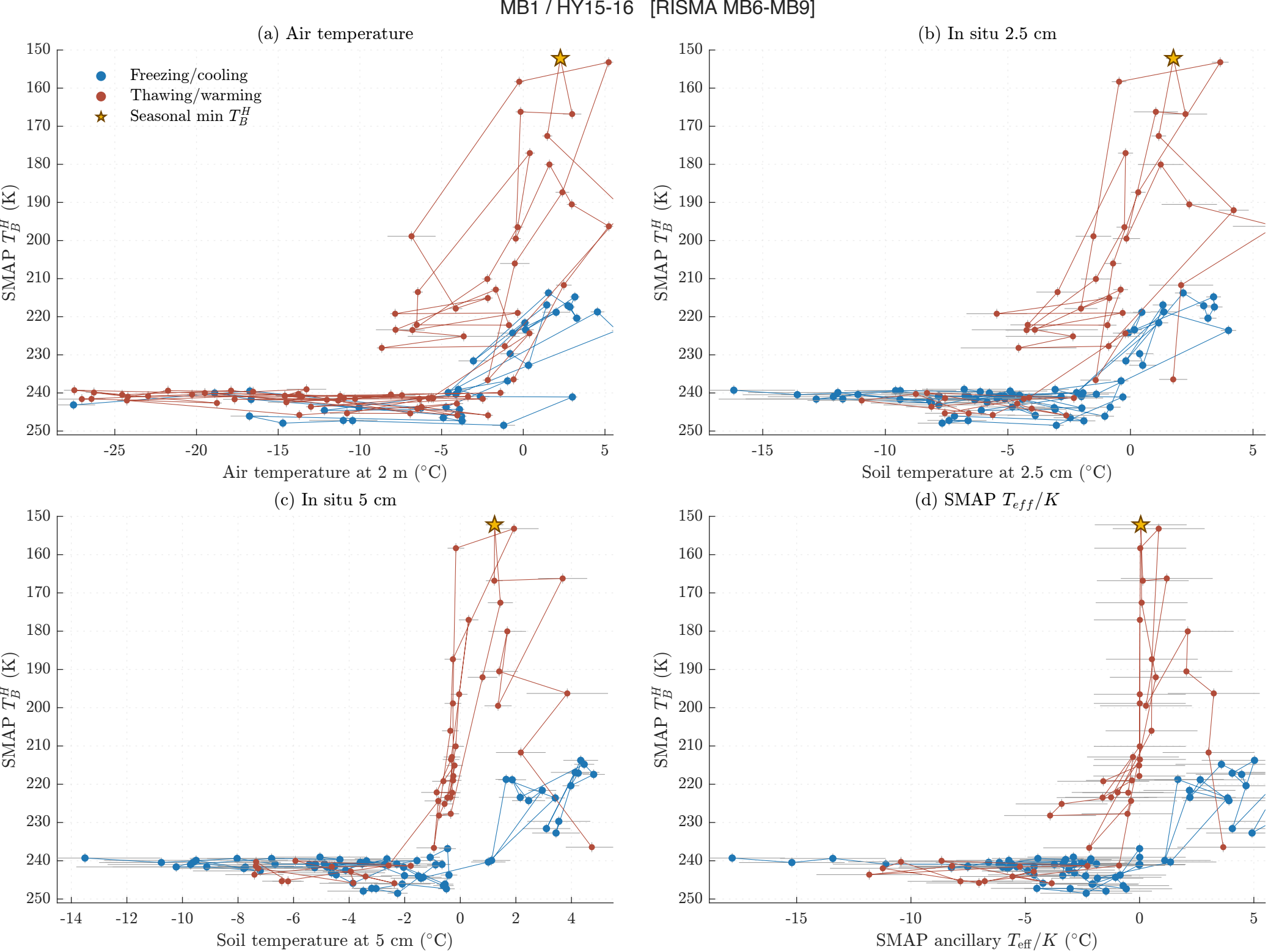
MB1 / HY15-16 [RISMA MB6-MB9]
(a) Air temperature
(b) In situ 2.5 cm
(c) In situ 5 cm
(d) SMAP T_{eff}/K
Freezing/cooling
Thawing/warming
Seasonal min T_B^H
SMAP T_B^H (K)
Air temperature at 2 m (°C)
Soil temperature at 2.5 cm (°C)
Soil temperature at 5 cm (°C)
SMAP ancillary T_{eff}/K (°C)

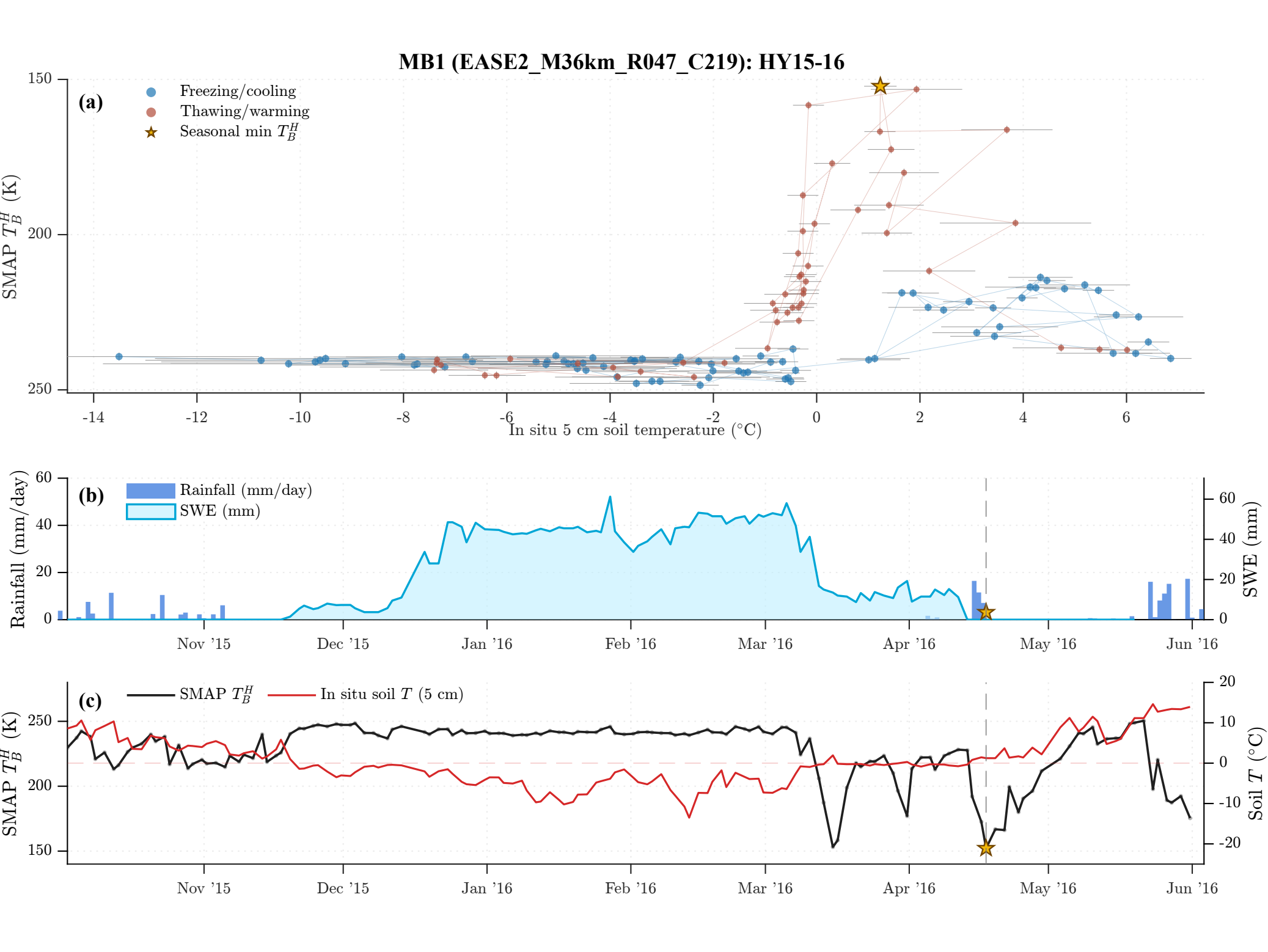
MB1 (EASE2_M36km_R047_C219): HY15-16
(a)
Freezing/cooling
Thawing/warming
Seasonal min T_B^H
SMAP T_B^H (K)
In situ 5 cm soil temperature (°C)
(b)
Rainfall (mm/day)
SWE (mm)
Nov '15
Dec '15
Jan '16
Feb '16
Mar '16
Apr '16
May '16
Jun '16
(c)
SMAP T_B^H
In situ soil T (5 cm)
Soil T (°C)

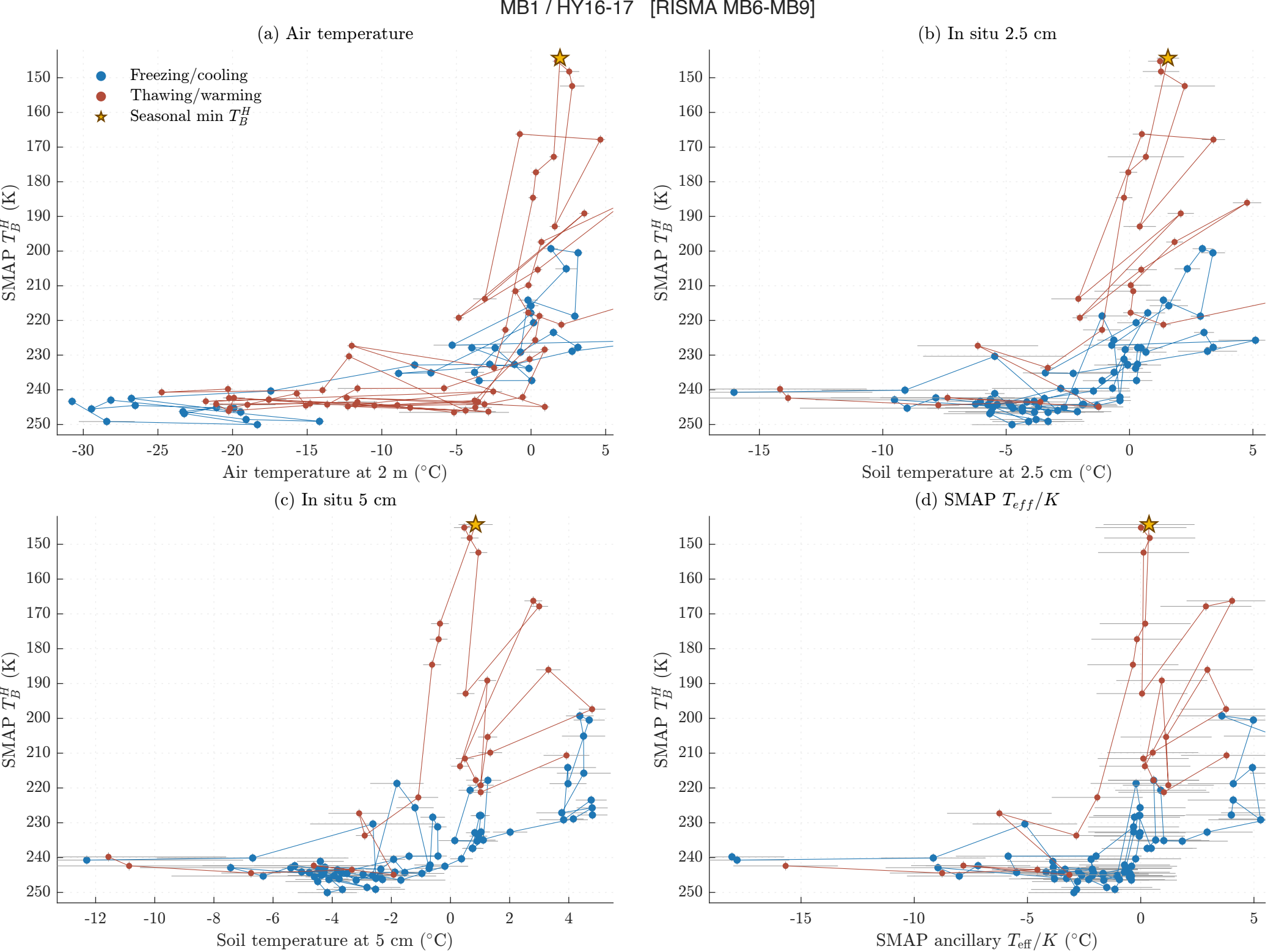
MB1 / HY16-17 [RISMA MB6-MB9]
(a) Air temperature
(b) In situ 2.5 cm
(c) In situ 5 cm
(d) SMAP T_{eff}/K
Freezing/cooling
Thawing/warming
Seasonal min T_B^H
SMAP T_B^H (K)
Air temperature at 2 m (°C)
Soil temperature at 2.5 cm (°C)
Soil temperature at 5 cm (°C)
SMAP ancillary T_{eff}/K (°C)

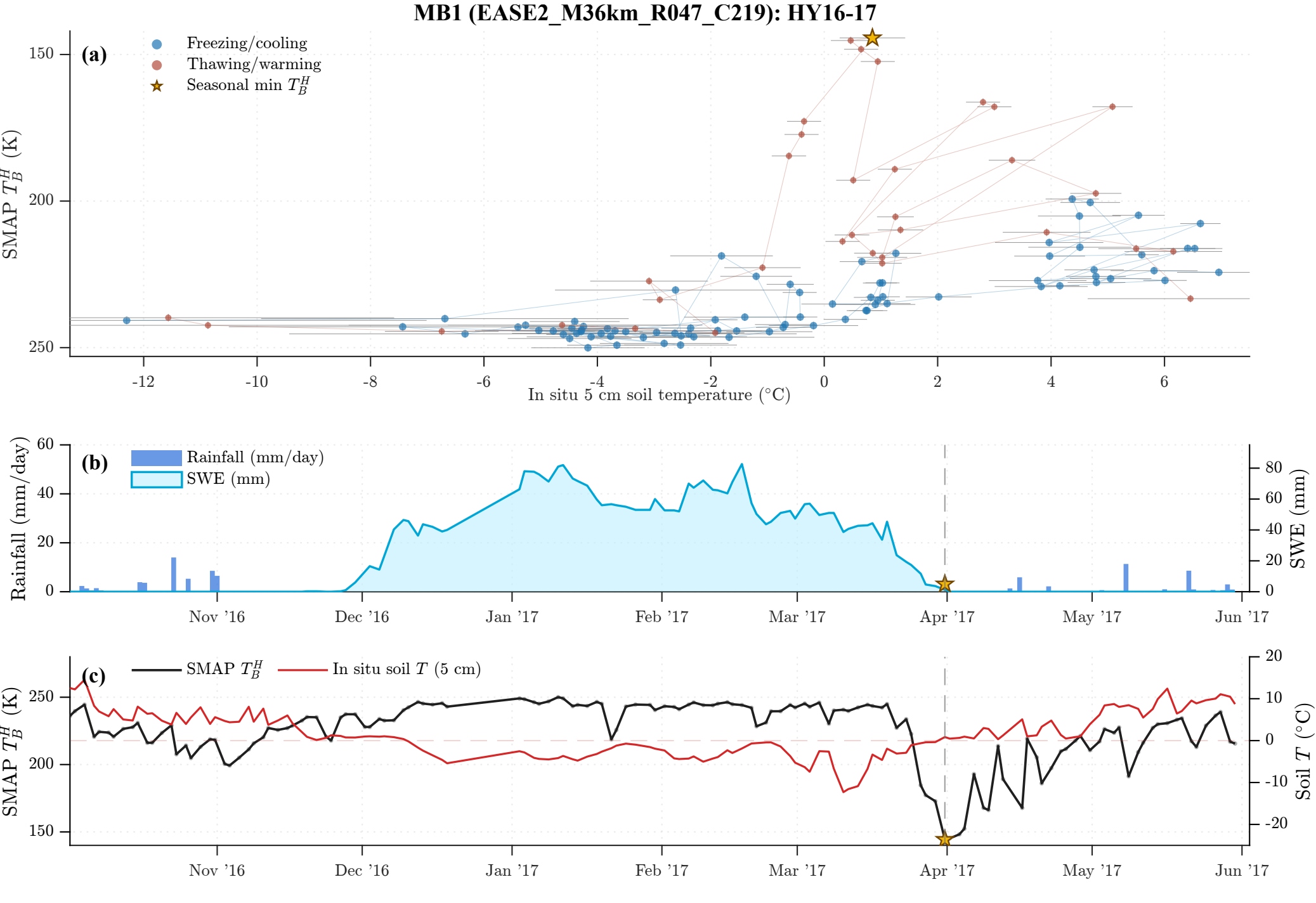
MB1 (EASE2_M36km_R047_C219): HY16-17
(a)
Freezing/cooling
Thawing/warming
Seasonal min T_B^H
SMAP T_B^H (K)
In situ 5 cm soil temperature (°C)
(b)
Rainfall (mm/day)
SWE (mm)
Nov '16
Dec '16
Jan '17
Feb '17
Mar '17
Apr '17
May '17
Jun '17
(c)
SMAP T_B^H
In situ soil T (5 cm)
Soil T (°C)

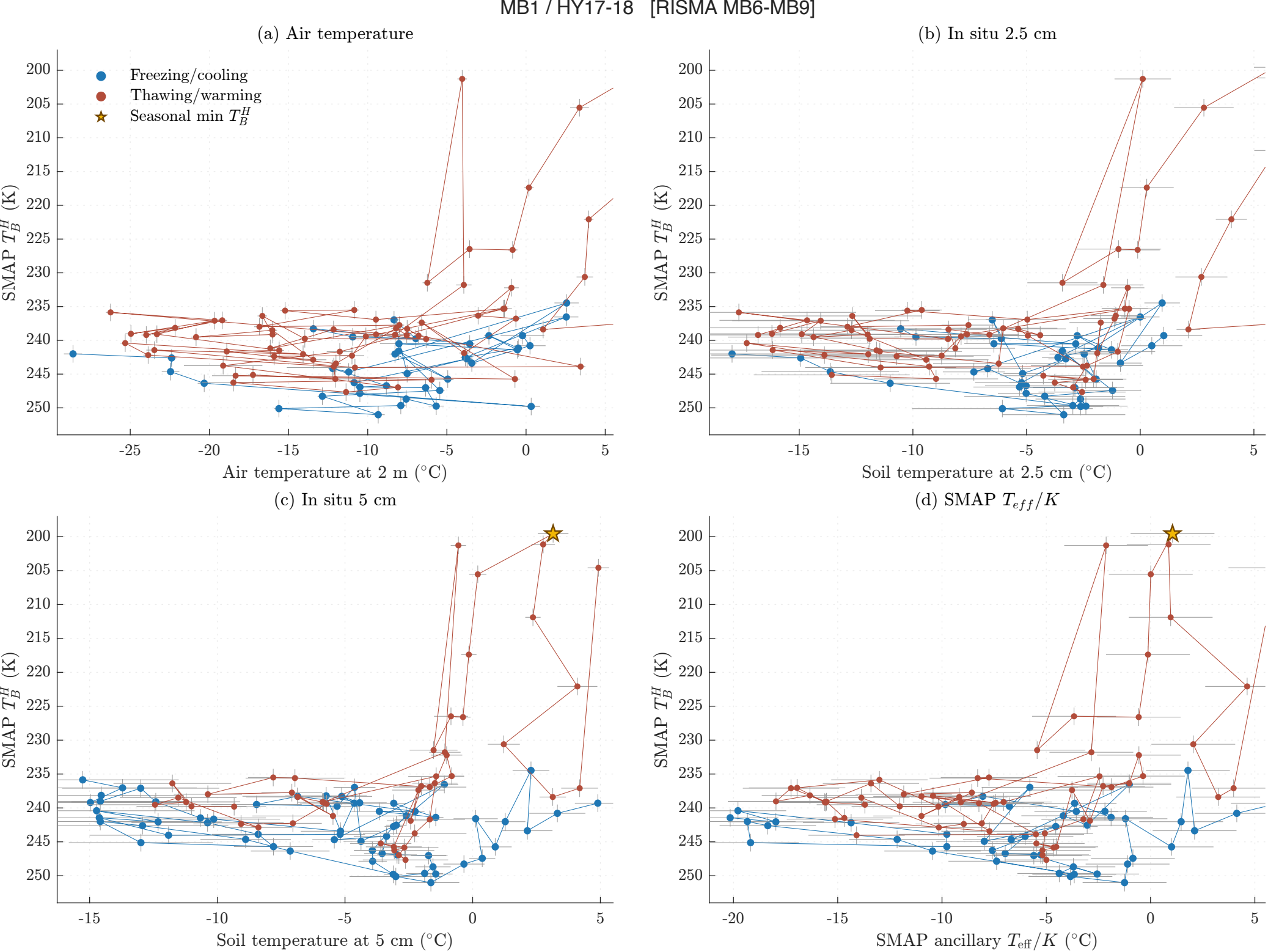
MB1 / HY17-18 [RISMA MB6-MB9]
(a) Air temperature
(b) In situ 2.5 cm
(c) In situ 5 cm
(d) SMAP T_{eff}/K
Freezing/cooling
Thawing/warming
Seasonal min T_B^H
SMAP T_B^H (K)
Air temperature at 2 m (°C)
Soil temperature at 2.5 cm (°C)
Soil temperature at 5 cm (°C)
SMAP ancillary T_{eff}/K (°C)

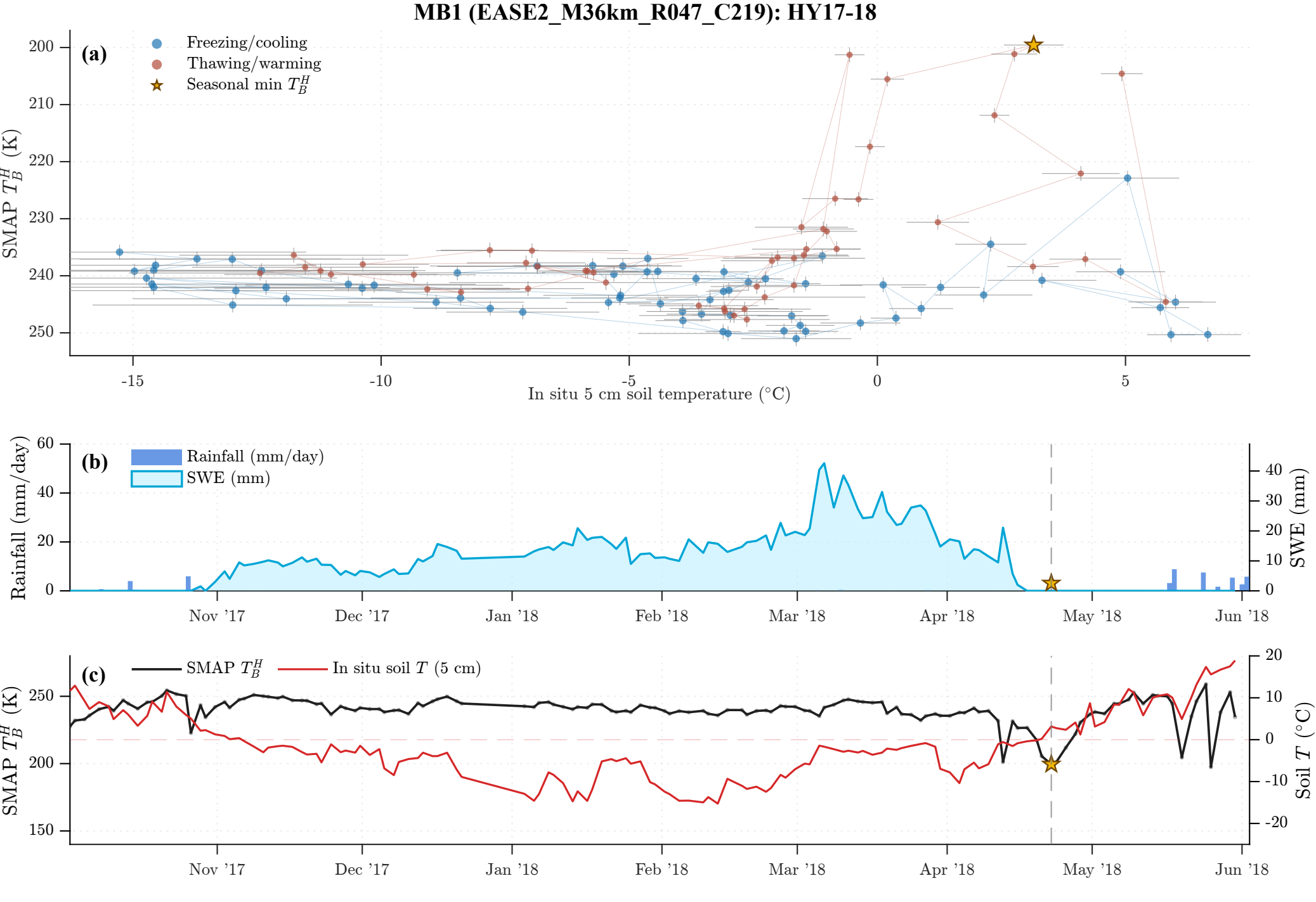
MB1 (EASE2_M36km_R047_C219): HY17-18
(a)
Freezing/cooling
Thawing/warming
Seasonal min T_B^H
SMAP T_B^H (K)
In situ 5 cm soil temperature (°C)
(b)
Rainfall (mm/day)
SWE (mm)
(c)
SMAP T_B^H
In situ soil T (5 cm)
Soil T (°C)
Nov '17
Dec '17
Jan '18
Feb '18
Mar '18
Apr '18
May '18
Jun '18

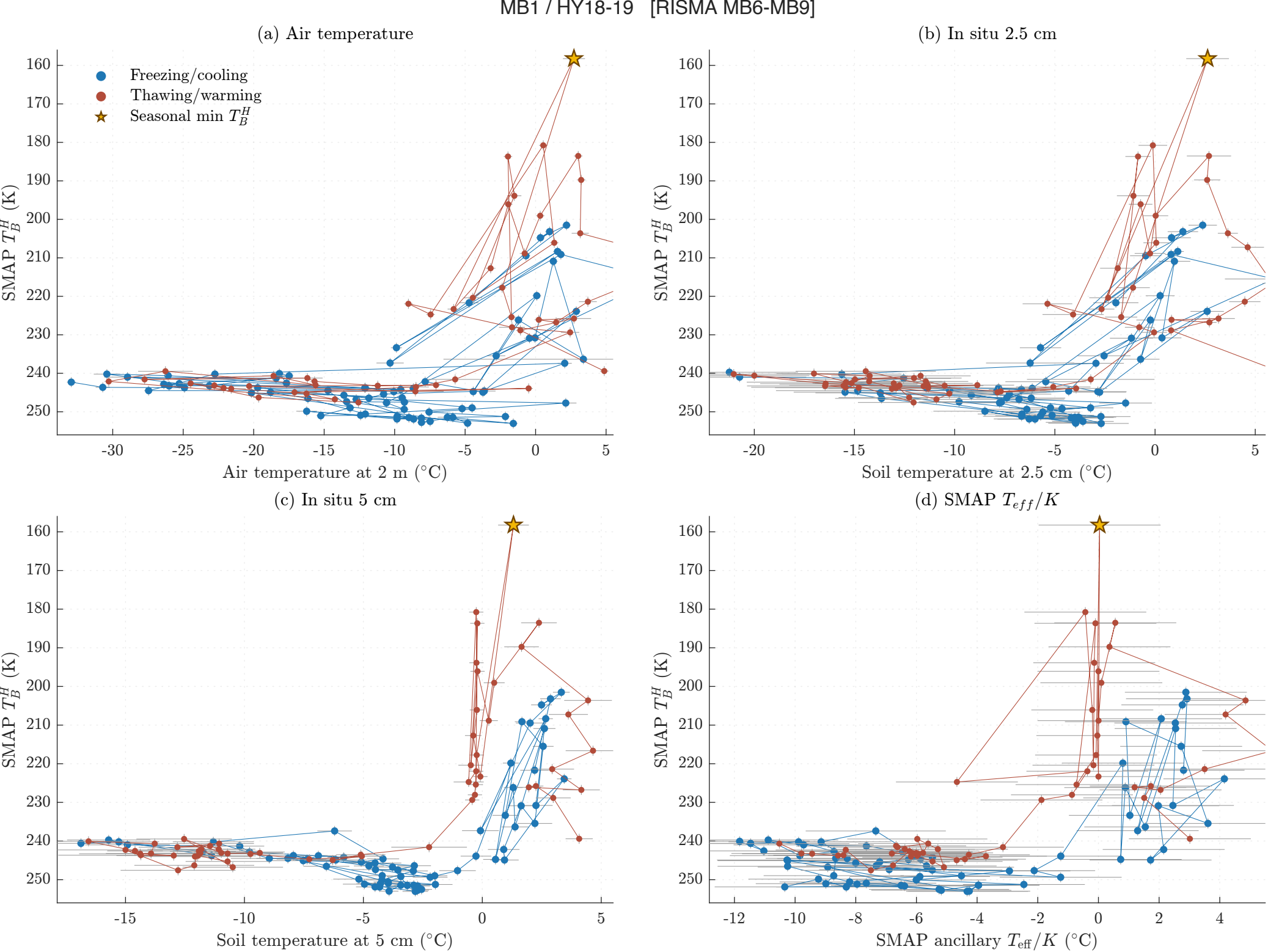
MB1 / HY18-19 [RISMA MB6-MB9]
(a) Air temperature
(b) In situ 2.5 cm
(c) In situ 5 cm
(d) SMAP T_{eff}/K
Freezing/cooling
Thawing/warming
Seasonal min T_B^H
SMAP T_B^H (K)
Air temperature at 2 m (°C)
Soil temperature at 2.5 cm (°C)
Soil temperature at 5 cm (°C)
SMAP ancillary T_{eff}/K (°C)

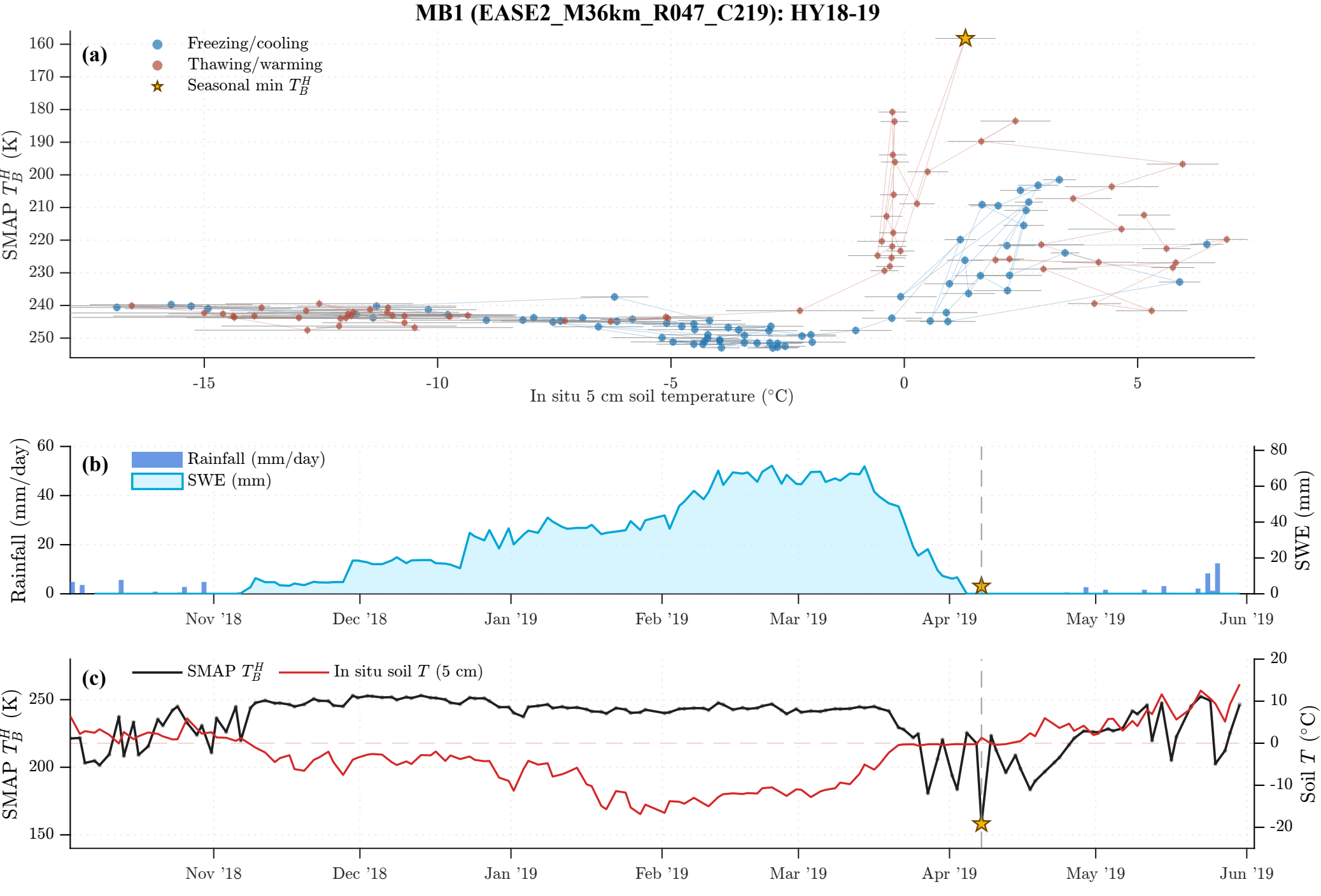
MB1 (EASE2_M36km_R047_C219): HY18-19
(a)
Freezing/cooling
Thawing/warming
Seasonal min T_B^H
SMAP T_B^H (K)
In situ 5 cm soil temperature (°C)
(b)
Rainfall (mm/day)
SWE (mm)
Nov '18
Dec '18
Jan '19
Feb '19
Mar '19
Apr '19
May '19
Jun '19
(c)
SMAP T_B^H
In situ soil T (5 cm)
Soil T (°C)

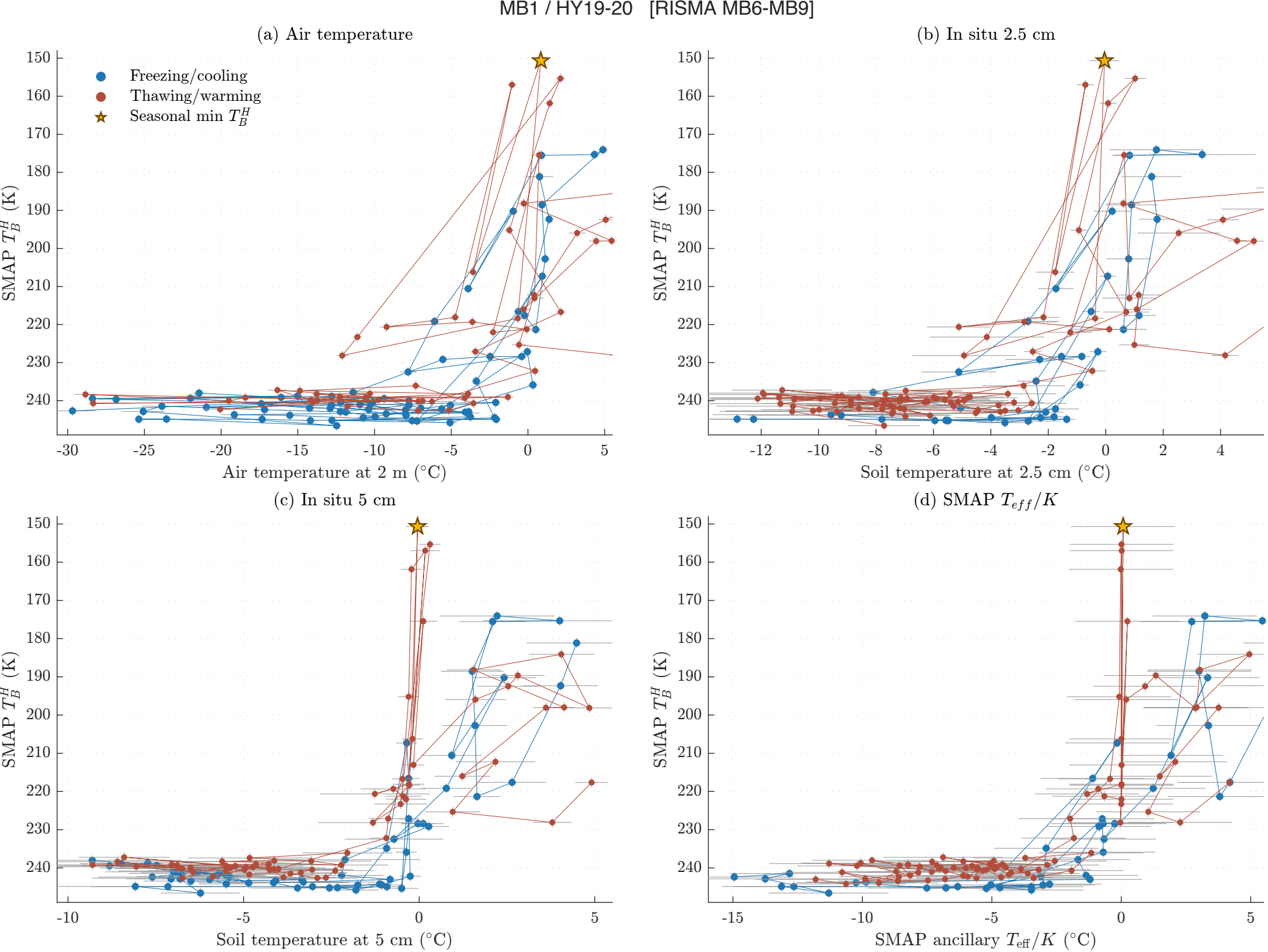
MB1 / HY19-20 [RISMA MB6-MB9]
(a) Air temperature
(b) In situ 2.5 cm
(c) In situ 5 cm
(d) SMAP T_{eff}/K
Freezing/cooling
Thawing/warming
Seasonal min T_B^H
SMAP T_B^H (K)
Air temperature at 2 m (°C)
Soil temperature at 2.5 cm (°C)
Soil temperature at 5 cm (°C)
SMAP ancillary T_{eff}/K (°C)

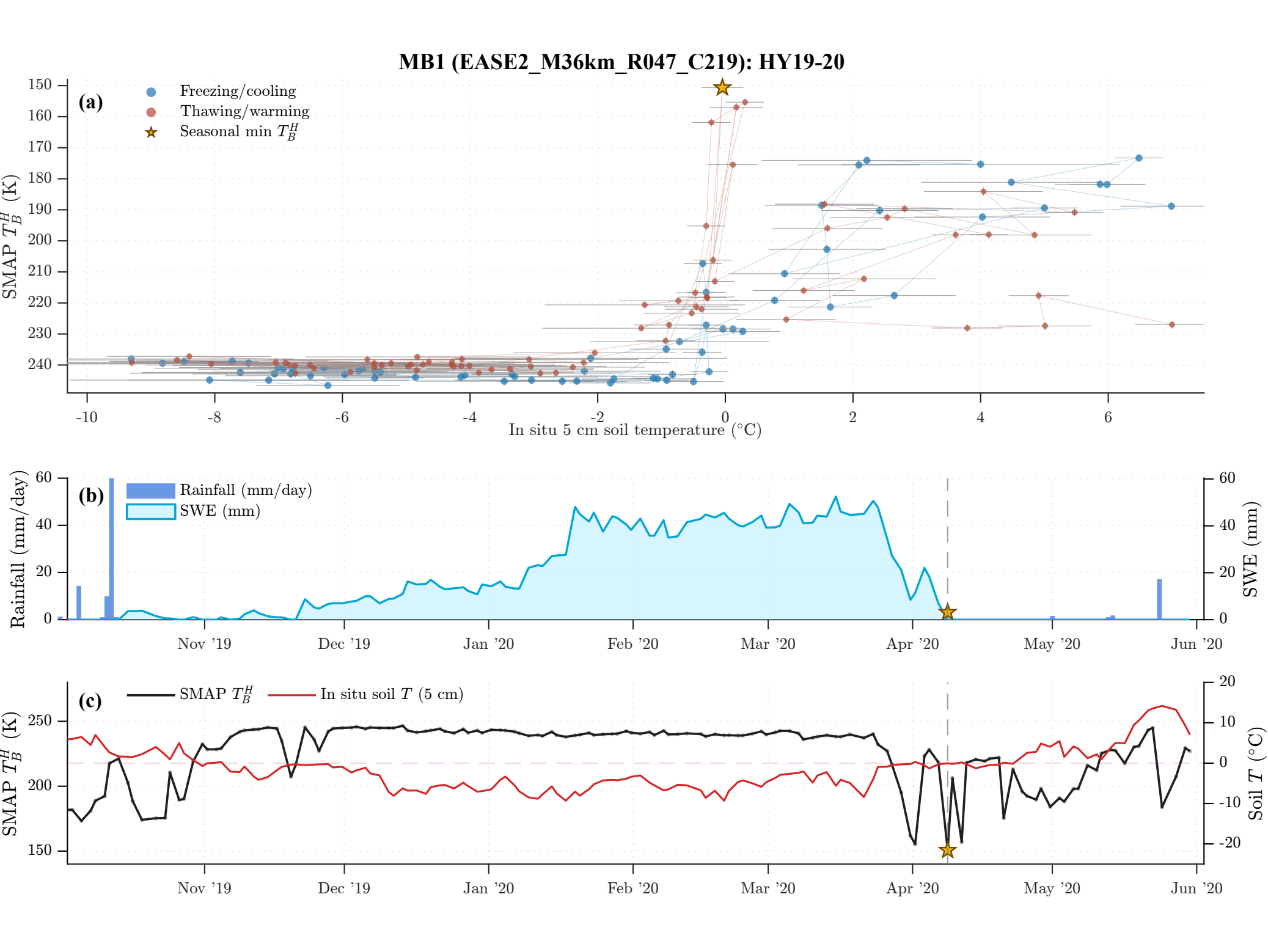
MB1 (EASE2_M36km_R047_C219): HY19-20
(a)
Freezing/cooling
Thawing/warming
Seasonal min T_B^H
SMAP T_B^H (K)
In situ 5 cm soil temperature (°C)
(b)
Rainfall (mm/day)
SWE (mm)
Nov '19
Dec '19
Jan '20
Feb '20
Mar '20
Apr '20
May '20
Jun '20
(c)
SMAP T_B^H
In situ soil T (5 cm)
Soil T (°C)

MB1 / HY20-21 [RISMA MB6-MB9]
(a) Air temperature
(b) In situ 2.5 cm
(c) In situ 5 cm
(d) SMAP T_{eff}/K
Freezing/cooling
Thawing/warming
Seasonal min T_B^H
SMAP T_B^H (K)
Air temperature at 2 m (°C)
Soil temperature at 2.5 cm (°C)
Soil temperature at 5 cm (°C)
SMAP ancillary T_{eff}/K (°C)

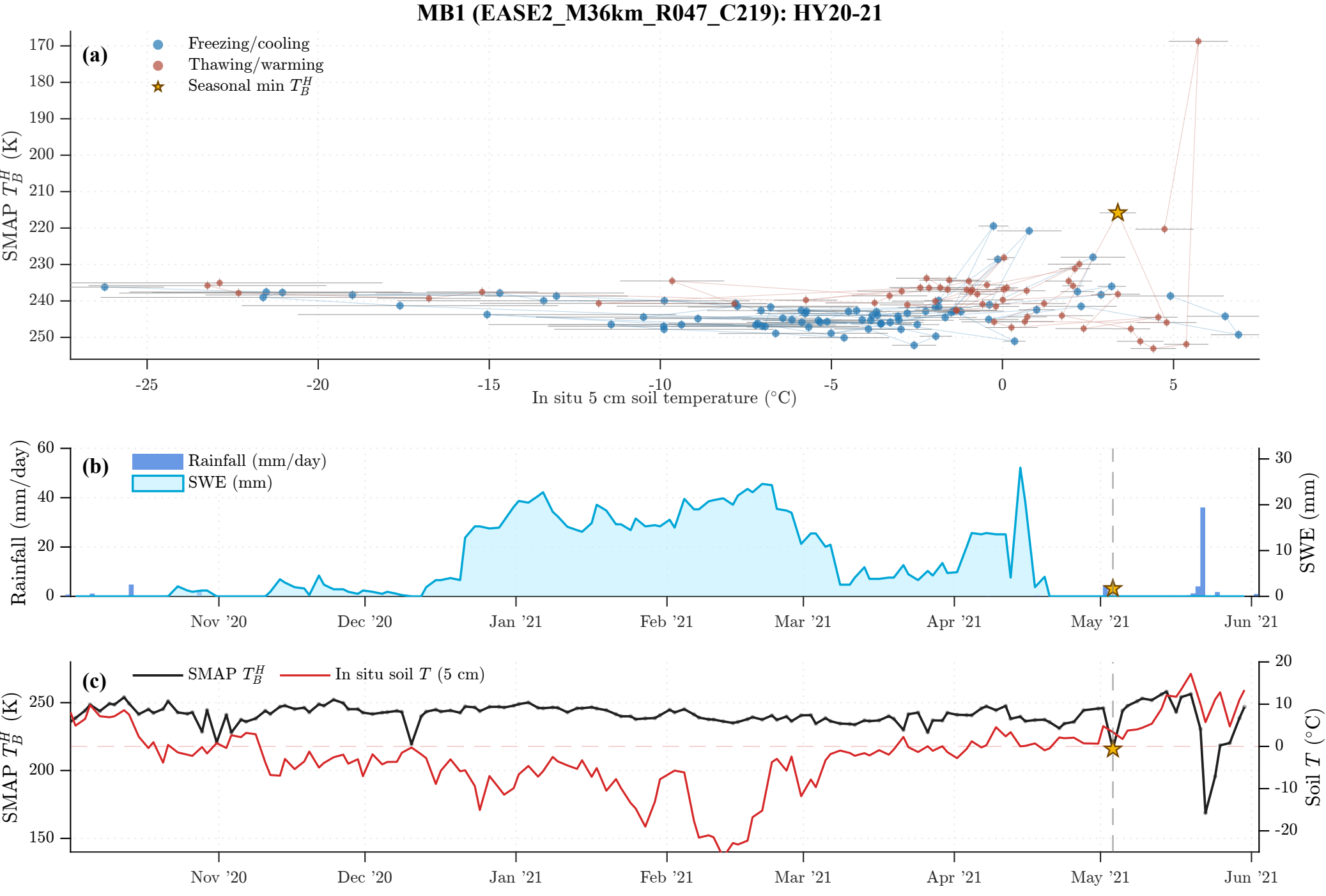
MB1 (EASE2_M36km_R047_C219): HY20-21
(a)
Freezing/cooling
Thawing/warming
Seasonal min T_B^H
SMAP T_B^H (K)
In situ 5 cm soil temperature (°C)
(b)
Rainfall (mm/day)
SWE (mm)
Nov '20
Dec '20
Jan '21
Feb '21
Mar '21
Apr '21
May '21
Jun '21
(c)
SMAP T_B^H
In situ soil T (5 cm)
Soil T (°C)

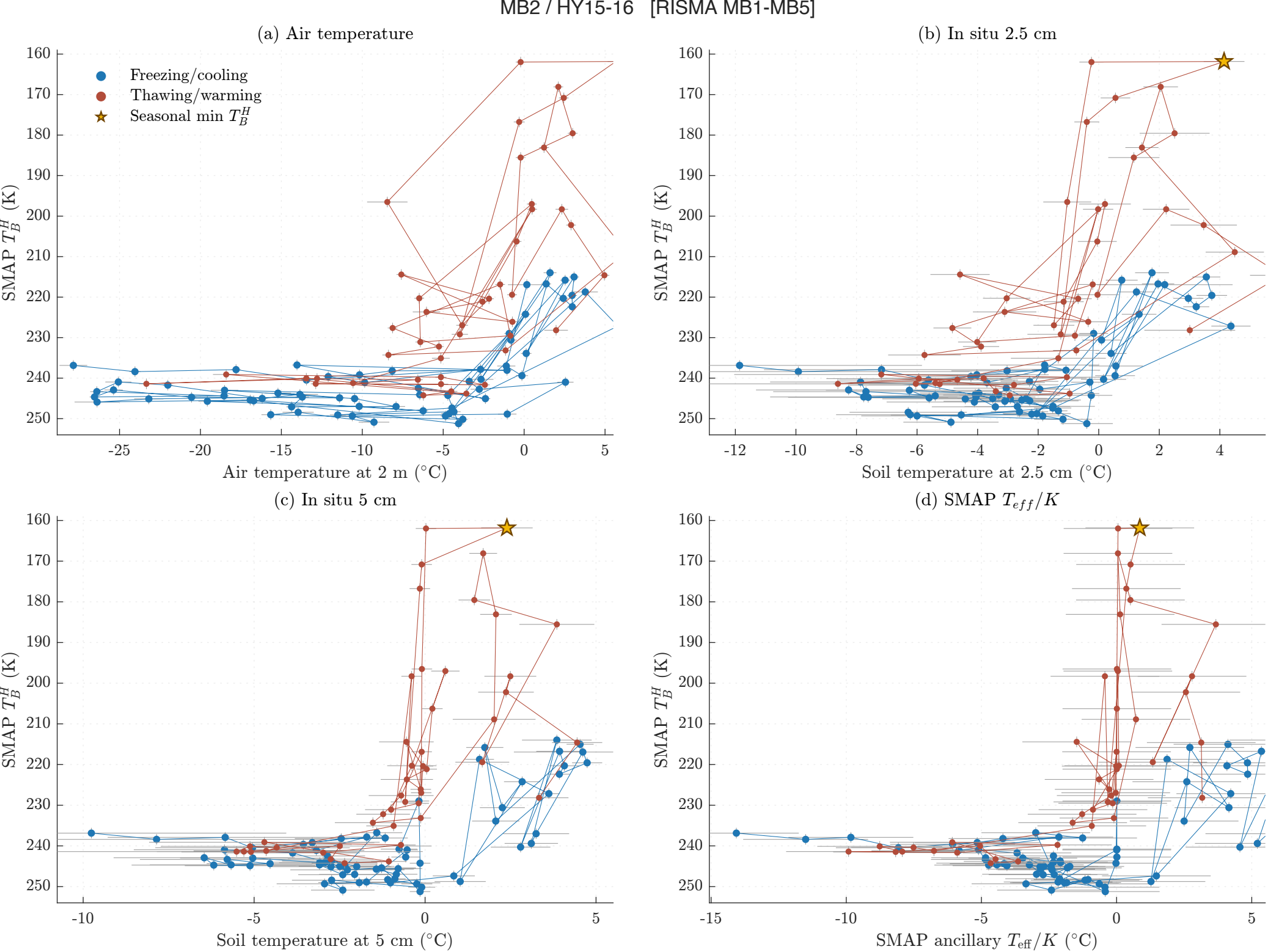
MB2 / HY15-16 [RISMA MB1-MB5]
(a) Air temperature
(b) In situ 2.5 cm
(c) In situ 5 cm
(d) SMAP T_{eff}/K
Freezing/cooling
Thawing/warming
Seasonal min T_B^H
SMAP T_B^H (K)
Air temperature at 2 m (°C)
Soil temperature at 2.5 cm (°C)
Soil temperature at 5 cm (°C)
SMAP ancillary T_{eff}/K (°C)

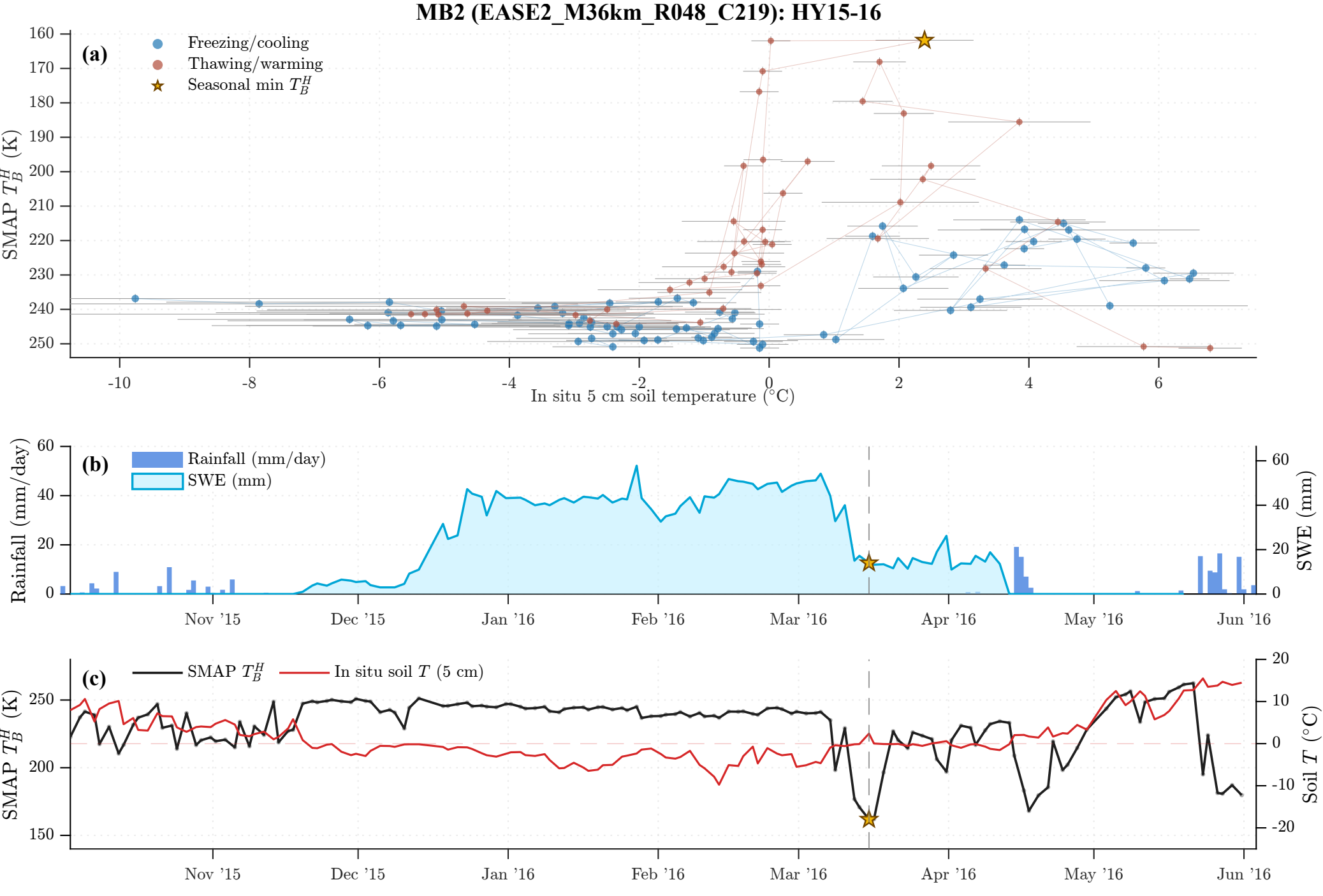
MB2 (EASE2_M36km_R048_C219): HY15-16
(a)
Freezing/cooling
Thawing/warming
Seasonal min T_B^H
SMAP T_B^H (K)
In situ 5 cm soil temperature (°C)
(b)
Rainfall (mm/day)
SWE (mm)
Nov '15
Dec '15
Jan '16
Feb '16
Mar '16
Apr '16
May '16
Jun '16
(c)
SMAP T_B^H
In situ soil T (5 cm)
Soil T (°C)

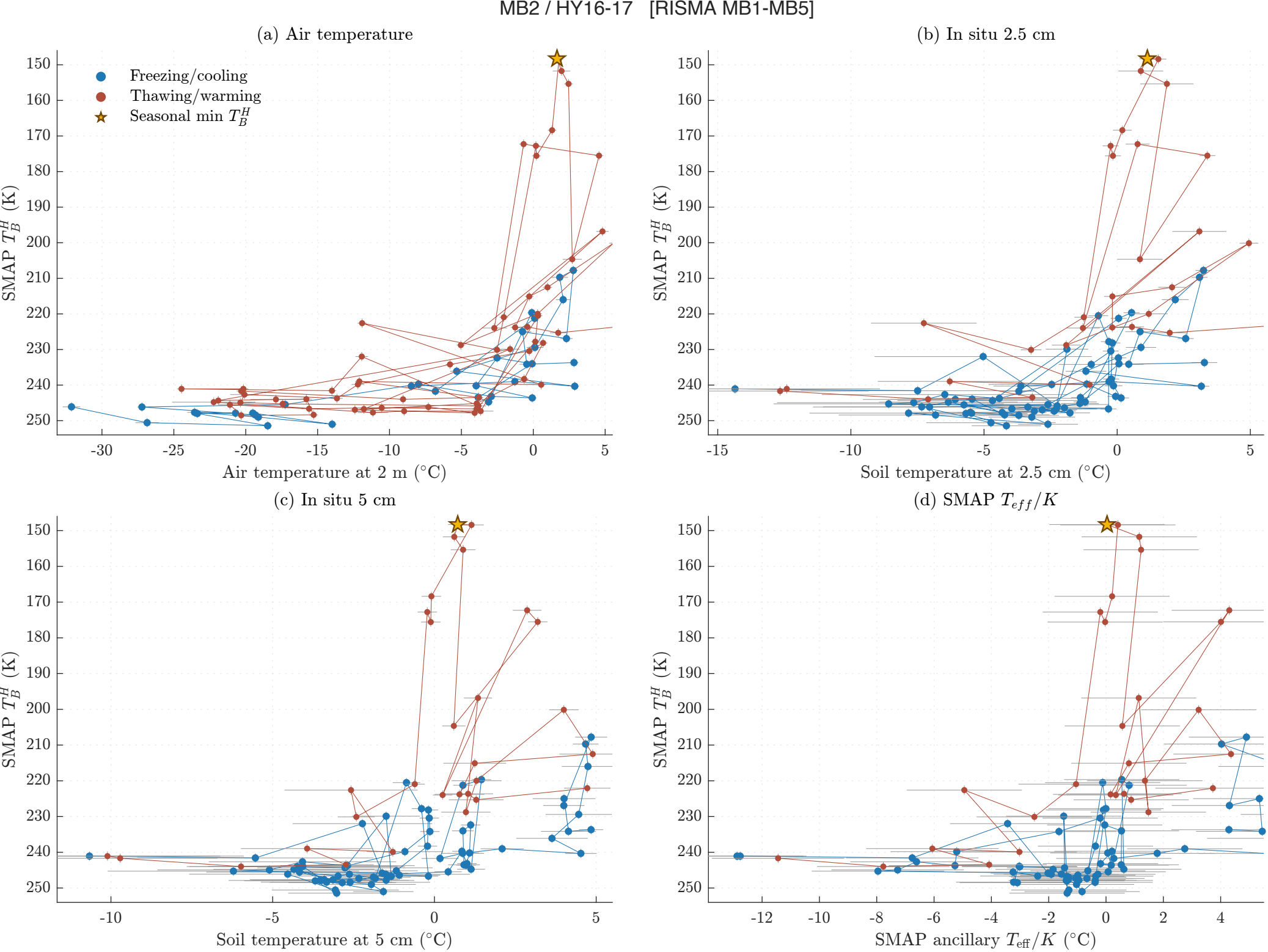
MB2 / HY16-17 [RISMA MB1-MB5]
(a) Air temperature
(b) In situ 2.5 cm
(c) In situ 5 cm
(d) SMAP T_{eff}/K
Freezing/cooling
Thawing/warming
Seasonal min T_B^H
SMAP T_B^H (K)
Air temperature at 2 m (°C)
Soil temperature at 2.5 cm (°C)
Soil temperature at 5 cm (°C)
SMAP ancillary T_{eff}/K (°C)

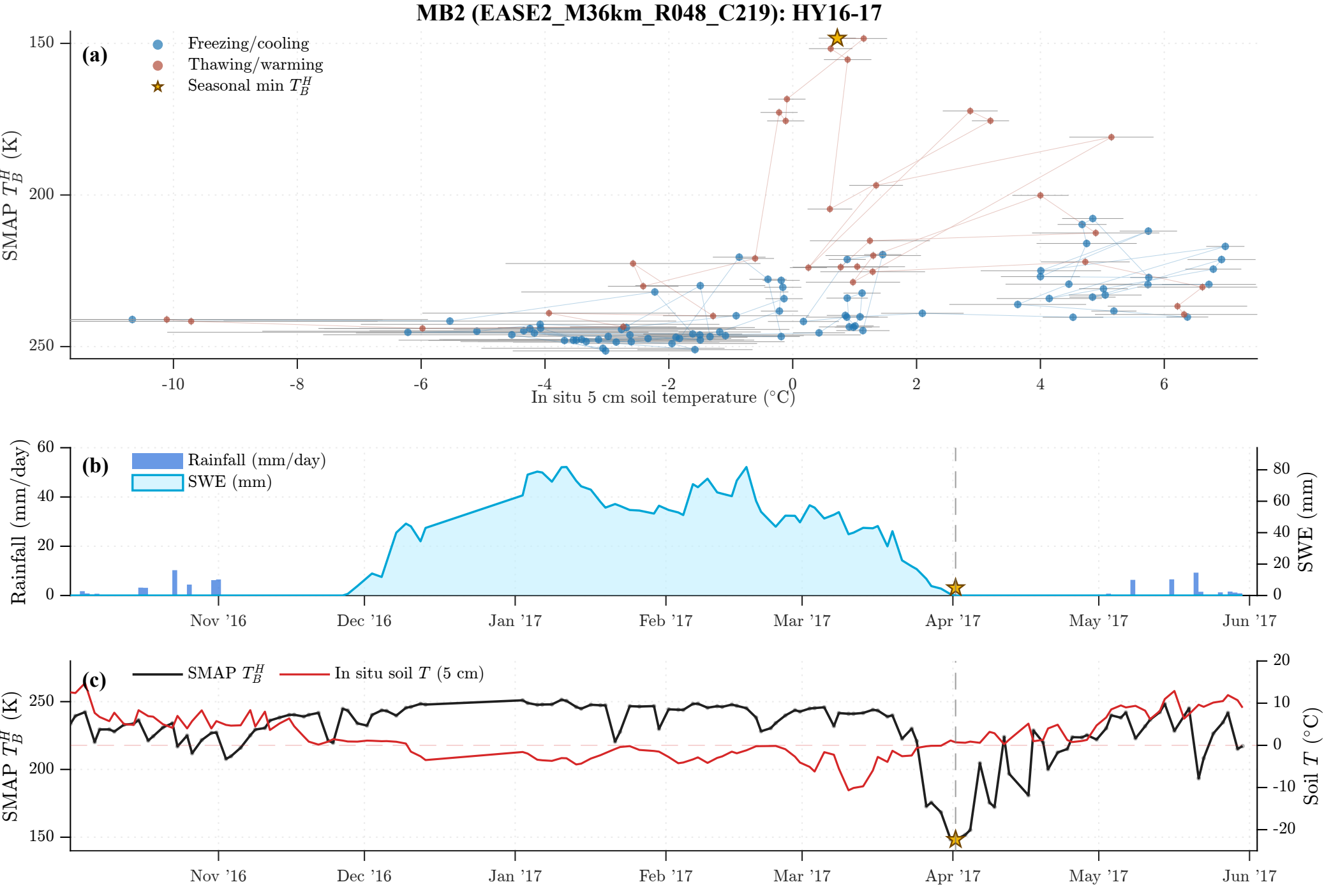
MB2 (EASE2_M36km_R048_C219): HY16-17
(a)
Freezing/cooling
Thawing/warming
Seasonal min T_B^H
SMAP T_B^H (K)
In situ 5 cm soil temperature (°C)
(b)
Rainfall (mm/day)
SWE (mm)
Nov '16
Dec '16
Jan '17
Feb '17
Mar '17
Apr '17
May '17
Jun '17
(c)
SMAP T_B^H
In situ soil T (5 cm)
Soil T (°C)

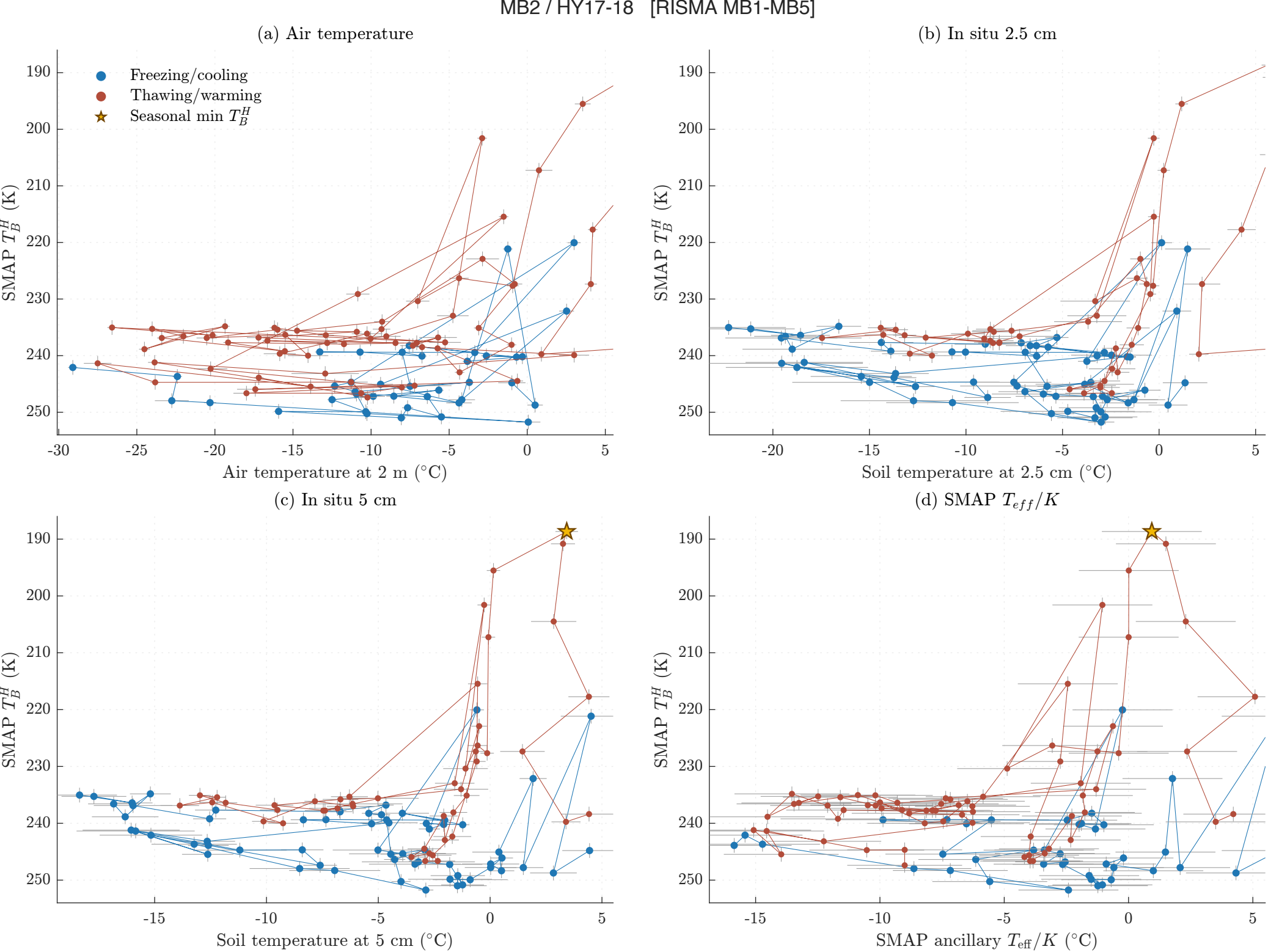
MB2 / HY17-18 [RISMA MB1-MB5]
(a) Air temperature
(b) In situ 2.5 cm
(c) In situ 5 cm
(d) SMAP T_{eff}/K
Freezing/cooling
Thawing/warming
Seasonal min T_B^H
SMAP T_B^H (K)
Air temperature at 2 m (°C)
Soil temperature at 2.5 cm (°C)
Soil temperature at 5 cm (°C)
SMAP ancillary T_{eff}/K (°C)

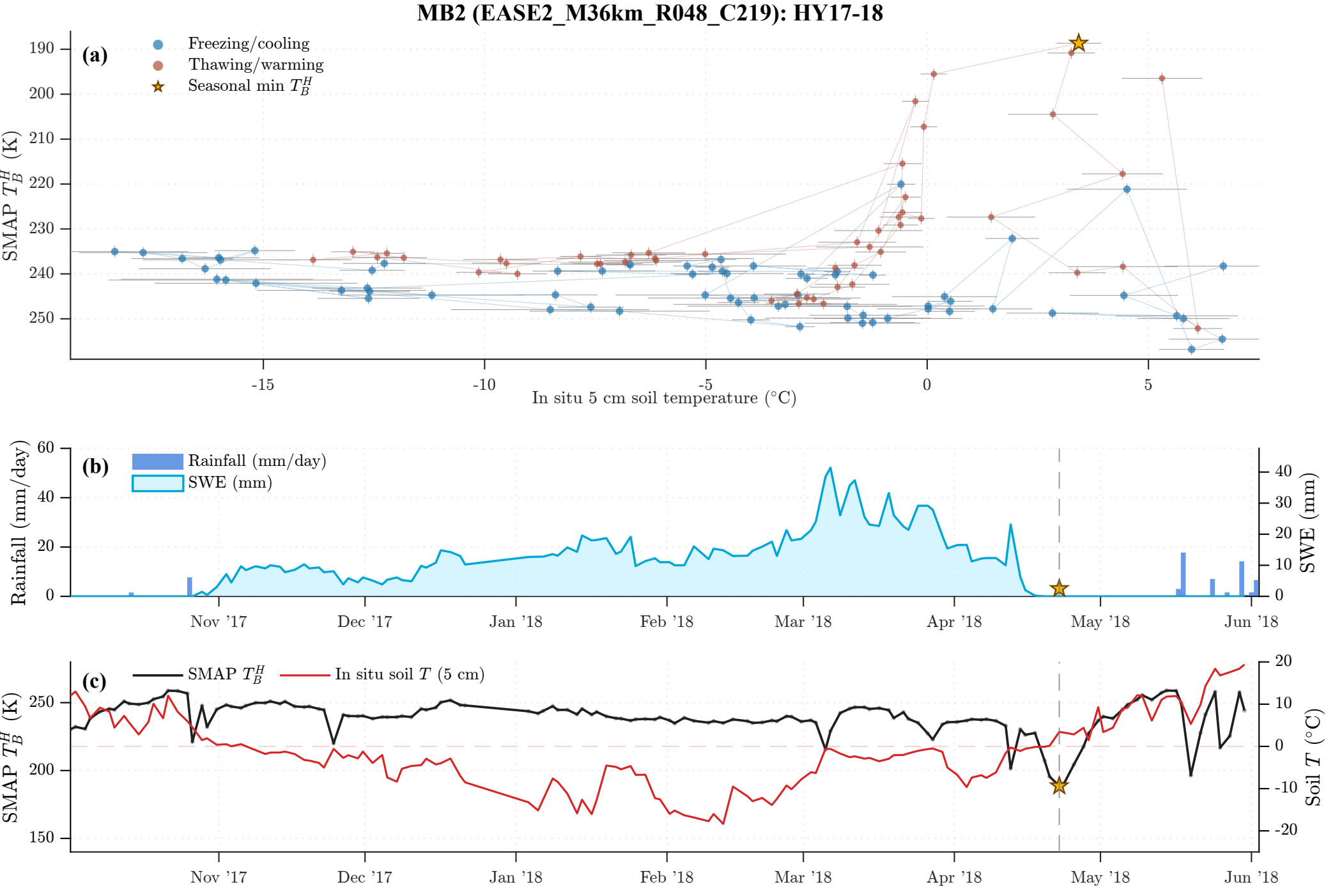
MB2 (EASE2_M36km_R048_C219): HY17-18
(a)
Freezing/cooling
Thawing/warming
Seasonal min T_B^H
SMAP T_B^H (K)
In situ 5 cm soil temperature (°C)
(b)
Rainfall (mm/day)
SWE (mm)
Nov '17
Dec '17
Jan '18
Feb '18
Mar '18
Apr '18
May '18
Jun '18
(c)
SMAP T_B^H
In situ soil T (5 cm)
Soil T (°C)

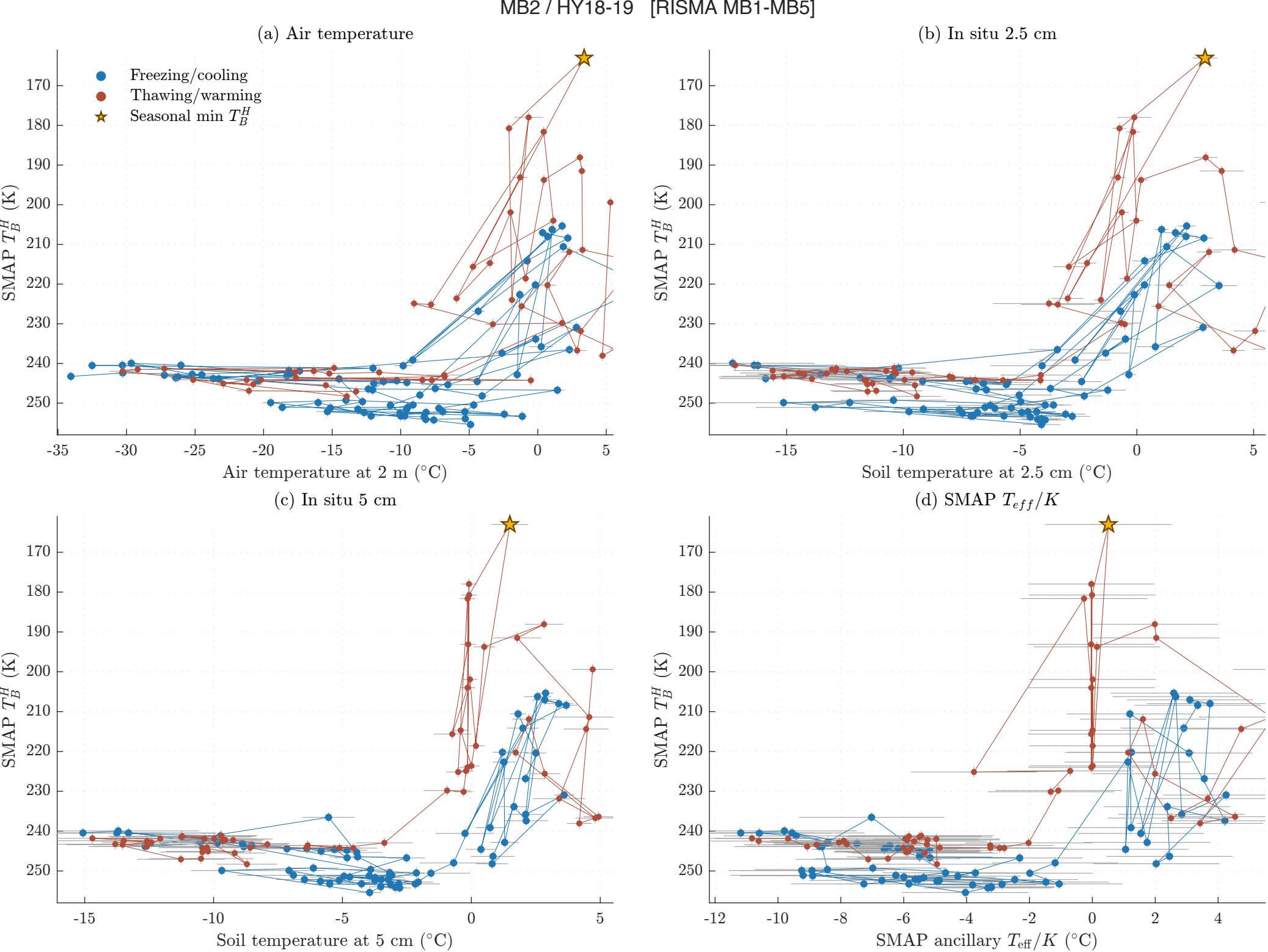
MB2 / HY18-19 [RISMA MB1-MB5]
(a) Air temperature
(b) In situ 2.5 cm
(c) In situ 5 cm
(d) SMAP T_{eff}/K
Freezing/cooling
Thawing/warming
Seasonal min T_B^H
SMAP T_B^H (K)
Air temperature at 2 m (°C)
Soil temperature at 2.5 cm (°C)
Soil temperature at 5 cm (°C)
SMAP ancillary T_{eff}/K (°C)

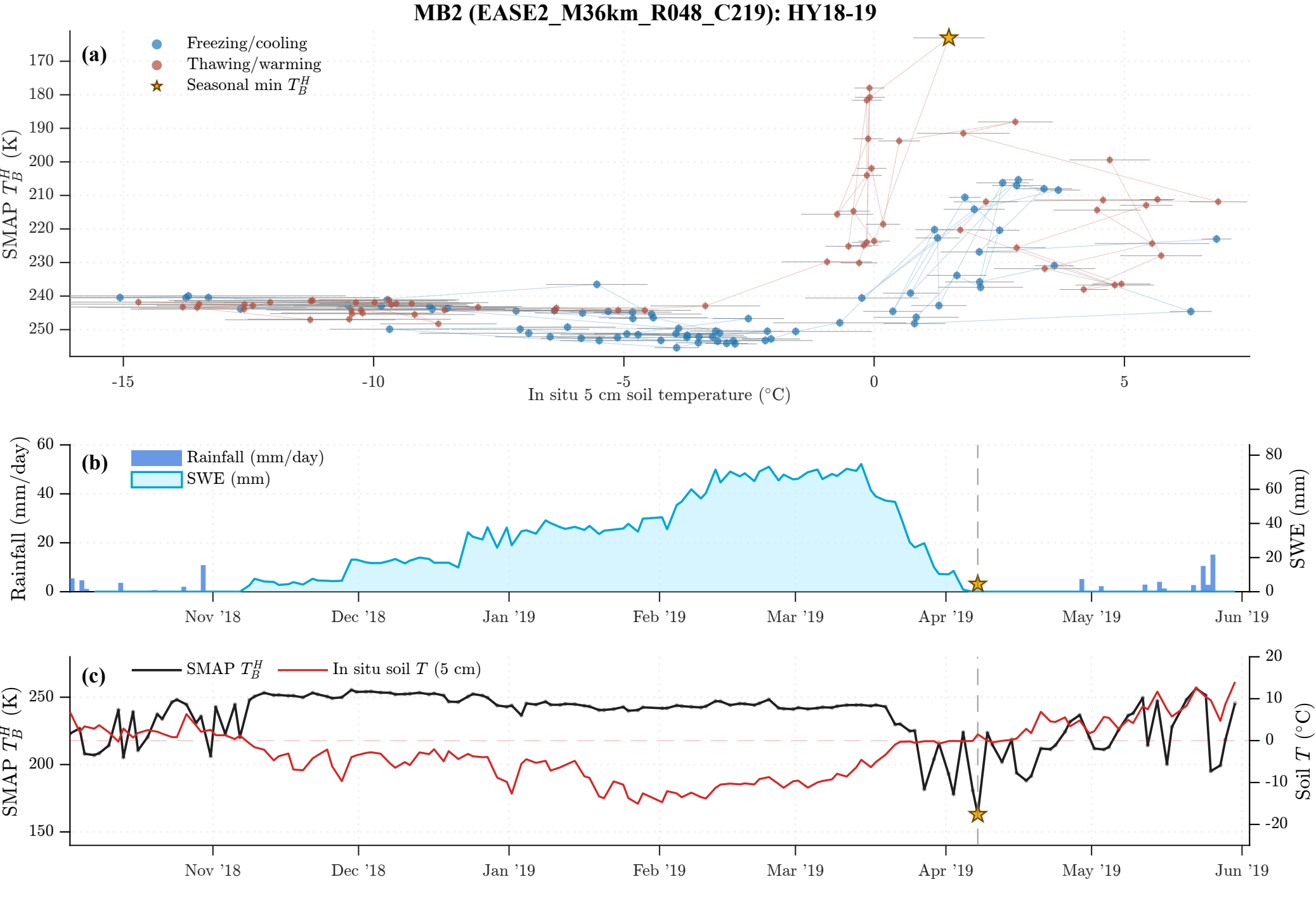
MB2 (EASE2_M36km_R048_C219): HY18-19
(a)
Freezing/cooling
Thawing/warming
Seasonal min T_B^H
SMAP T_B^H (K)
In situ 5 cm soil temperature (°C)
(b)
Rainfall (mm/day)
SWE (mm)
Nov '18
Dec '18
Jan '19
Feb '19
Mar '19
Apr '19
May '19
Jun '19
(c)
SMAP T_B^H
In situ soil T (5 cm)
Soil T (°C)

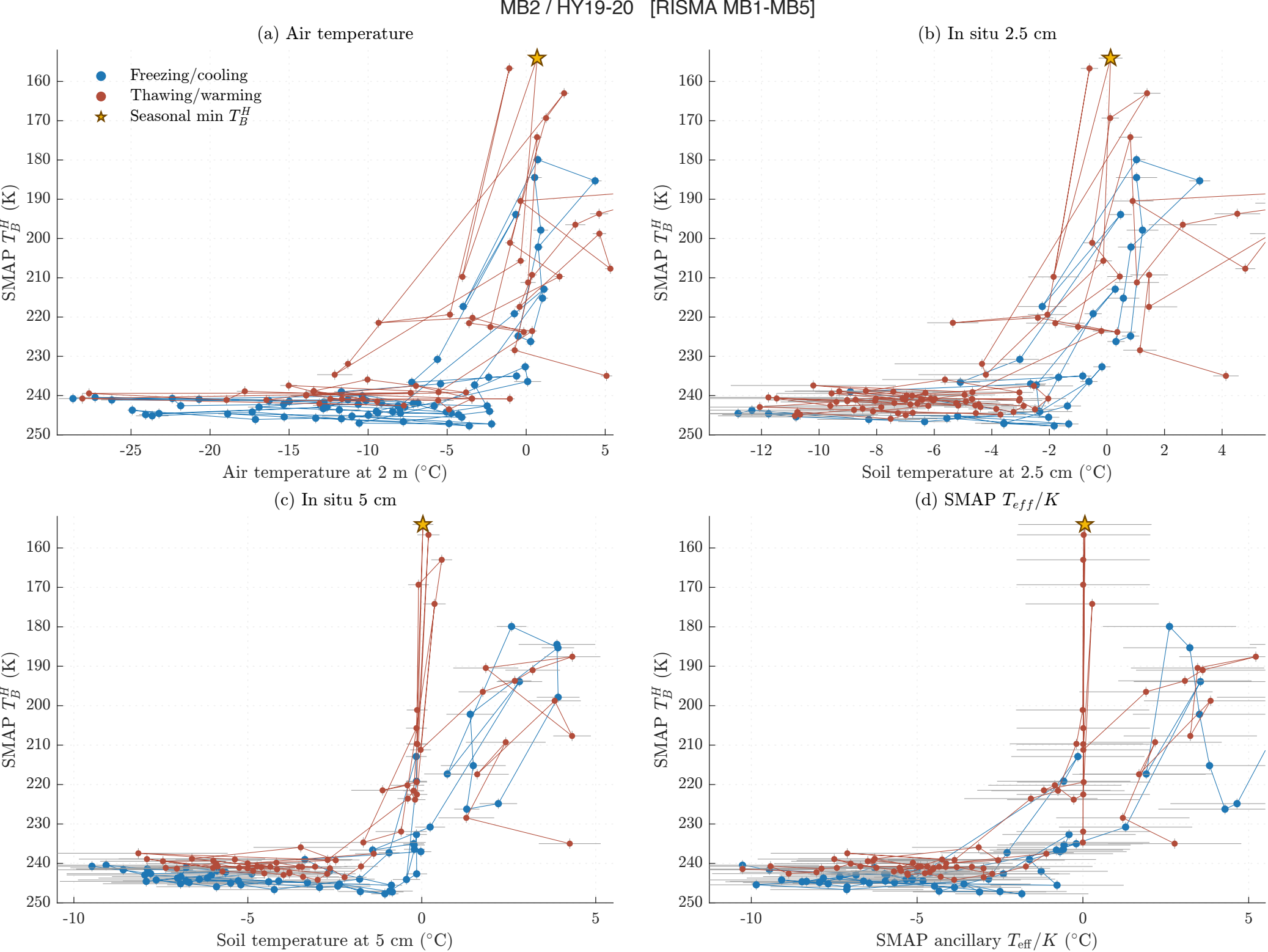
MB2 / HY19-20 [RISMA MB1-MB5]
(a) Air temperature
(b) In situ 2.5 cm
(c) In situ 5 cm
(d) SMAP T_{eff}/K
Freezing/cooling
Thawing/warming
Seasonal min T_B^H
SMAP T_B^H (K)
Air temperature at 2 m (°C)
Soil temperature at 2.5 cm (°C)
Soil temperature at 5 cm (°C)
SMAP ancillary T_{eff}/K (°C)

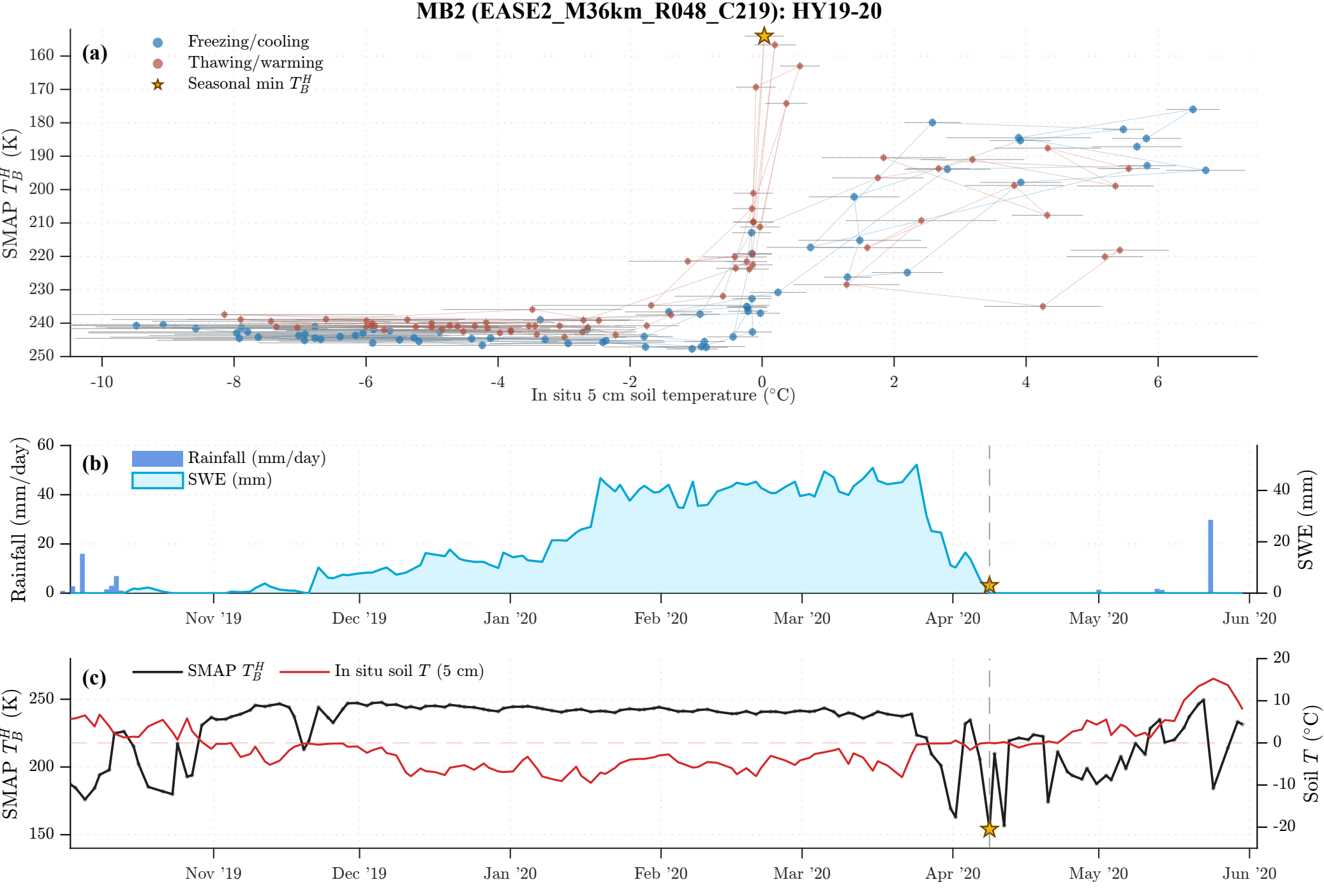
MB2 (EASE2_M36km_R048_C219): HY19-20
(a)
Freezing/cooling
Thawing/warming
Seasonal min T_B^H
SMAP T_B^H (K)
In situ 5 cm soil temperature (°C)
(b)
Rainfall (mm/day)
SWE (mm)
Nov '19
Dec '19
Jan '20
Feb '20
Mar '20
Apr '20
May '20
Jun '20
(c)
SMAP T_B^H
In situ soil T (5 cm)
Soil T (°C)

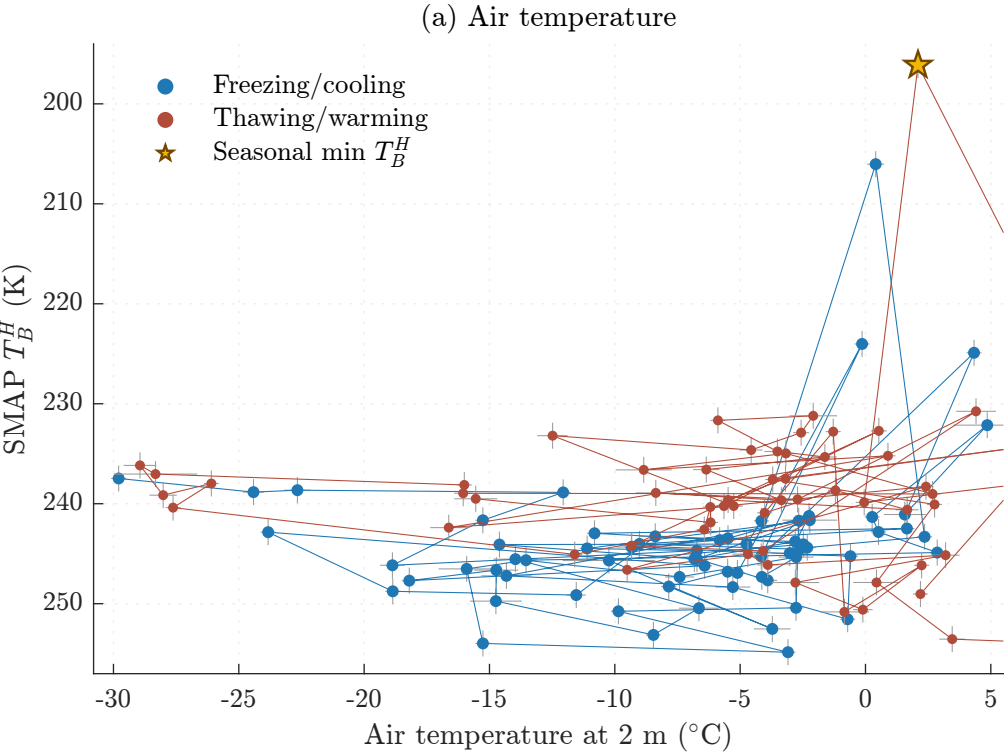
(a) Air temperature
Freezing/cooling
Thawing/warming
Seasonal min T_B^H
SMAP T_B^H (K)
Air temperature at 2 m (°C)

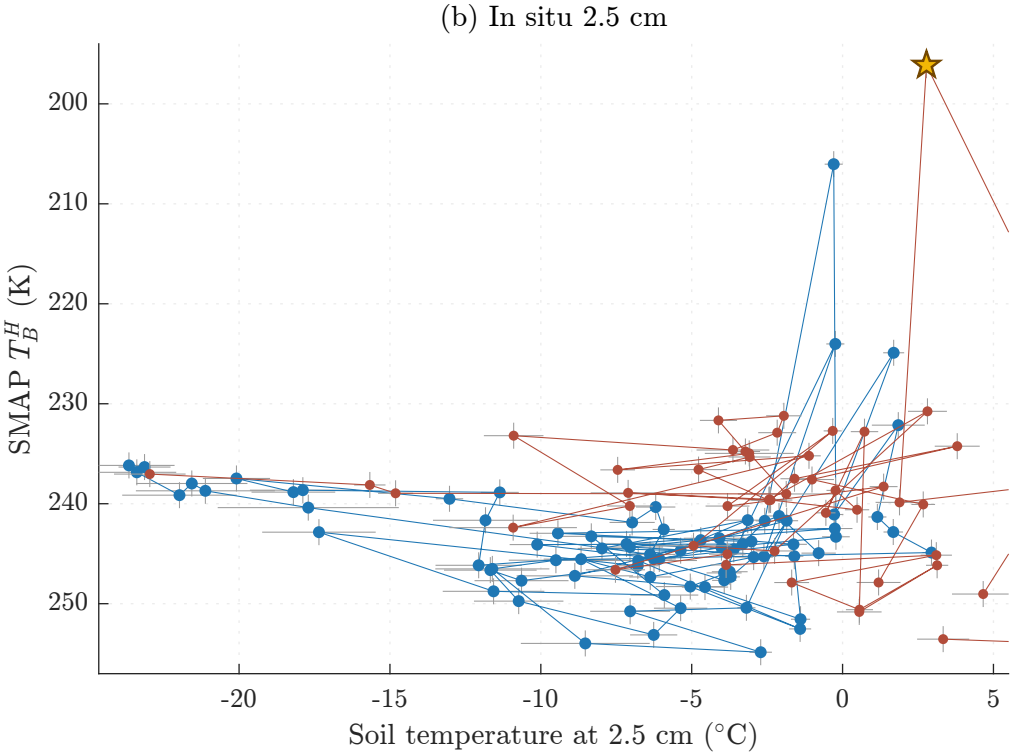
(b) In situ 2.5 cm
SMAP T_B^H (K)
Soil temperature at 2.5 cm (°C)

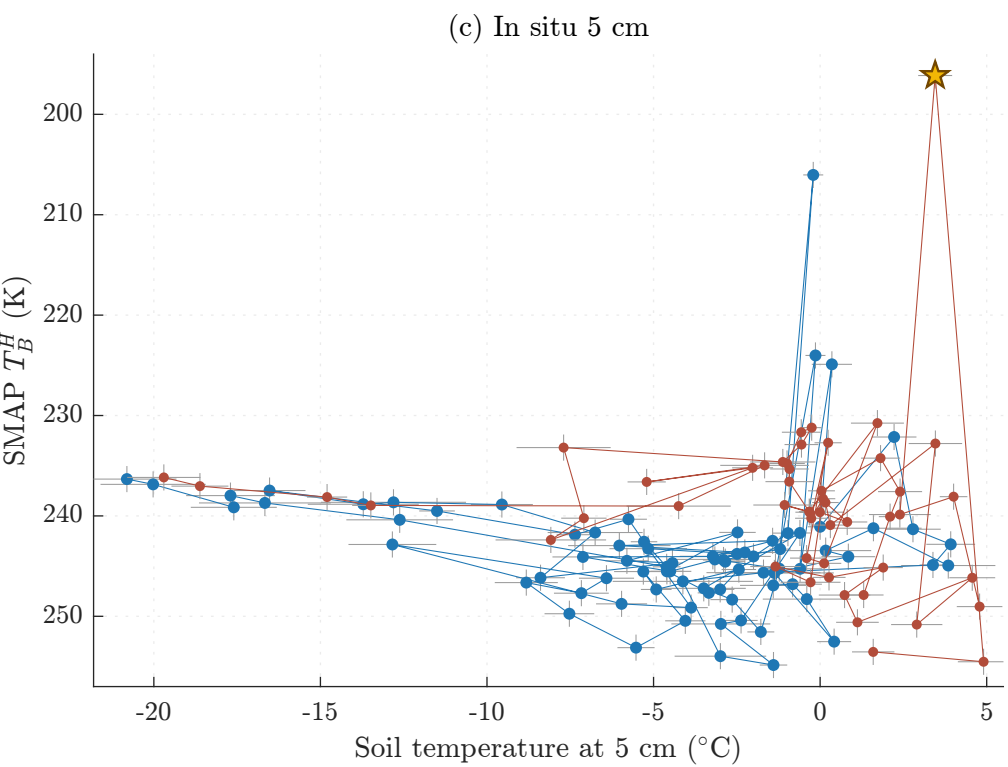
(c) In situ 5 cm
SMAP T_B^H (K)
Soil temperature at 5 cm (°C)

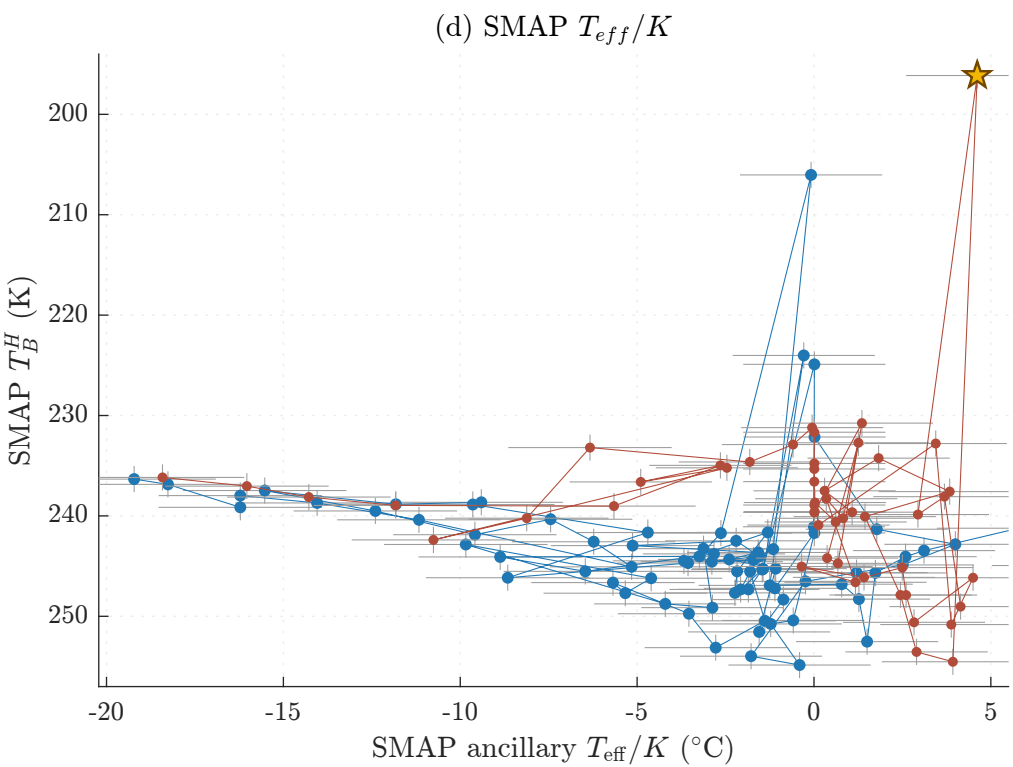
(d) SMAP T_{eff}/K
SMAP T_B^H (K)
SMAP ancillary T_{eff}/K (°C)

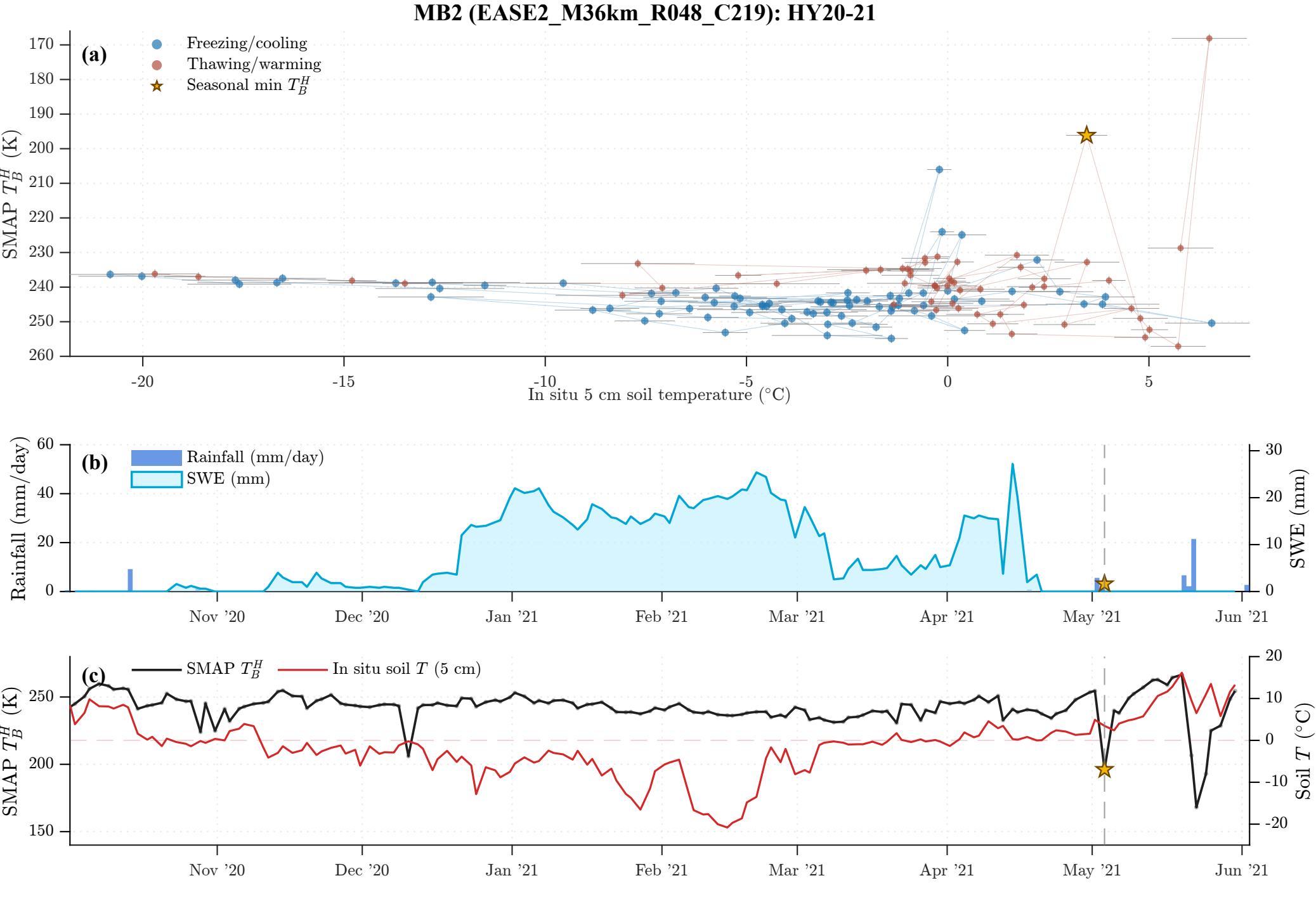
MB2 (EASE2_M36km_R048_C219): HY20-21
(a)
Freezing/cooling
Thawing/warming
Seasonal min T_B^H
SMAP T_B^H (K)
In situ 5 cm soil temperature (°C)
(b)
Rainfall (mm/day)
SWE (mm)
Nov '20
Dec '20
Jan '21
Feb '21
Mar '21
Apr '21
May '21
Jun '21
(c)
SMAP T_B^H
In situ soil T (5 cm)
Soil T (°C)